Towards novel lab-on-a-chip electrochemical detection of infectious disease biomarkers

Author: Amy Elizabeth Valera

TOWARDS NOVEL LAB-ON-A-CHIP ELECTROCHEMICAL DETECTION OF INFECTIOUS DISEASE BIOMARKERS

Amy E. Valera

A dissertation

submitted to the Faculty of

the department of Biology

in partial fulfillment

of the requirements for the degree of

Doctor of Philosophy

Boston College
Morrissey College of Arts and Sciences
Graduate School

October 2018

TOWARDS NOVEL LAB-ON-A-CHIP ELECTROCHEMICAL DETECTION OF INFECTIOUS DISEASE BIOMARKERS

Amy E. Valera

Advisor: Thomas C. Chiles, Ph.D.

Rapid diagnosis of infectious disease at the site of the patient is critical for preventing the escalation of an outbreak into an epidemic. This is particularly true for cholera, a disease known to spread swiftly within resource-limited populations. A device suited to point-of-care (POC) diagnosis of cholera must not only demonstrate laboratory levels of sensitivity and specificity, but it must do so in a highly portable, low-cost manner, with a simplistic readout. Here, we report novel proof-of-concept lab-on-a-chip (LOC) electrochemical immunosensors for the detection of cholera toxin subunit B (CTX), based on two nanostructured architectures: the gold dendritic array, and the extended core coax (ECC).

The dendritic array has an ~18x greater surface area than a planar gold counterpart, per electrochemical measurements, allowing for a higher level of diagnostic sensitivity. An electrochemical enzyme-linked immunosorbant assay (ELISA) for CTX performed *via* differential pulse voltammetry (DPV) on the dendritic sensor demonstrated a limit-of-detection of 1 ng mL^{-1}, per a signal-to-noise ratio of 2.6, which was more sensitive than a simple planar gold electrode (100 ng mL^{-1}). This sensitivity also matches a currently available diagnostic standard, the optical ELISA, but on a miniaturized platform with simple electrical readout.

The ECC was optimized and explored, undergoing several changes in design to facilitate sensitive LOC electrochemical detection. The ECC matched the off-chip sensitivity towards CTX demonstrated by a previous non-extended core coaxial iteration, which was comparable to a standard optical ELISA. In contrast to the previous coaxial architecture, the ECC is amenable to functionalization of the gold core, allowing for LOC detection. ECCs were functionalized using a thiolated protein G, and CTX was detected *via* an electrochemical ELISA. While this work is ongoing, the ECC shows promise as a platform for LOC electrochemical ELISA.

The ability to potentially meet POC demands makes biofunctionalized gold dendrites and ECCs promising architectures for further development as LOC sensors for the de- tection of infectious disease biomarkers.

Contents

List of Tables

List of Figures

ACKNOWLEDGEMENTS

I would first like to thank my advisor, Dr. Thomas C. Chiles, for his support over the last five years. I leave Boston College as a capable and independent researcher thanks to him. I would also like to thank my collaborator, Dr. Michael J. Naughton, for his guidance in navigating the interdisciplinary science landscape. Thank you also to my committee members Dr. Babak Momeni, Dr. Daniel Kirschner, and Dr. Sarah McMenamin, for your time and flexibility.

To the Chiles' lab members, both graduate and undergraduate, who have moved on to bigger things, thank you for everything. Most especially, I want to thank Dr. Shannon Argueta for not only being an amazing scientific mentor and sympathetic ear, but also one of my most supportive friends. My last few years at Boston College would have been impossible if not for our weekly dinner dates. Thank you also to Emma Geiger, for being an amazing undergraduate researcher in the lab, and an even more amazing roommate outside of it.

Thank you to the Naughton lab members, past and present, who have been both collaborators and friends. I would especially like to thank Luke D'Imperio and Dr. Nathan Nesbitt for all they have done to make this thesis possible, through their commitment to interdisciplinary science. Luke in particular has fabricated

over 100 ECC chips for me in the past 3 years, which is an incredible feat.

Thank you to everyone in the Biology office for making sure that I never fell through the cracks. Especially Dina Goodfriend, without whom the last few years, which included moving to a new lab space, would have been impossible. Dina made certain that I could always make research my main concern, by taking care of the rest. She and the rest of the biology staff truly go above and beyond for the students in the department.

I want to thank all my friends within Boston College, specifically Dr. Joshua A. Walker who has been helping me hone my scientific writing since my comprehensive exam, and Elizabeth Bearce for all the craft nights. To my friends from outside Boston College, thank you for making this journey possible, especially John Bufe and countless others who never doubted I would finally graduate. I would also like to thank my family for their support through all of my schooling, especially my sister, Emily Valera.

Most importantly, I would like to thank my partner, Michael Mogenson who came into my life while I was writing my comprehensive exam proposal, and still decided to stick around all the way through to me writing my thesis. In the intervening years, he has dealt with the ups and downs of my time at Boston College with unimaginable and unending support and grace. He has been my biggest cheerleader, and an amazing scientific sounding board.

List of Abbreviations

Ab	antibody
ALD	atomic layer deposition
ALP	alkaline phosphatase
4-AP	4-aminophenol
A.S.S.U.R.E.D	accessible, sensitive, specific, user-friendly, rapid/robust, equipment-free, delivered
AuNP	gold nanoparticle
BSA	bovine serum albumin
CE	counter electrode
CFTR	cycstic fibrosis transmembrane conductance regulator
C_{dl}	double layer capacitance
CTX	cholera toxin subunit b
CV	cyclic voltammetry
DENA	directed electrochemical nanowire assembly
DPV	differential pulse voltammetry
ECC	extended core nanocoax
EDTA	ethylenediaminetetraacetic acid
ELISA	enzyme-linked immunosorbant assay
Fab	antigen-binding fragment

FBS	fetal bovine serum
Fc	crystallizable fragment
FCA	ferrocenecarboxylic acid
GOx	glucose oxidase
I_p	peak current
LFA	lateral flow assay
LOC	lab-on-a-chip
NIL	nanoimprint lithography
pAPP	p-aminophenylphosphate
PBS	phosphate buffered saline
PCEPy	poly-(2-cyano-ethylpyrrole)
PCR	polymerase chain reaction
PDMS	polydimethylsiloxane
POC	point of care
PSA	prostate specific antigen
QD	quantum dot
RE	reference electrode
SDS	sodium dodecyl sulfate
SEM	scanning electron microscopy
SPR	surface plasmon resonance
TBS	tris buffered saline
TBST	tris buffered saline with tween-20
VOC	volatile organic compound
WE	working electrode

WHO World Health Organization

This dissertation is dedicated to Michael J. Mogenson

Chapter 1

Introduction

1.1 Cholera remains a global disease burden

The World Health Organization (WHO) describes cholera as "a disease of inequity - an ancient illness that today sickens and kills only the poorest and most vulnerable people" (*1*). Indeed, for close to a century, industrialized countries have seen almost no cholera outbreaks, largely due to modern sanitation infrastructure. Despite this, cholera remains a global disease burden affecting ~2.9 million people per year, resulting in ~95,000 deaths (*1*). The map of reported cholera cases from the last decade could as well be a map of poverty (Fig. 1.1). It is for this reason that the world is currently in the midst of the 7^{th} pandemic of cholera which has persisted since 1961 despite the availability of highly effective treatment, preventative measures, and even vaccines (*2*, *3*). The endemic presence of cholera in many parts of the world, and the frequent re-emergence of large scale cholera outbreaks, means that strategies for containment that were effective in the developed world must be reevaluated.

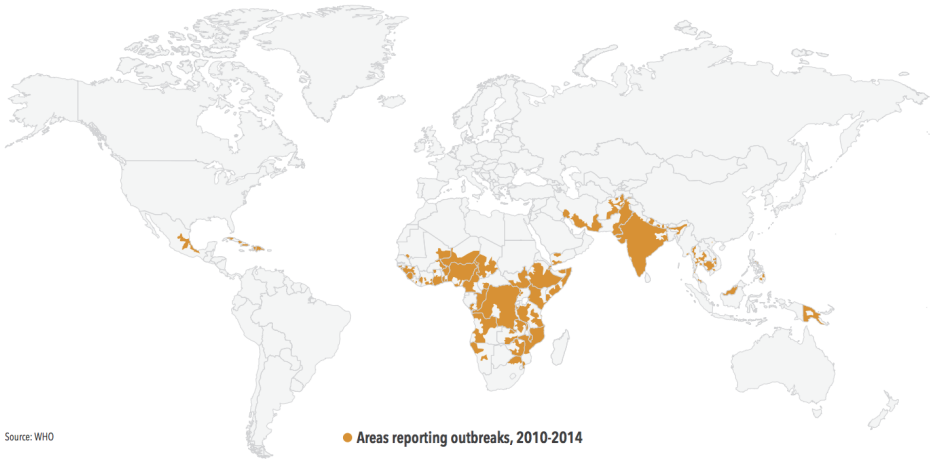

FIGURE 1.1: A map of areas reposting cholera outbreaks from 2010 to 2014. Image from reference (*1*).

1.1.1 Causative agent and pathogenesis

Vibrio cholerae is a gram-negative, highly motile rod-shaped bacterium of the Vibrionaceae family. It thrives in salt water, but can also be found in low-salinity water if it is warm and contains sufficient nutrients (*4*). While there are hundreds of serogroups of *V. cholerae*, only two, O1 and O139, are known to cause epidemics (*5*). Infection occurs via a fecal-oral transmission, usually from contaminated drinking water, but also through contaminated food. Once ingested, most *V. cholerae* is destroyed by the stomach's gastric juices. As is the case in areas where cholera is endemic, if a person is malnourished, the stomach produces less acid and the bacteria survives to colonize the small intestine (*6*). Cholera enterotoxin is secreted and adheres to the cells of intestine via an interation between the toxin's pentameric β subunit and the GM1 ganglioside of

the enterocyte. Once attached, the toxin's single α subunit is cleaved into two domains, A1 and A2, after which the enzymatic A1 subunit enters the cell where it continuously stimulates the production of cAMP. High cAMP levels lead to activation of the cystic fibrosis transmembrane conductance regulator (CFTR), an ATP-gated anion channel, which allows for an efflux of Cl^- ions and water (*7*, *8*). This leads to the acute "rice water" diarrhea characteristic of cholera, which can cause death within hours if untreated (*9*).

1.1.2 Early detection and response to prevent outbreaks

The WHO has recently developed a roadmap for the elimination of cholera worldwide by the year 2030. Given the ample knowledge about both the prevention and treatment of its infections, it is a reality that every death from cholera is avoidable. However, it still continues to thrive in crowded, resource-limited areas of the world with suboptimal centralized health care and sanitation facilities (*10*). Additionally, it disproportionately strikes communities already weakened by famine, war and natural disasters. For example, after an earthquake devastated Haiti in 2010, an epidemic of cholera was able to spread so rapidly that only 2 months after the first laboratory-confirmation case, it had affected 120,000 people, with 2,500 deaths reported (*11*).

Fundamental to the WHO's roadmap is the importance of early detection and rapid response to control future outbreaks. In fact, this comprises "Axis 1" of

the plan, highlighting that early detection is the foundation for preventing epidemics. However, a lack of sophisticated medical infrastructure available to the people most affected by cholera means that any potential diagnostic tool must meet the demands unique to this environment. This means that for a tool to be useful at the point-of-care (POC) in a resource-limited area, it must also be low-cost, portable, and give unambiguous results that could be easily interpreted by untrained personnel, in addition to being highly sensitive and specific. An ideal tool would also open up the possibility of transmitting diagnostic data to a centralized data bank for epidemiological monitoring. The WHO uses the acronym A.S.S.U.R.E.D. to describe the characteristics necessary for an ideal POC diagnostic test (Fig. 1.2) (*12*, *13*).

1.1.3 Current assays for cholera detection

Current benchmark assays for cholera detection do not meet POC diagnostic demands. Fecal culturing remains the best method, as it allows for serogroup distinction which is important for monitoring outbreaks. This method, however, is time consuming, typically requiring 2 full days for cultures to develop (*9*, *14*). As a result, true POC diagnosis typically is made on the basis of symptoms, which for diarrheal diseases tend to be almost identical (*14*). This creates a scenario where already limited resources, both financial and medical, may be wasted on incorrect diagnosis. In turn, this contributes to the cycle of cholera and poverty that is responsible for endemic infection in the first place (Fig. 1.3).

FIGURE 1.2: The acronym A.S.S.U.R.E.D. is used to describe the ideal features of a POC diagnostic device, as dictated by the WHO.

While breaking free of this cycle can be accomplished through interventions at several points, the role of roper diagnosis in the prevention of the spread of cholera is essential.

Cholera outbreaks account for an estimated $2 billion financial burden in the countries it affects. This is mainly in the form of loss of productivity from prolonged convalescence and the death of otherwise healthy workers (*1*). Enhanced epidemiological surveillance, facilitated by sensitive detection, allows for quick identification of endemic areas, which directs medical response and may decrease the total monetary loss from a large outbreak.

To this end, since 1990, 24 commercially available cholera diagnostic tests have been developed. Many of these are polymerase chain reactions (PCR) or ELISA-based, which provide high levels of specificity and sensitivity. Yet both require access to clinical laboratory infrastructure, which may be limited or nonexistent at the site of the patient (*15*). Conversely, the most rapid and portable of these 24 tests all rely either on colorimetric lateral flow assays (LFA) or agglutination readouts (*16*). Agglutination techniques are highly cost-effective and can give rapid results, but are only semi-quantitative, and reagents require refrigeration after reconstitution (*17*). LFAs (or "dipstick" tests) represent currently the most promising technologies for POC diagnosis (*18*, *19*). While low-cost and highly user friendly, LFAs are qualitative or semi-quantitaive at best (*20*), and the sensitivity and specificity of many available LFA tests are still not optimal (*17*).

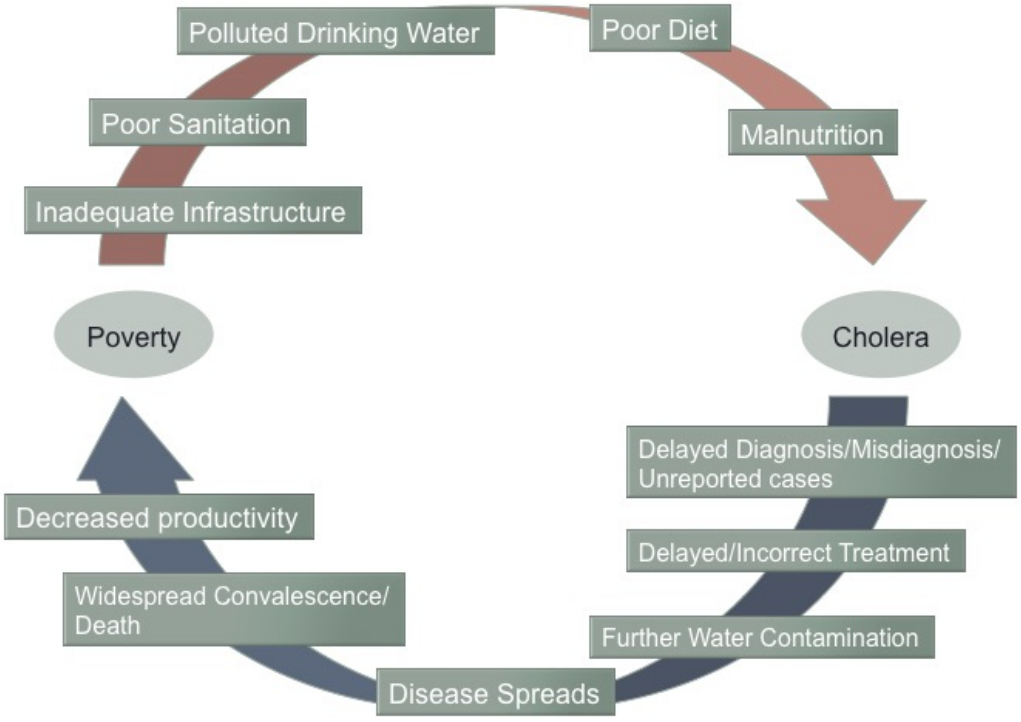

FIGURE 1.3: Cholera outbreaks in the developed world have been unheard of in the last century. This is because poverty and cholera are intrinsically linked.

Further, LFAs rely on a visual readout with a colored strip appearing if sufficient analyte is present in the test area. The drawback of such visual methods was highlighed by Ley, *et. al.* in their review of one LFA tool, the Crystal VC dipstick (Fig. 1.4) (*21*). They found that optical readouts increase the possibility of misdiagnoses by human error, such that the rate of false positives nearly doubled, from 26% to 44%, when it was performed by workers in the field, *vs.* a trained laboratory technician (*22*). In fact, it is recommended that the Crystal VC dipstick not replace standard fecal culturing in diagnosis, but instead be used as an intermediate tool for evaluating treatment options (*23*). As stated previously, this can result in wasted time and resources, which contributes to the severity of an outbreak. While at the present time LFA and agglutination assays may be adequate, diagnostic sensors with simple, quantitative electrochemical readouts may be more desirable towards outbreak prevention.

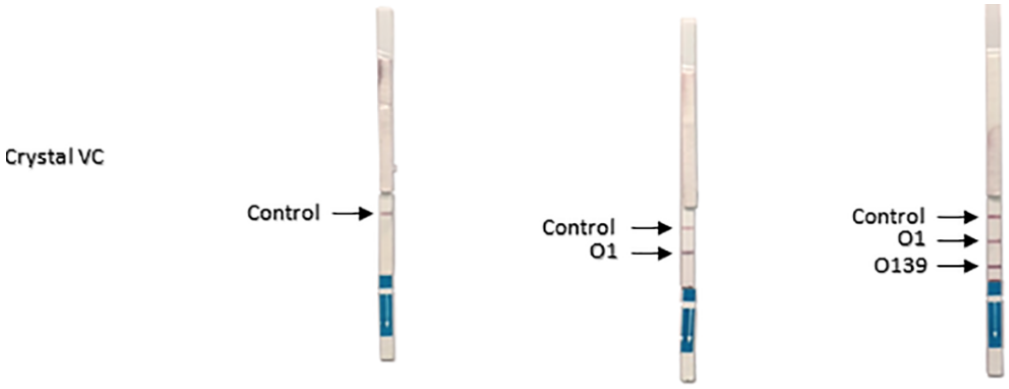

FIGURE 1.4: The Crystal VC dipstick test provides an optical readout similar to a pregnancy test. The reliance on colored strips can lead to a high rate of misdiagnoses by workers in the field. Image from reference (*21*).

1.2 Lab-on-a-chip sensors for POC diagnostics

Lab-on-a-chip (LOC) biosensors are those that integrate laboratory functions onto a miniaturized chip-based platform (*24*). The field of biosensing is being revolutionized by LOC technology, with numerous fully integrated detection systems utilizing a wide variety of sensing methods being reported recently (*25*–*30*). In addition to being used as medical diagnostic tools, LOCs are being employed in pathogen detection (*31*), trace metal detection (*32*), water monitoring (*33*), and in drug discovery (*34*). These devices, due to their size, function with diminished reagent needs and, depending on their detection strategy, are often low powered and highly portable. To this end, the use of LOC technologies are particularly attractive as it pertains to public health care in the developing world,

as these miniaturized tools hold the potential for sensitive, low-cost, POC diagnosis (*35*). While many advances have been made in the field, it remains largely unproven outside of the laboratory, especially for POC applications.

LOC biosensors typically incorporate microfluidic technology to further remove the human element from diagnosis (*36*). The field of microfluidics involves the use of micrometer-scale microfabricated channels to manipulate the flow of minute amounts of liquid, on the order of 10^{-9} to 10^{-18} liters (*34*, *37*, *38*). The most frequently used elastomer for microfluidic channels, polydimethylsiloxane (PDMS), allows for manufacturing that is low-cost and high production (*39*). Microfluidic channels integrated on a LOC biosensor therefore represent a cost-effective alternative to LFAs for small-volume, user-friendly and potentially automated detection at the site of the patient. The commercial promise of the field is reflected in the number of patents issued for microfluidic devices, which has been steadily increasing since the mid-90s (Fig. 1.5) (*40*). As the field rapidly expands, new methods of miniaturizing conventional laboratory assays are being explored. Detection strategies employed in LOC microfluidic sensors have ranged from magnetic beads, to capillary electrophoresis, to electrochemical immunodetection (*41*–*45*). Microfluidics have also been utilized to decrease the analysis time and reagent consumption of common immunoassays (*46*).

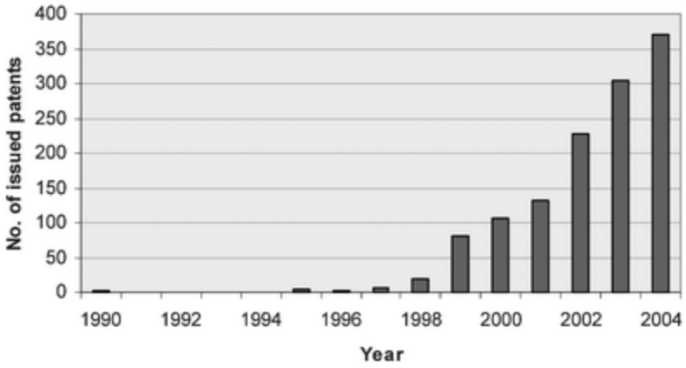

FIGURE 1.5: The number of patents being issued for microfluidic devices reflects the commercial promise of the field. Image from reference (*40*).

1.2.1 Optics-based LOC sensors

For diagnostic assays, tests with an optical readout mechanism are by far the most prevalent (*47*). This includes the detection of either fluorescent tags or color changes as a result of an enzymatic reaction (as in an ELISA); such tests are called intensity assays. Optical detection also encapsulates the category of surface plasmon resonance (SPR) assays. Intensity assays are more amenable to portability, low cost and limited equipment needs, but the choice of detection method is driven by a trade-off between POC benefits and diagnostic benefits, which must be considered.

The use of a fluorescent signal in immunodetection is popular due to the commercial availability of components required for detection (*e.g.* excitation source, light collection apparatus and photodetector) (*47*). In addition to numerous

available fluorophores, quantum dots (QD) also exist in a wide variety of emission spectra colors, and may in fact be more desirable as a reporter. QDs are nanometer-scale semiconductor particles, whose unique optical and electronic properties make them popular in LOC detection. When conjugated to biomolecules (*e.g.* antibodies), QDs can provide ~100x reduced risk of photobleaching, and 20x the brightness as compared to a fluorophore (*48*). In fact, Jokerst, *et. al.* were able to use QDs in a microfluidic biosensor in order to detect 3 cancer biomarkers in both serum and whole saliva, with 30x more signal amplification relative to a fluorphore (*49*). The color of the light emitted by a QD can be finely tuned by only changing the particles' size, shape or material (Fig. 1.6) (*50*, *51*). In this way, QDs allow for highly sensitive detection, such as the femtomolar levels of cancer biomarker sensing achieved by Hu, *et. al.* (*52*). QDs remain limited by their optical nature, however. They can experience a phenomenon called "blinking", where the QD may become invisible due to surface defects trapping electrons. Surface defects can also cause deterioration in quantum yield, meaning that the ratio of absorption to emission is low, and they may become undetectable, or may require much more sensitive instrumentation to detect (*53*).

Besides fluorescent and colorimetric assays, LOCs have also been reported that take advantage of SPR. SPR is a method of exploiting the unique behavior of metal surfaces wherein conduction electrons oscillate when excited by light, in order to measure the adsorption of molecules onto the surface (*54*). This method offers the POC advantages of being label-free, highly sensitive, and real-time (*55*). Specifically, the resonance amplifies optical phenomena such as scattering,

(a)

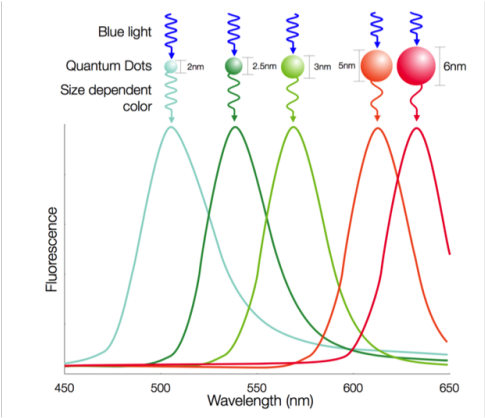

(b)

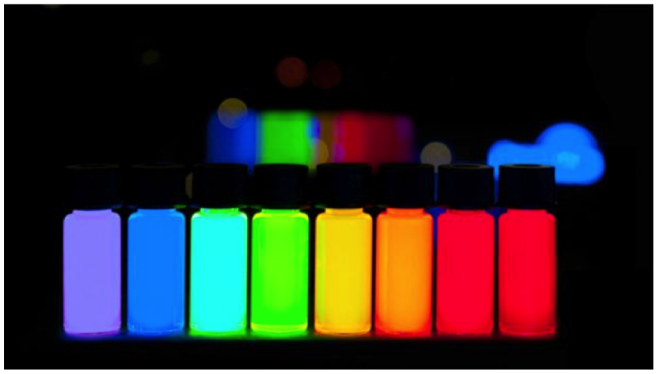

FIGURE 1.6: (a) The color of a QD emission can be finely tuned by changing its size. (b) A wide range of extremely bright fluorescent colors are achievable using QDs. Images adapted from references (a) (*50*) and (b) (*51*).

transmission, adsorption (*56*, *57*), and photoluminescence (*58*, *59*).

SPR on flat metal films has been the most popular architecture for biosensing applications, with commercially available sensors sold by GE Healthcare (*60*). This system (Fig. 1.7), however, requires extremely large and expensive equipment, making it unsuitable for use in POC work. Additionally, further drawbacks to SPR sensing must be addressed, which include the inability to distinguish specific from non-specific binding at the sensor surface, inadequate sensitivity for low molecular weight molecules, and the limited size of the sensor area (*61*).

On this latter point, altering the surface architecture of the sensor may offer a solution. Research recently has focused on producing surface architectures with their own interesting resonance behaviors, which can interface with portable microfluidic devices for POC diagnosis. Specifically, gold nanoparticles (AuNP) have been particularly useful in LOC style sensors, which can increase sensor surface area (*62*). Integration of SPR sensors with microfluidic channels to facilitate low volume and portable detection has also been extensively reported (*63*–*67*). But despite the potential of optical detection methods like SPR and QDs, the simple readout offered by electrochemical assays may be more desirable towards POC applications.

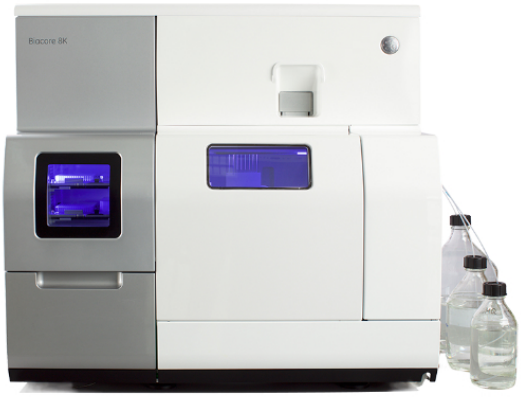

FIGURE 1.7: The GE Healthcare Biacore 8k SPR sensing platform, used for assessing biomolecule interactions in drug discovery. Image from reference (*60*).

1.2.2 Electrochemical LOC sensors

For medical purposes, tools that can offer a quantification of biological processes are better suited than those that only offer qualitative data. Qualitative tools, such as LFAs, can lead to ambiguous results and potentially misdiagnoses. However, connecting electronics to a biological environment for quantitative monitoring can be difficult, and so assays which provide electrochemical readouts are attractive as biosensors for their ability to directly transduce biological events into an electronic signal (*68*). Electrochemical biosensors require a bioreceptor for analyte recognition, which will interface with a surface architecture where biological events take place, and a transducing element (for example, current generated as a result of the biological event), which is turned into an electronic signal, and is processed for display (Fig. 1.8).

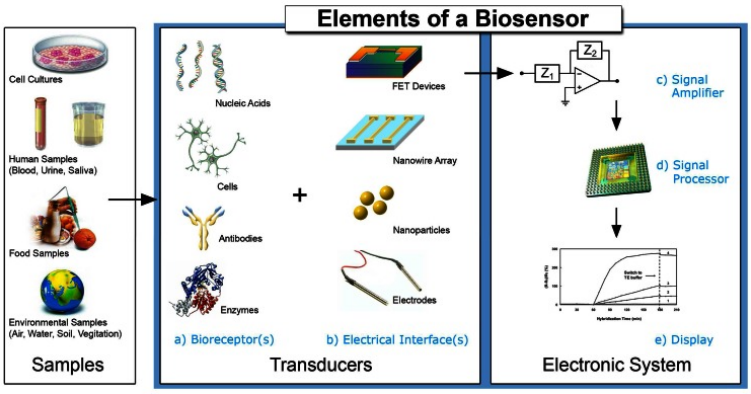

FIGURE 1.8: Elements required for an electrochemical biosensor. A wide range of sensors have be developed through mixing of different combinations of bioreceptor elemnts and electrical interfaces. Portability can be achieved through miniaturization of signal amplification and processing components, such as through the use of a microprocessor with a smart phone. Image from reference (*68*).

Electrochemical sensors largely fall into three categories for signal transduction: amperometric, potentiometric, and capacitive (*69*, *70*). In response to a biological event, amperometric sensors generate a current, potentiometric sensors accumulate a charge, and capacitive sensors alter conductive properties (*71*). Of these, amperometric sensors are the most popular and widespread for use in commercial devices, if only for the fact that the most well-known electrochemical biosensor is the glucose meter (*72*). In fact, this device alone accounts for 85% of the world's biosensor market (*73*).

Glucose meters rely on the following reaction scheme for electrochemcial detection (where GOx-FAD^+ is glucose oxidase conjugated to a redox cofactor which acts as an initial electron acceptor):

1. $\mathbf{Glucose + GOx - FAD^+ \longrightarrow Glucolactone + GOx - FADH_2}$

2. $\mathbf{GOx - FADH_2 + O_2 \longrightarrow GOx - FAD^+ + H_2O_2}$

Hydrogen peroxide is then oxidized at an electrode, and the flow of electrons is recorded as a current that is proportional to the amount of glucose in the original sample:

3. $\mathbf{H_2O_2 \longrightarrow 2\,H^+ + O_2 + 2\,e^-}$

While it has undergone some refinement, this principle for glucose detection has not changed drastically since it was first described, over 40 years ago (*74*). While the ubiquity and utility of the glucose sensor highlights the potential for a next generation of electrochemcial biosensors, its success has yet to be matched by any other tool. This detection scheme is based on a redox reaction that is linked to the oxidation of glucose, limiting its use in the detection of other analytes (*75*). For the development of novel electrochemcial biosensors, new detection strategies must be explored. Currently, the most popular bioreceptor elements used in electrochemical sensing are enzymes, due to their specificity (*76*, *77*), like the glucose sensor. Increasingly reported, however, are those that utilize antibodies, whole cells, and nucleic acids (*78*).

In POC applications, miniaturization is one of the most important features afforded by electrochemical detection strategies. Miniaturization opens up the possibility for multiplexing and portability (*79*–*84*). Additionally, the low power needs of miniaturized devices means that measurements could feasibly be taken using a smart phone USB port both as a power source and as an analyzer, potentially allowing for epidemiological monitoring by automatically uploading results to a centralized databank (*85*).

For example, Lillehoj, *et. al.* demonstrated a microfluidics-based LOC diagnostic sensor for the detection of malaria biomarkers which was integrated with a compact mobile phone platform (Fig. 1.9) (*86*). They developed a microchip-sized potentiostat, and a phone application with a simple user interface to walk

users through the detection process, all *via* the phone's USB port. Their device was based on capturing antibodies in a polypyrrole matrix on a simple planar gold electrode, which limited sensitivity to about 16 ng mL^{-1}. Smartphones are growing in ubiquity in the developed world, and with the advent of low-cost Android phones, they are poised to become even more common in the developing world (*87*, *88*). As such, tailoring LOC development towards devices amenable to smartphone integration is proving an exciting avenue for the future of electrochemical diagnostics.

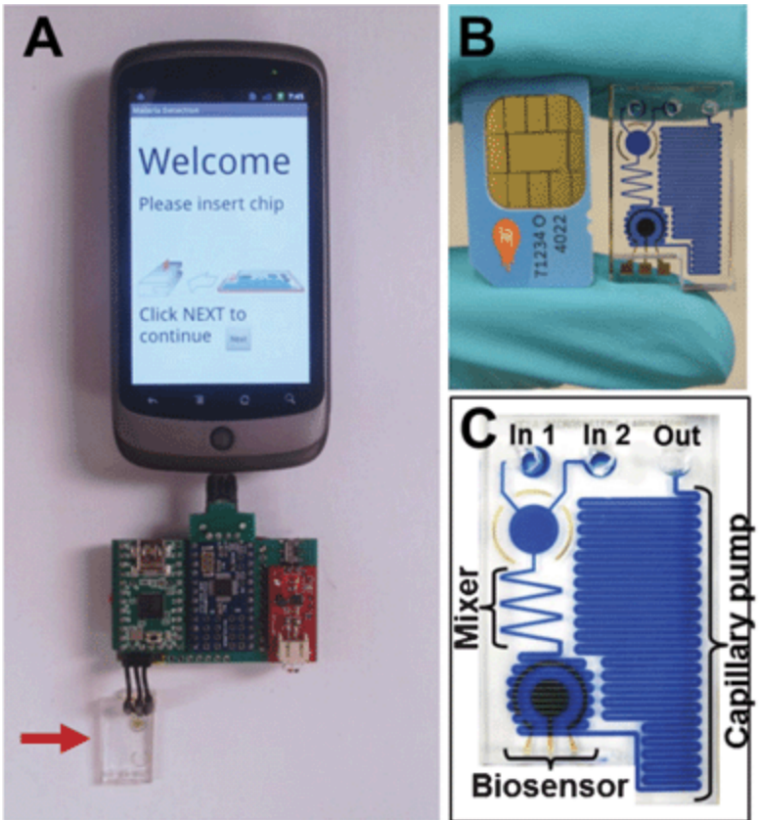

FIGURE 1.9: A prototype fully integrated LOC for malaria biomarker detection. This setup incorporated an electrochemical biosensor with a microfluidic channel system. Detection parameters (*e.g.* redox potential) were transmitted from a custom application *via* USB to a microcontroller. The microcontroller transmits detection parameters to a potentiostat module, which will measure voltage and current signals from the microfluidic chip. The microcontroller processes these signals and transmits them back to the phone in real-time. Red arrow points to the microfluidic sensing device. Image from reference (*86*).

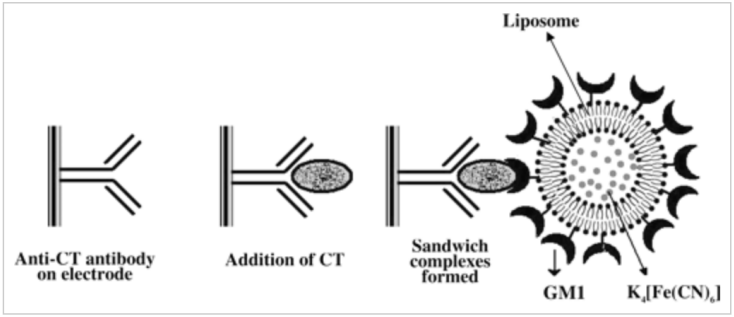

FIGURE 1.10: A capture antibody is adorbed onto an electrode, and captures cholera toxin. A GM1 functionalized liposome filled with a redox species is tethered to the electrode surface *via* a sandwich format, allowing for electrochemical detection of cholera toxin. Image from reference (*90*).

1.3 Strategies for sensor functionalization

Electrochemical sensors utilize a variety of recognition elements. For example, research into POC cholera sensors has generally sought to exploit the affinity of cholera toxin's beta subunit for GM1 gangliosides (*9*, *89*). Viswanathan *et. al.* used an assay similar to a sandwich ELISA to detect cholera toxin by binding cholera toxin to the surface of carbon nanotubes *via* antibody capture (Fig. 1.10). Toxin was then detected when GM1 functionalized liposomes encapsulating potassium ferricyanide bound to the immobilized cholera toxin, and the potassium ferricyanide was detected by square wave stripping voltammetry (*90*). However, while GM1 is a natural receptor for cholera toxin and *E. coli* heat-labile enterotoxin, this strategy cannot be employed for other biomarkers.

1.3.1 Methods of antibody tethering

Antibodies remain a much more attractive bioreceptor element due to both their specificity and due to their high commercial availability. In fact, antibodies have been used extensively in traditional diagnostic immunoassays, and so it would follow that they would be adopted for the use in POC sensor applications as well (*91*, *92*).

Indeed, a number of electrochemical antibody-based sensing platforms have been reported for detecting oncogenic biomarkers (*93*–*95*). Surface immobilization of antibodies can have severe impacts on their function, however, so care must be taken in choosing an immobilization technique that preserves the availability of the antigen binding region. One of the most well known uses of antibodies in diagnostics is the the ELISA. Adsorption of the capture antibody to the polystyrene substrate is achieved through hydrophobic and electrostatic interactions (*96*). Due to the random nature of this method, microtiter plates for ELISA must be sufficiently large to overcome the deficiencies caused by sub-optimally bound antibodies, leading to the need for volumes in the hundreds of microliters of sensing reagents for detection.

An antibody is comprised of two fragment antigen binding regions (Fab), and a fragment crystallizable region (Fc). Studies have shown that the activity of antibodies covalently bound to a solid surface is about half that of soluble antibodies, which is a major hinderance for antibody-based sensor development

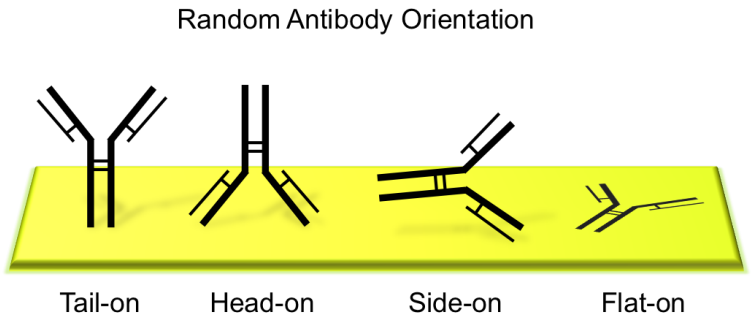

FIGURE 1.11: Antibodies allowed to adsorb onto a bare gold substrate will do so in a random manner, resulting in diminished availability of the antigen sensing region for analyte detection.

(*97*, *98*). If allowed to adsorb with no direction, antibodies adopt variable orientations, including tail-on (Fc attached to surface), head-on (Fab attached to surface), side-on (one Fc and one Fab attached to surface), or flat-on (all fragments attached to surface) (Fig. 1.11) (*99*). Tail-on is the most desirable due to the unobstructed availability of the Fab (*100*–*103*). Since the Fab is unique from the Fc in physical structure, isoelectric point and and composition, methods for oriented antibody attachment to a solid surface have been developed which exploit their distinction. (*104*).

The use of bacteria-derived protein A and protein G are particularly attractive for oriented antibody tethering, as they constrain surface binding to only the Fc region of the antibody (Fig. 1.12) (*105*–*107*). Of the two, protein G shows the most promise, as protein A has been demonstrated to bind the Fc in a highly reversible manner, and to also sometimes bind to the Fab and to albumin (*104*). Using protein G as an intermediate binding protein not only aids in the orientation of the

antibody, but also helps to reduce the negative effects of steric hindrance that may result from the proximity of attached antibodies to each other (*108*).

In biosensor development, conductive polymers are also gaining popularity as a means of tethering antibodies to electrode surfaces. This method is facile, cost-effective and stable; all useful features towards POC diagnostics development (*109*). Conducting polymers are well-suited to integration with a redox-based detection mechanisms because alternating single and double bonds in the polymer allow it to transfer charge efficiently (*110*). Polypyrrole specifically has emerged as a frequently-used polymer in biosensing applications, due to the gentle conditions of its one-step electropolymerization (*110*). Polypyrroles have been used in amperometric biosensors due to the tight adherence of the polymer to the working electrode (*111*), the potential for adding functional groups that allow for protein tethering, the stability at ambient conditions (*112*), and the ability to polymerize in neutral aqueous solutions (*113*). Much work has been directed towards the entrapment of recognition elements within the polymeric matrix, particularly for the enzyme glucose oxidase. Fouldes and Lowe demonstrated almost 30 years ago that GOx, which is negatively charged at pH 7.0, can be easily ionically incorporated into a polypyrrole matrix, which is net positive charged at the same pH (*114*). Their glucose sensor was limited, however, due to leeching of the enzyme out of the matrix, and due to polymer degradation in the presence of H_2O_2. Such a method of immobilization also leaves open the possibility for biomolecules to be denatured (*102*). An ideally suited biosensor would allow biomolecules to remain correctly oriented while maintaining their

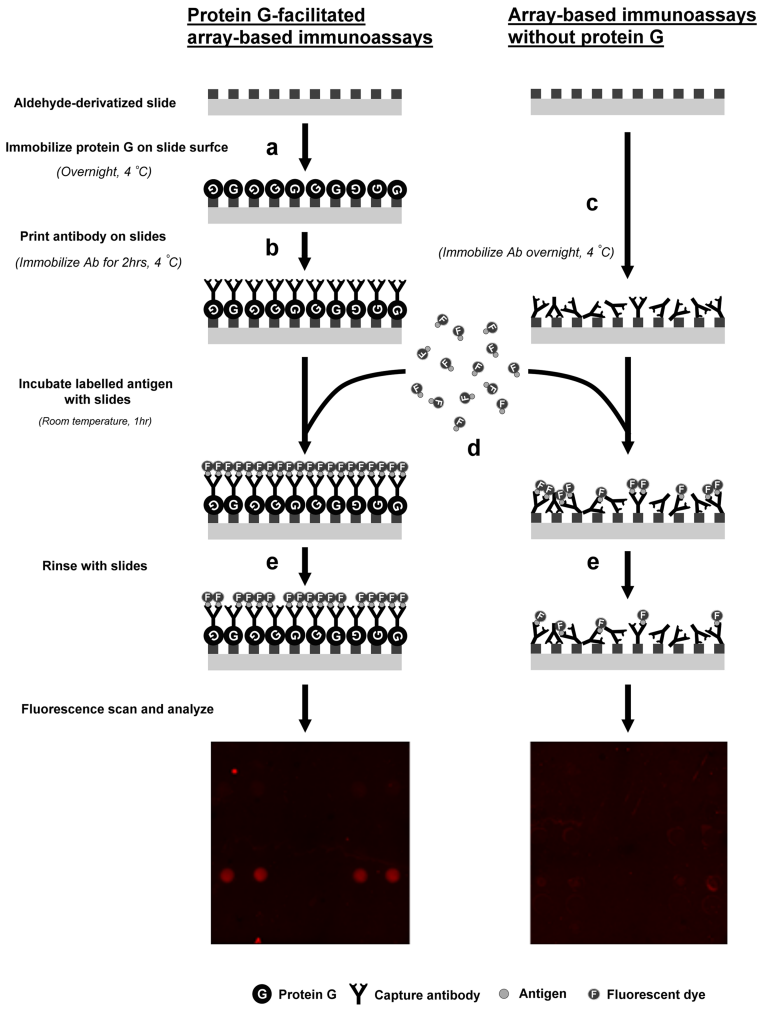

FIGURE 1.12: Oriented antibody binding can be achieved by using protein G as an intermediate. Image from reference (*105*).

native state.

For this reason, functional groups have been added to pyrrole polymers that allow for covalent bonding (*via* terminal reactive groups such as COOH and NH_2) (*115*, *116*) or electrostatic interaction with the polymer surface, rather than matrix entrapment (*117*, *118*). Electrostatic binding requires the least amount of work, but is limited by sensitivity to solution pH, which can cause the release of the protein from the polymer. However, Ouerghi, *et. al.* demonstrated that this method can be used for antibody biofunctionalization with a decent amount of control over antibody orientation. They reported the use of a polypyrrole with a terminal CN group, which electrostatically interacted with OH groups on the Fc region of their antibody (*102*).

Um, *et. al.* took this protocol even further to achieve better antibody orientation. They utilized a cyclic voltammetry (CV) scheme in order to attract negatively charged antibodies to the polymer surface at times when the surface was positively charged (*103*). This allowed the antibody to be tethered in one direction, leaving more antigen-binding regions available for sensing, as demonstrated by fluorescence imaging.

The mechanism of deposition of a polypyrrole film onto an electrode surface remains somewhat controversial due to the difficulty in following *in situ* what is happening at the electrode/solution interface, but it is generally accepted that

it begins by the anodic oxidation of the monomer in the presence of an electrolyte to create a cation free radical (*119*, *120*). Pyrrole can be electrodeposited potentiostatically (constant voltage), galvanostatically (constant current), or potentiodynamically (potential scans) (*121*).

1.4 Nanoarchitectures for sensitive electrochemical detection

An electrochemical reaction is detectable only in close proximity to the electrode surface. As such, the choice of electrode architecture can have huge implications in the sensitivity of electrochemical detection (*68*). Nanotechnology is a field that deals with the study of structures usually 1 to 100 nm in size, where materials exhibit unique properties (*122*–*124*). Nanoscale sensors may be desirable because their increased surface-area-to-volume ratio means that more atoms are available at the surface of the sensor for chemical reactions and signal detection (*125*). Sensors based on nanoarchitectures hold the potential to enable sensitive, specific, portable and low-cost diagnostics.

The field of nanotechnology is driven by the development of novel surface nanoarchitectures in the search for more sensitive devices. As stated previously, surface architectures exhibit unique characteristics at the nanoscale. This was demonstrated by a silicon nanowire array developed by Elfstrom, *et. al.*, who showed

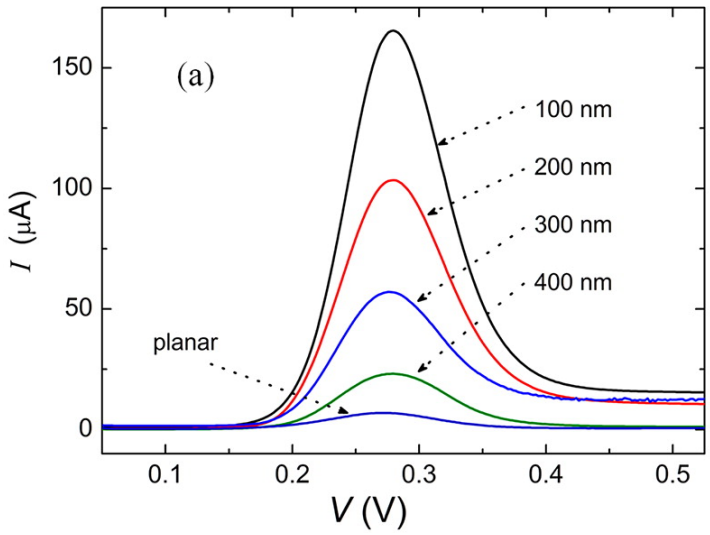

FIGURE 1.13: On a nanocoaxial array, decreasing the size of the annulus gap between the working and counter electrodes resulted in increasing sensitivity to the redox species ferrocenecarboxylic acid. Image adapted from reference (*127*).

that nanowires >150 nm in width were not sensitive to pH changes in a buffer, while smaller ones were (*126*). This was further demonstrated by Rizal *et. al.*, who showed that increasingly smaller nanometer scale distances between a nanocoaxial working and counter electrode resulted in greater and greater sensitvity to a redox species (Fig. 1.13) (*127*).

AuNPs are a prominent architecture for integration in electrochemical sensors, and protocols exist that allow for control over their size, dispersion, morphology and surface chemistry, providing for a broad range of sensor setups and detection methods (*128*). Of particular interest in the field of biosensing is the amenability

of AuNPs to biofunctionalization, specificically by antibodies. Antibody biofunctionalization of AuNPs was first reported in 1971, and so there have been over 40 years of development towards using these functionalized nanoparticles in numerous applications (*129*, *130*).

Antibody functionalization of AuNPs offers two major advantages in a sensing capacity: they enhance electrochemical signal transduction, and increase the overall surface area onto which antibodies can be stably bound, thus increasing the number of antigen-antibody recognition events that can be detected. Electrochemical biosensors based on antibody/AuNP tethering have been reported for the amperometric and potentiomtric detection of hepatitis B surface antigens (*131*) and for the potentiometric detection of diptheria (*132*, *133*). Additionally, Chen *et. al.* demonstrated the utility of AuNPs as the actual electrochemical label for detection, by measuring the number of $AuCl_4^-$ anions generated upon oxidation of the AuNP (Fig. 1.14) (*134*).

Nanowire arrays are another class of nanostructure used extensively in electrochemcial sensing, which have been reported using a variety of materials. For example, Si nanowires were fabricated by Patolsky, *et.al.*, which were capable of the electrical detection of a single virus (*135*), while Yin, *et. al.* incorporated silver nanoparticles on Si nanowires for the detection of H_2O_2 (*136*). In the context of biosensing and disease diagnosis, Zheng, *et. al.* demonstrated highly sensitive and multiplexed detection of prostate specific antigen (PSA) using a Si nanowire array (*137*). This setup detected down to an impressive 0.9 pg mL^{-1} of

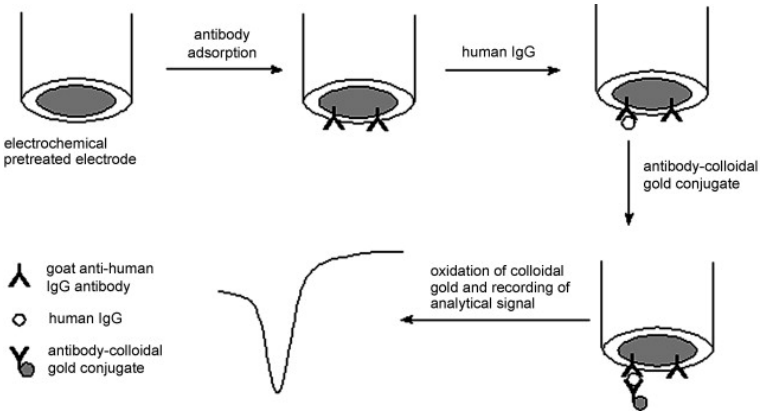

FIGURE 1.14: A biosensor based on AuNP/antibody tethering. In this example, a sandwich style assay is employed for detection. The AuNP is oxidized, and the resultant $AuCl_4^-$ anions are measured at the electrode surface. Image from reference (*134*).

PSA in a label-free manner, compared to 3 pg mL^{-1} for a standard optical ELISA.

Electrochemical sensors based on nanostructured electrodes, and integrated with microfluidic fluid handling systems represent one of the most promising combinations for true A.S.S.U.R.E.D. diagnostics. But while the potential is there, the actual application is essentially nonexistent. Use of such devices seems largely relegated to the laboratory, with few systems seeing any sort of commercial interest, especially so for the detection of infectious diseases of poverty. As such, the field remains open to the contribution of novel nanoscale surface architectures, and to the development and refinement of assays with which to integrate them.

1.5 Aims of study

This research detailed in this dissertation involves the exploration of different methods of surface biofunctionalization on two different nanostructured sensing platforms: gold dendrites and the extended core nanocoax (ECC). After functionalization, the sensors were evaluated for proof-of-concept utility as electrochemical LOC diagnostic sensors. This work was completed in collaboration with the physics laboratory of Dr. Michael J. Naughton.

The dendritic architecture has been previously characterized and utilized in CO_2 electrolysis. Here, the structure was given biological utility through the electrodeposition of a conductive polypyrrole film. Capture antibody was electrostatically tethered to this film, creating a biofunctionalized substrate for cholera detection *via* electrochemical ELISA. Its performance was compared to a planar LOC and a standard optical ELISA.

The novel ECC architecture was investigated, and its fabrication was optimized. Electrochemcial performance of the ECC was evaluated relative to a standard set by a previous nanocoaxial iteration (which lacked an extended core). ECCs were then biofunctionalized using protein G to tether capture antibody. An electrochemical ELISA was performed on-chip, and the performance was compared to a standard optical ELISA.

Cholera toxin subunit B was used in this study due to its clinical relevance, stability, safety and availability. However, it is conceivable that the procedures detailed in this thesis could be applied to any biomarker for which antibodies are commercially available.

Chapter 2

Materials and Methods

2.1 Chemicals and Reagents

Cholera toxin subunit B (CTX), ferrocenecarboxylic acid (FCA), ethanol, ethylenediaminetetraacetic acid (EDTA), poly-(2-cyano-ethyl)pyrrole (PCEPy), sodium perchlorate ($NaClO_4$), HEPES, glycerol and H_2SO_4 were purchased from Sigma-Aldrich (St. Louis, MO). Anti-cholera toxin subunit B polyclonal and monoclonal antibodies and alkaline phosphatase (ALP) conjugated antibody were obtained from Abnova (Taipei, Taiwan). p-Aminophenylphosphate (pAPP) was acquired from Gold Biotechnology, Inc. (St. Louis, MO). The BluePhos phosphatase substrate system was purchased from KPL (Gaithersburg, MD). Hydrogen tetrachloroaurate(III) trihydrate ($HAuCl_4$), bovine serum albumin (BSA), Tween-20, phosphate buffered saline (PBS), and Tris base were obtained from Fisher Scientific (Pittsburgh, PA). Protein G was purchased from Protein Mods (Madison, WI). The Innovacoat ® Gold nanoparticle 40 nm conjugation kit was

obtained from Novus Biologicals (Littleton, CO).

Shipley 1813 photoresist, Mf-319 developer, Microposit 1165, LOR-3B resist, and SU-8 were purchased from MicroChem Corp. (Westborough, MA). Transetch-N and Cr 1020 etchants were purchased from the Transene Company, Inc. (Danvers, MA). Epon^{TM} resin 828 and Epikure 3140 curing agent were obtained from Miller-Stephenson Chemical Co. Inc. (Danbury, CT). Hydrogen peroxide (27%) and ammonium hydroxide (28%) were procured from Alfa Aesar (Ward Hill, MA).

2.2 Fabrication of dendritic arrays

Dendritic arrays were fabricated with the guidance of Dr. Nathan T. Nesbitt in collaboration with the laboratory of Dr. Michael J. Naughton as described below.

2.2.1 Preparation of planar substrates

Planar silicon wafers (University Wafers, Boston, MA) were cleaned via sonicaton in acetone for 10 minutes. Using an AJA sputtering system (AJA International, Inc., Scituate, MA), a 10 nm adhesion layer of Ti was deposited, followed by ~120 nm of Au. Samples were diced into 16x30 mm^2 chips using a DAD3220 dicing saw (Disco, USA). Samples were cleaned for 10 minutes prior to well attachment, using a 1:1:5 mixture of hydrogen peroxide (27%), ammonium hydroxide (28%) and diH_2O heated to 80°C, in a procedure called RCA

cleaning (*138*). Chips were then rinsed thoroughly with diH_2O and 200 proof ethanol, and allowed to dry. If chips were to be used as planar controls, wells were attached using the Epon^{TM} resin 828 and Epikure 3140 two part epoxy system (*139*). Plastic wells were made from pipette tips (Denville, USA) with a base area of ~19 mm^2, which were cut to a height of ~1 cm, with the manufactured end attached to the substrate surface to ensure a tight seal. Substrates were placed into a 50°C oven to prevent epoxy from spreading into the sensing region, and allowed to cure overnight.

2.2.2 Directed electrochemical nanowire assembly (DENA)

Gold electrodeposition onto Ti/Au (10 nm/120 nm) coated chips was carried out with a waveform generator (Agilent 33600A Series) using a two-electrode setup (Fig. 2.1). The waveform was monitored with an oscilloscope (Agilent MSO-X 3024A) during electrochemical deposition, using a 10:1 passive probe (Agilent N2863B) to minimize the oscilloscope's disturbance of the waveform. The Au flat film served as the working electrode (WE), and a platinum coiled wire as the counter electrode (CE). A square waveform with frequency of 30 MHz, peak-to-peak amplitude of 10 V, offset of -2 V, and duty cycle of 50% was applied for 20 min in a solution of 30 mM $HAuCl_4$. For dendritic samples, an epoxy-free removable and reusable well system was utilized, to prevent the wicking properties of the dendrites pulling epoxy into the functional sensor area. The reusable well system (Fig. 2.2) creates 7 water-tight sensing arrays, in order to

minimize the effects of dendritic growth differences that are observed chip-to-chip.

FIGURE 2.1: The two electrode setup for DENA. A platinum coil acts as a counter electrode, and the gold surface of the chip acts as the working electrode.

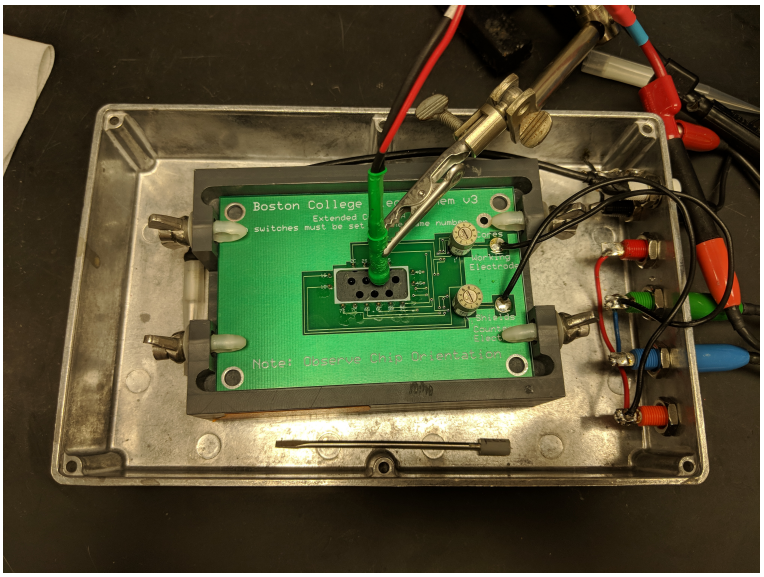

FIGURE 2.2: A removable well system is used to divide each chip into 7 sensing regions. An external CE and RE are inserted into the well of interest, and the chip is hooked up to a potentiostat for electrochemical measurements.

2.3 Fabrication of extended core nanocoaxial arrays

Fabrication of extended core nanocoaxial arrays was generously carried out by Luke D'Imperio in collaboration with the laboratory of Dr. Michael J. Naughton as described below.

2.3.1 Preparation of pillar substrates

Silicon pillar chips 16x30 mm^2 in size were prepared for metal deposition. A 3:1:H_2SO_4:H_2O_2 *piranha* cleaning mixture was prepared (*140*). Briefly, H_2SO_4 was heated to 150°C, and H_2O_2 was added slowly. The Si wafer was submerged in the mixture, and after 20 min it was thoroughly rinsed with diH_2O, and dried with N_2 air.

2.3.2 Photolithography and metal deposition

Before beginning the first round of photolithographic patterning, the Si wafer was plasma cleaned. After, LOR-3B resist was added using a spinner set to ramp to 500 rpm for 8 s, followed by 1,000 rpm for 30 s. The chip was then baked on a hot plate for 5 min at 150°C. Next, Shipley 1813 photoresist was spun on with a ramp of 500 rpm for 8 s followed by 2,000 rpm for 45 s, followed by 5 s at 3,000 rpm. The sample was baked a further 2 min at 110°C, and then exposed for 7.5 s using a Suss mask aligner (SUSS Microtec, Germany). After

exposure, the sample was developed with MF-219 for 50 s, then immediately rinsed with diH_2O and dried with N_2 air. This leaves behind open areas where the first metals should be deposited.

After initial patterning, Ti and Au were sputtered on to a thickness of 10 nm and 110 nm, respectively. Microposit 1165 solution heated to 75°C was then used to lift off the Ti/Au from any areas where photoresist remained over a span of 2 h, leaving behind gold pads and leads.

Atomic layer deposition using a Cambridge ALD machine (Cambridge NanoTech, Waltham, MA) was used to deposit 200 nm of alumina (Al_2O_3). After, an etch-layer mask was applied, and the same photolithographic steps as detailed above were followed. Chips were submerged in Transetch-N for a minimum of 10 h to open up macropads for final metal deposition. After etching, the sample is again washed thoroughly with diH_2O and dried with N_2 air.

Finally, chromium was sputtered on using the AJA system. Cr is deposited to a thickness of 110 nm, and a liftoff process is followed as previously described.

2.3.3 Formation of extended core

Shipley 1813 was spun on at 500 rpm for 5 s, then 1000 rpm for 45 s. The samples were soft baked at 110°C for 3 min following photoresist application.

The sample was exposed on the Suss mask aligner, without any mask, for 1.2 s. The sample was developed in MF-319 for no more than 30 s to expose the top of the Cr layer (Fig. 2.3a). The Cr layer was then etched away using a Cr specific etchant, Cr 1020, for 60-70 s at room temperature. The sample was rinsed with diH_2O and dried with N_2 air, then imaged by scanning electron microscopy (SEM) at a 30° tilt to ensure that the Al_2O_3 layer is exposed (Fig. 2.3b).

Once the Cr layer was confirmed to be etched sufficiently, Transetch-N was used to etch away the Al_2O_3 layer for about 15-20h (Fig. 2.3c).

Finally, the Cr layer is again etched to the desired height, creating an extended gold core. Remaining photoresist is removed with either Microposit 1165 solution, or acetone. The chip is finally rinsed and washed diH_2O and dried with N_2 air.

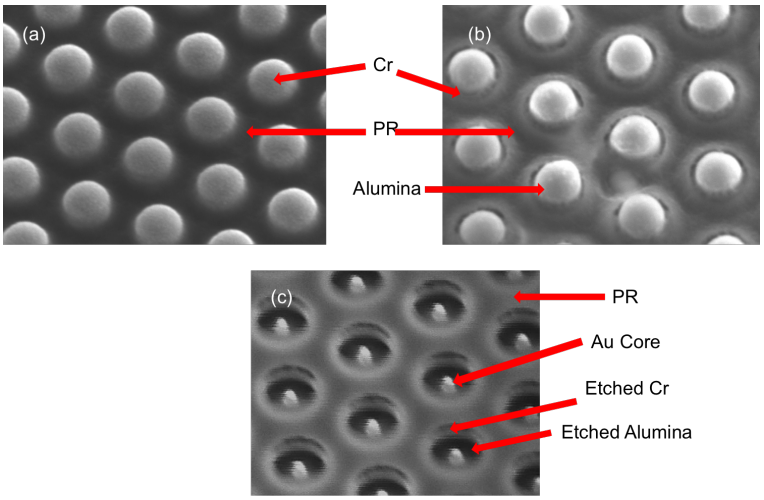

FIGURE 2.3: The extended core of the ECC is fabricated using a series of etching steps. (a) After final deposition of Cr, a layer of photoresist (PR) is added and briefly exposed. Subsequent development uncovers the top of the Cr layer. (b) The Cr layer is etched down to reveal the alumina (Al_2O_3) dielectric layer. This was then also etched (c) to reveal the gold core. A final Cr etching step completes the ECC architecture. (Images courtesy of Luke D'Imperio)

2.4 Characterization of nanostructures

2.4.1 Scanning electron microscopy

All nanostructures were imaged by SEM for appropriate dendritic growth and correct extended core formation, respectively. That is, dendrites should be grown relatively homogeneously over the surface of the electrode, and extended cores should be about 200 nm above the shield. SEM images of ECCs during and post fabrication, as well as all gold nanoparticle images were taken using a JEOL JSM-7001F SEM. SEM images of dendrite arrays were taken using a JEOL JCM-6000 NeoScope benchtop SEM.

Proof-of-concept of the amenability toward biofunctionalization of both dendritic and ECC structures was evaluated *via* SEM using a gold nanoparticle conjugation kit. Anti-mouse IgG/alkaline phosphatase, which acts the final antibody in the ELISA protocol, was conjugated to a 40 nm gold nanoparticle using the kit.

Feasibility of antibody functionalization of ECCs was evaluated using a Protein G monolayer. Thiolated protein G was diluted to 1 mg mL^{-1} in tris buffered saline (TBS), and incubated on chip surfaces for 2 h at room temperature. After rinsing thoroughly 3x in TBST (0.05% Tween-20, 50 mM Tris, 150 mM NaCl, pH 7.4), the anti-mouse IgG, which was tagged with a 40 nm gold nanoparticle, was added to the chips for 1 h at room temperature. Chips were washed 3x in

TBST and allowed to air dry for SEM visualization.

Dendrites were evaluated for the success of antibody tethering to the PCEPy film. The same AuNP-tagged antibody described above was utilized, with the PCEPy film taking the place of the protein G layer. A full ELISA was performed on the chip, up to the application of the tertiary antibody. Chips were then removed from their housings and washed thoroughly in TBS, then allowed to dry for SEM visualization.

2.4.2 Resistivity Measurements

ECC arrays were first tested for electrical integrity using a 610B Electrometer (Kiethley Instruments, Cleavland, OH). Resistance between the working and counter electrodes were measured, and any array with a resistance less than 10^6 Ω was considered to be shorted, and not used.

2.4.3 Ferrocenecarboxylic acid redox sensitivity assay

Sensing capabilities of both ECCs and dendrites were appraised using the redox species ferrocenecarboxylic acid (FCA). Differential pulse voltammetry (DPV) was used to oxidize 1 mM FCA in phosphate buffered saline (PBS), pH 7.4. The potential range was 0 mV to 500 mV (in order to encompass FCA's redox

potential at 300 mV), the potential step was 2 mV, the pulse amplitude was 50 mV, the pulse width was 50 ms, the pulse sample period was 100 ms, and the equilibrium time was 10 s.

2.4.4 Dendrite surface area assessment

To assess the increase in dendritic surface area over a planar control, cyclic voltammetry was performed to sweep across the reduction and oxidation potentials of Au (*141*). Briefly, the working electrode was the Au sample, the reference electrode was Ag/AgCl in saturated KCl solution, and the counter electrode was a Pt wire spiral. A tape mask exposed a geometric surface area of 2 cm^2 of the Au working electrode to the electrolyte. All three electrodes were immersed in 500 mM H_2SO_4. Electrolytes were prepared from pure sulfuric acid and deionized water.

2.5 Electrochemistry

2.5.1 Dendrites

Electrochemical readout on dendritic sensors was performed using a three-electrode system on a Reference 1000 potentiostat (Gamry Instruments, Warminster, PA). The gold surface of the chip functioned as the working electrode (WE). External

Ag/AgCl and Pt wires served as the reference electrode (RE) and counter electrode (CE), respectively (*141*). DPV was used as the method of electrochemical analysis for its suppression of background signal (*142*, *143*).

2.5.2 Extended core coax

Electrochemical readout on the ECC arrays was identical to the dendritic arrays, with the exception that the outer Cr shield of the nanocoax served as the counter electrode. An external Ag/AgCl wire served as the RE. DPV was again used as the method of electrochemical analysis.

2.6 Substrate biofunctionalization

2.6.1 Conductive polymer functionalization

Conductive polymer biofunctionalization was carried out in a 3-electrode system: the gold chip surface served as the WE, an Ag/AgCl wire as the RE, and a Pt wire as the CE. A poly(2-cyano-ethyl)pyrrole (PCEPy) film was formed using 10 mM 2-cyano-ethylpyrrole in 0.1 M $NaClO_4$ (acting as an electrolyte) (*103*). PCEPy was chosen as an antibody tethering substrate for dendritic arrays because it resulted in minimal nonspecific antibody binding.

The pyrrole monomer was electrooxidized with a chronopotentiometric scan at 800 mV for 100 s (*144*). To confirm the generation of a PCEPy coated dendrite

chip, the electrode was washed thoroughly in diH_2O, and an aqueous $NaClO_4$ solution containing no monomer was applied. DPV was performed in a range of 0 to 700 mV. A peak around 400 mV is in good agreement with the oxidation potential of PCEPy (*119*). Primary capture antibody was then incubated on the polymer-coated substrate for 48 h to allow for sufficient electrostatic interaction.

2.6.2 Protein G biofunctionalization

Protein G biofunctionalization was carried out using a thiolated protein G diluted to 1 mg mL^{-1} in TBS (*145*). Cleaned substrates were incubated with protein G for 2 h at room temperature with rocking. Chips were then rinsed thoroughly 3x in TBST, after which primary capture antibody was incubated on the chip surface for 48 h, allowing the antibody to be tethered by its nonantigenic region to the protein G.

2.7 Enzyme-linked immunosorbant assay (ELISA)

2.7.1 On-chip electrochemical ELISA

Modified electrodes (PCEPy or protein G) were incubated for 48 hours at 4°C with a primary anti-cholera toxin antibody diluted to 1 mg ml^{-1} in 10 mM HEPES. After incubation, electrodes were rinsed 3x with TBST, and blocked for 1 hour at room temperature using 5% bovine serum albumin (BSA) and 5% glycerol in

TBST to prevent nonspecific binding to the well or, for PCEPy modified electrodes, to any remaining free cyano sites.

Several concentrations of cholera toxin beta subunit antigen (CTX) were prepared in 2% BSA/TBST, ranging from 0.5 ng mL^{-1} to 500 ng mL^{-1}, and were added to the chip surface and incubated for 1 h at room temperature. The chip was again rinsed 3x with TBST. A secondary anti-cholera toxin antibody was diluted to 50 ng mL^{-1} in 2% BSA/TBST and was added to the chip surface for 1 h at room temperature, after which the surface was washed 3x with TBST.

A final tertiary antibody, anti-mouse IgG conjugated to alkaline phosphatase was added at a concentration of 2.7 μg mL^{-1} for 1 h at room temperature. The chip was washed 6x with TBST. Finally, 1 mM p-aminophenylphosphate (pAPP) was added to the chip surface for 30 min in the dark. The reaction was stopped with 20 μL of 50 mM EDTA in TBS. The 4-aminophenol (4-AP) generated was oxidized directly on the chip surface via DPV in a potential range of -300 mV to 200 mV, with a potential step of 2mV, a pulse amplitude of 50 mV, a pulse width of 50 ms, a sample period of 100 ms, and an equilibrium time of 10 s (*142*).

The chemical reactions taking place are the following:

1. $\mathbf{H_2O + pAPP \longrightarrow 4\,AP + HPO_4^{2-}}$

2. 4 AP $\longrightarrow$ 4 QI + 2 H^+ + 2 e^-

2.7.2 Off-chip electrochemical ELISA

Off-chip electrochemcial ELISA assessments were carried out similarly to on-chip, with the following modifications. A 96-well microtiter plate was used in place of the gold chip surface for tethering of the primary capture antibody. In order to facilitate binding to the plastic microtiter plate, the primary antibody was diluted in 0.1 M $NaHCO_3$ for only 2 h. The plate was then blocked overnight in 5% BSA in TBST. All subsequent reagent application (cholera toxin, secondary antibody, tertiary antibody, and enzyme substrate) and wash steps were performed in the microtiter plate as previously described. The final redox product, 4-AP, was applied to the surface of the nanostructure being examined for electrochemical measurement. DPV settings were as previously described.

2.7.3 Conventional optical ELISA

Optical ELISAs were performed identically to the off-chip ELISA, with the exception that for the last step, the BluePhos phosphatase system took the place of pAPP as the reaction substrate. Absorbance was measured spectroscopically at λ=600nm on a SpectraMax M5 (Molecular Devices, Sunnyvale, CA).

2.8 Data analysis

Titrations of cholera toxin were analyzed by overlapping DVP signals. Any nonspecific peaks were subtracted from all data points. Raw DPV signals were also subtracted to zero at -200 mV to ensure that observed peak currents were accurate (Fig. 2.4). Baselining to zero allows for true comparison of different concentrations of CTX when assessing the performance of devices. Peak current (I_p) for each signal and plotted against CTX concentration to determine detection limits and range of detection.

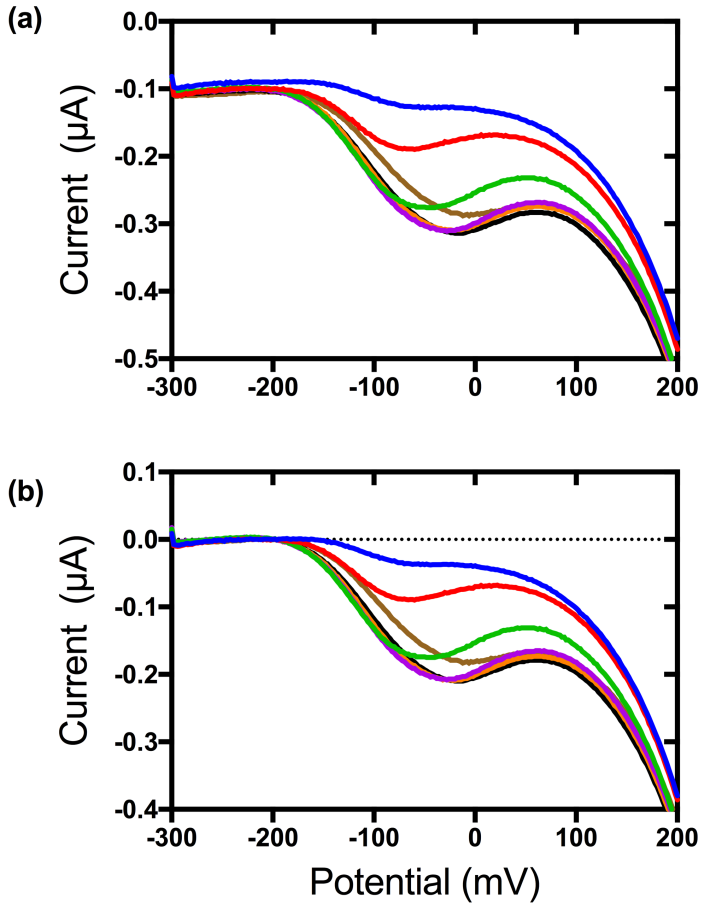

FIGURE 2.4: (a) Raw DPV signals for a titration of alkaline phosphatase (ALP) antibody. (b) DPV signals baselined at -200 mV to assess true peak current

Chapter 3

Gold Dendrites

3.1 Introduction

The importance of POC diagnostic technologies has been highlighted by several recent high-profile infectious disease outbreaks. In 2017, Yemen's cholera epidemic became one of the largest and most rapidly spreading in modern history (*146*). While several factors have contributed to the severity of this and many other outbreaks, such as Ebola, a lack of rapid diagnostic tools and epidemiological monitoring cannot be ignored, as these are critical in controlling the spread of disease within human populations. Fecal culturing remains the benchmark of cholera diagnosis, but this method is a process which is both time-consuming, requiring up to 2 full days for cultures to develop, and necessitates clinical laboratory infrastructure (*14*). A more portable and rapid diagnostic tool exists, the Crystal VC Dipstick, but it suffers from a relatively high rate of false positives (*21*). There remains an unmet need for portable, cost effective detection methods, which exhibit specificity and sensitivity at the POC. Robust POC

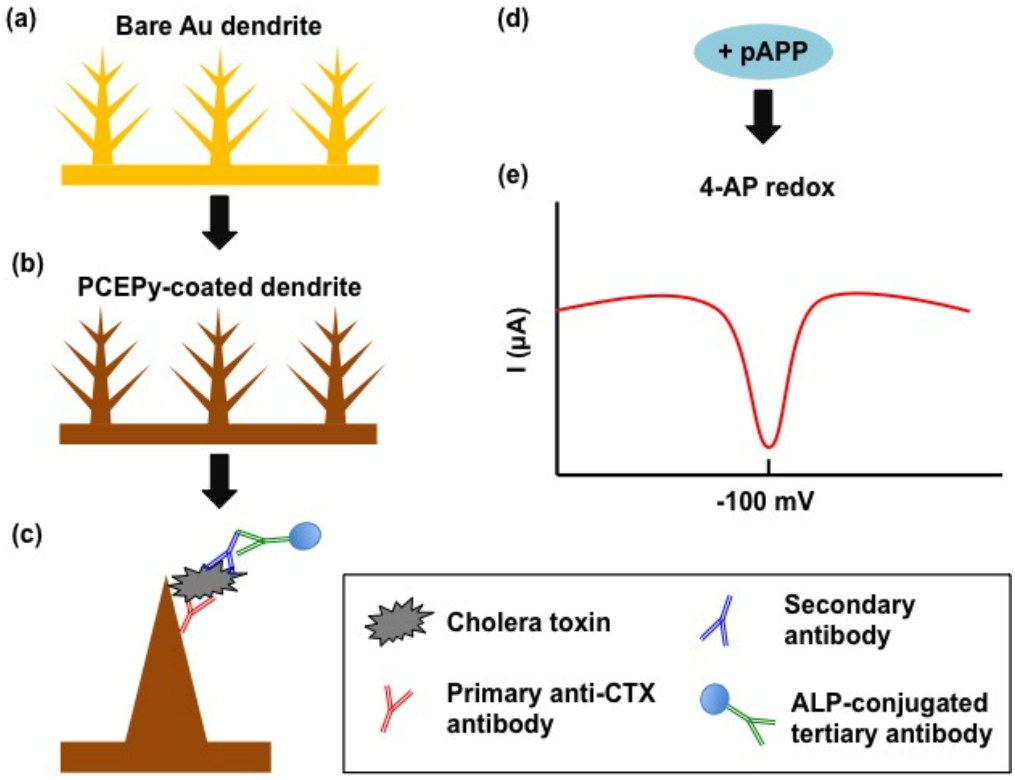

FIGURE 3.1

technologies can facilitate better prevention and earlier response, enabling accurate diagnosis and proper treatment, and thus improved patient prognosis and limited economic impact (*147*). Here, we combined directed electrochemical nanowire assembly (DENA) with a conductive polypyrrole polymer (poly-(2-cyano-ethyl)pyrrole (PCEPy)), which facilitates biofunctionalization of dendrite surfaces, in order to fabricate proof-of-concept electrochemical sensors for the detection of CTX (Figure 3.1).

FIGURE 3.1: A schematic overview of the dendrite-based lab-on-a-chip ELISA. (a) Dendrites grown on a planar gold substrate. (b) Dendrites coated in a film of poly-(2-cyano-ethyl)pyrrole (PCEPy). (c) Primary ELISA antibody tethered to PCEPy coated dendrites *via* electrostatic interactions. Cholera toxin (CTX), secondary anti-CTX antibody, and tertiary antibody are added, with wash steps between each. (d) Alkaline phosphatase (ALP) conjugated to the tertiary antibody reacts with the substrate p-aminophenylphosphate (pAPP) to form 4-aminophenol (4-AP), which (e) redoxes at -100 mV. This redox peak is proportional to the amount of CTX in the sample.

3.1.1 Metallic dendrites as biosensor substrates

Metallic dendrites are an important class of nanostructures for LOC development. They consist of branching, tree-like projections of crystals of a single metal or alloy. Directed electrochemical nanowire assembly (DENA) is a one-step, high growth rate technique to produce oriented, single-crystal metallic dendrites from an electrode surface at standard atmospheric and temperature conditions (*148*). This is accomplished by electrodeposition, where alternating electric field in the presence of a salt solution induces the crystallization of dendrites onto an electrode (*149*). The direction of dendrite growth is guided by the electric field (*150*). The dendritic structures form because of the diffusion limits of electrodeposition. That is, during deposition, only solute that is close to the surface is crystallized. This creates a diffusion boundary layer, as solute near the surface is used up, and new solute must diffuse from the bulk solution to the surface (*141*). Protrusions of the crystal are able to reach into this boundary and receive diffusing solute at a faster rate, creating dendrite structures (*151*).

DENA was first performed for the growth of palladium nanowires (*152*), but has since been used for the fabrication of structures composed of various metallic crystals, such as platinum, gold and silver (*153*–*155*). Gold was chosen in this study due to its biocompatibility and relative inertness.

Dendrites have found use as a substrate for numerous applications, including catalysis (*156*), chemical sensing (*155*), and electrochemical sensing (*157*). This

is due, in part, to an increase in the effective surface area that may afford higher detection sensitivity (*154*). This can be as a result of two features of the sensor: first, a greater number of the biomolecules used as recognition elements for specific antigens can be tethered to the electrode surface compared to a planar substrate of the same footprint area, and second, the increase in surface area means that more biological events are happening in proximity to the working electrode.

On this latter point, the direct positioning of both capture and detection reagents on the surface of an electrode has been exploited to create a highly sensitive diagnostic device for human immunodeficiency virus that was capable of detecting 1 ng mL^{-1} of HIV-1 and HIV-2 (*158*). We speculated that a sensing device based on a dendritic architecture may be capable of highly sensitive biomolecule detection due to both the increased number of recognition elements, as well as the localization of those elements in proximity to the electrode surface. The ability to maintain high sensitivity on a miniaturized electrode also means that a metallic dendrite-based sensor should require a smaller quantity of sensing reagents, decreasing the cost per assay and furthering the goal of A.S.S.U.R.E.D. diagnostics.

3.2 Aim of Study

Here, we used DENA to generate dendritic gold electrodes (Fig. 3.2), which were then modified with a conductive polypyrrole polymer PCEPy. In order to fabricate electrochemical sensors for the detection of CTX as a proof-of-concept LOC biosensor, anti-CTX antibodies were electrostatically tethered to the poylpyrrole film. An ELISA was then performed on the chip surface, and the presence of CTX antigen was determined *via* DPV of the redox product 4-AP. Electrochemical performance of these dendritic sensors was evaluated against a planar gold sensor and a standard optical ELISA to determine its potential for development as a POC diagnostic device.

3.3 Dendrite growth and characterization

Dendritic arrays were fabricated using DENA (Fig. 3.3). A Si wafter was first coated with an adhesion layer of Ti, then ~120 nm of Au. This Au film substrate served as the WE, which was situated across from the platinum wire that served as the CE. These were both submerged in a 30 mM solution of tetrachloroauric acid ($HAuCl_4$). A square waveform with a frequency of 30 MHz, a peak-to-peak amplitude of 10 V, an offset of -2 V, and a duty cycle of 50% was applied for 20 min. A comparison of a planar gold chip before and after dendrite growth is shown in Fig. 3.4 , in order to demonstrate the drastic morphological difference between both architectures. Variations in several parameters, including voltage

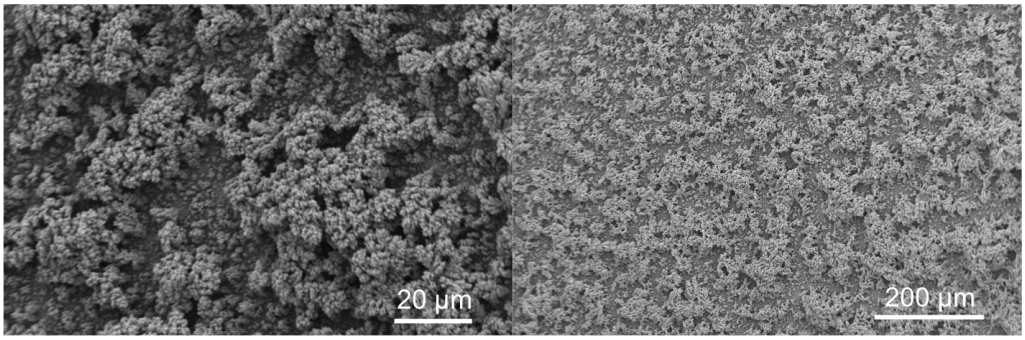

FIGURE 3.2

FIGURE 3.2: SEM of representative dendrite growth on a flat Au film. Dendrites show relatively consistent growth over large parts of the surface. That is, there are not large swaths of dendrite-free substrate, and likewise there are not regions with significantly larger or differently shaped dendrites. Images are shown at 900x (left) and 130X (right) for context.

offset (Fig. 3.5), solution concentration and peak-to-peak amplitude, can greatly impact the morphology of resultant dendrites. Previous work by collaborators has thoroughly characterized the effects of dendrite growth parameters, and so this study did not explore these further (*141*).

Growth parameters for this study were chosen based on consistency in dendrite formation over the area of the chip, and robustness of the crystals (*i.e.* dendrite crystals do not break off the base substrate with handling or with application of fluids). Immediate confirmation of electrodeposition can be initially optically confirmed, as the dendrite region will appear brown and rust-like compared to the bare gold surface. SEM was used to confirm proper fabrication, which was defined as uniform growth of crystals over the sensor surface, inasmuch can be achieved from a random process like crystallization. It should be noted, however, that dendrite growth closer to the bottom edge of submerged chips grew significantly more thin, branching dendrites, which can be explained by the presence of a corner which concentrates electric fields (Fig. 3.6). Exploiting this phenomenon could conceivably be achieved by using a pillared gold array as the substrate as opposed to a flat Au film. However, for the purposes of simplicity in this study, this extra step was not explored.

Individual dendrites demonstrate extensive branched structures that range from tens to hundreds of microns in length, increasing the surface area of the array. The increase in surface area over a planar control was measured by cyclic voltammetry (Fig 3.7a). Analysis was performed on three separate dendrite

chips, all grown following the same parameters described above. Analysis showed the effective dendrite surface area to be approximately 18 times greater than a planar chip of the same base area (Fig. 3.7b). However, the dendrites exhibited more variation in their peak current even though they were produced identically than was observed on planar electrodes. This is likely due to the hierarchical nature of dendrite formation, caused by the mass transport limitations in the crystallization, discussed above (*141*). This means that crystallization happens faster at protrusions that extend into the bulk liquid. Since this is a random process, it can result in differing chip surfaces.

As a baseline assessment of electrical functionality, dendrites were next used to measure the redox of ferrocenecarboxylic acid (FCA). This is done to ensure chips are functional and consistent, *i.e.* little-to-no drop in peak current should be observed from one run to the next on the same sensing region (Fig 3.8). Chips were set up in the three-electrode system previously described. A 1 mM solution of FCA was applied to the chip along with CE and RE wires. Measurements were performed with DPV, chosen as the method for electrochemical analysis due to its suppression of background current and high sensitivity (*159*). DPV was performed in the potential range of 0-500 mV, in order to encompass FCA's oxidation peak which occurs at ~300 mV.

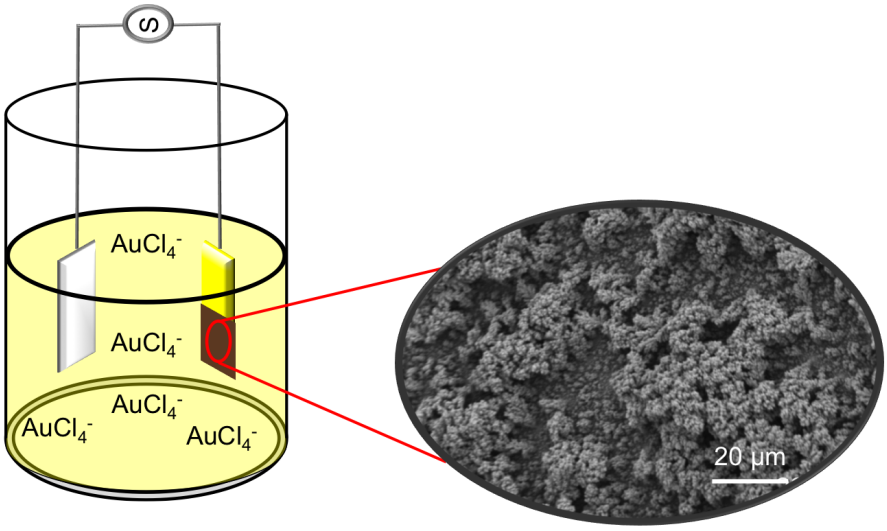

FIGURE 3.3

FIGURE 3.3: Experimental setup for dendritic growth on a planar gold substrate (WE) (right) with a parallel CE (Pt) (left). Dendrite growth is visible as a rust-like area on portions of the WE that are submerged in the $HAuCl_4$. Inset illustrates an example of correctly formed dendrites.

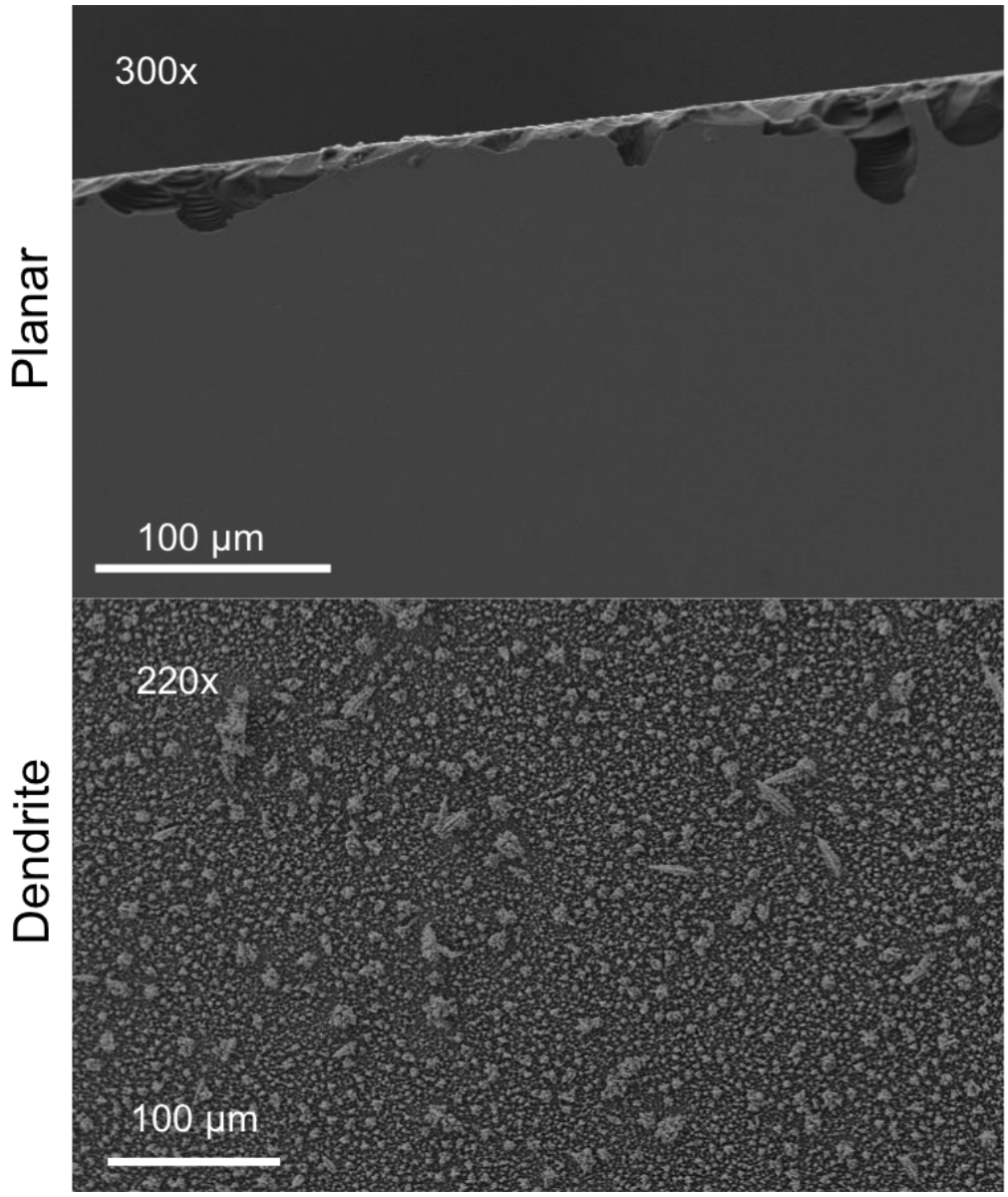

FIGURE 3.4

FIGURE 3.4: SEMs taken at 300 and 220x of a planar chip before and after DENA demonstrate the change in surface architecture. Planar chip was imaged on an edge to aid in visualization, as the planar surface lacks any appreciable features otherwise. Defects on the planar chip are a result of the dicing process.

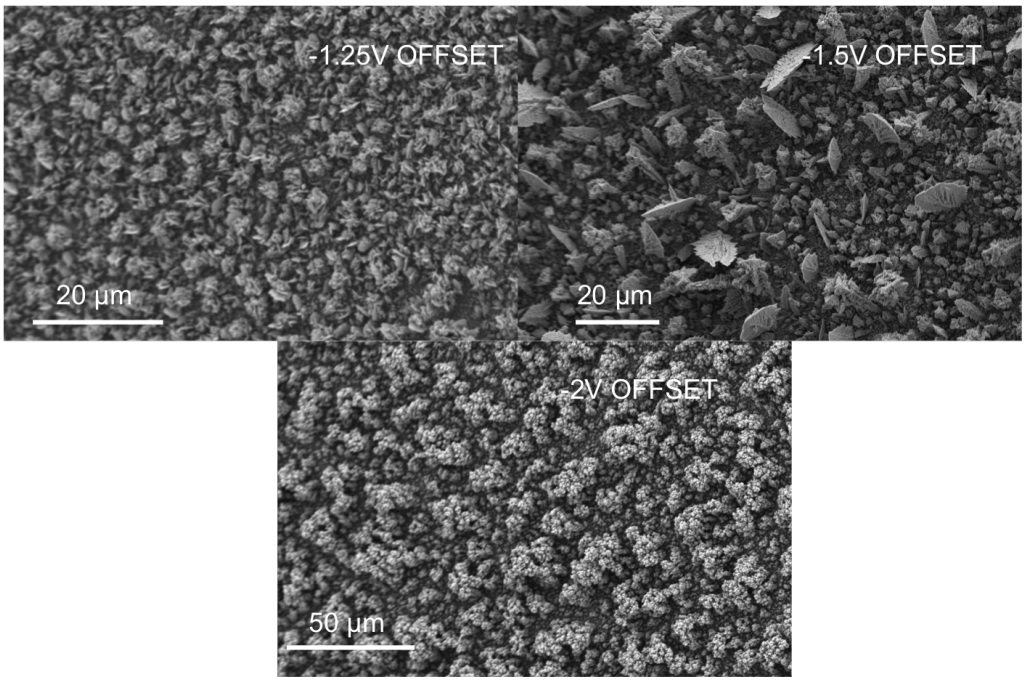

FIGURE 3.5

FIGURE 3.5: SEMs of the effects of varying just one parameter (voltage offset) on the resulting shape of dendrite crystals. Morphology can also be controlled by the length of deposition, solution concentration, and peak-to-peak amplitude, but these parameters were not explored in this study. An offset of -2 V was chosen for use in chips for biofunctionalization.

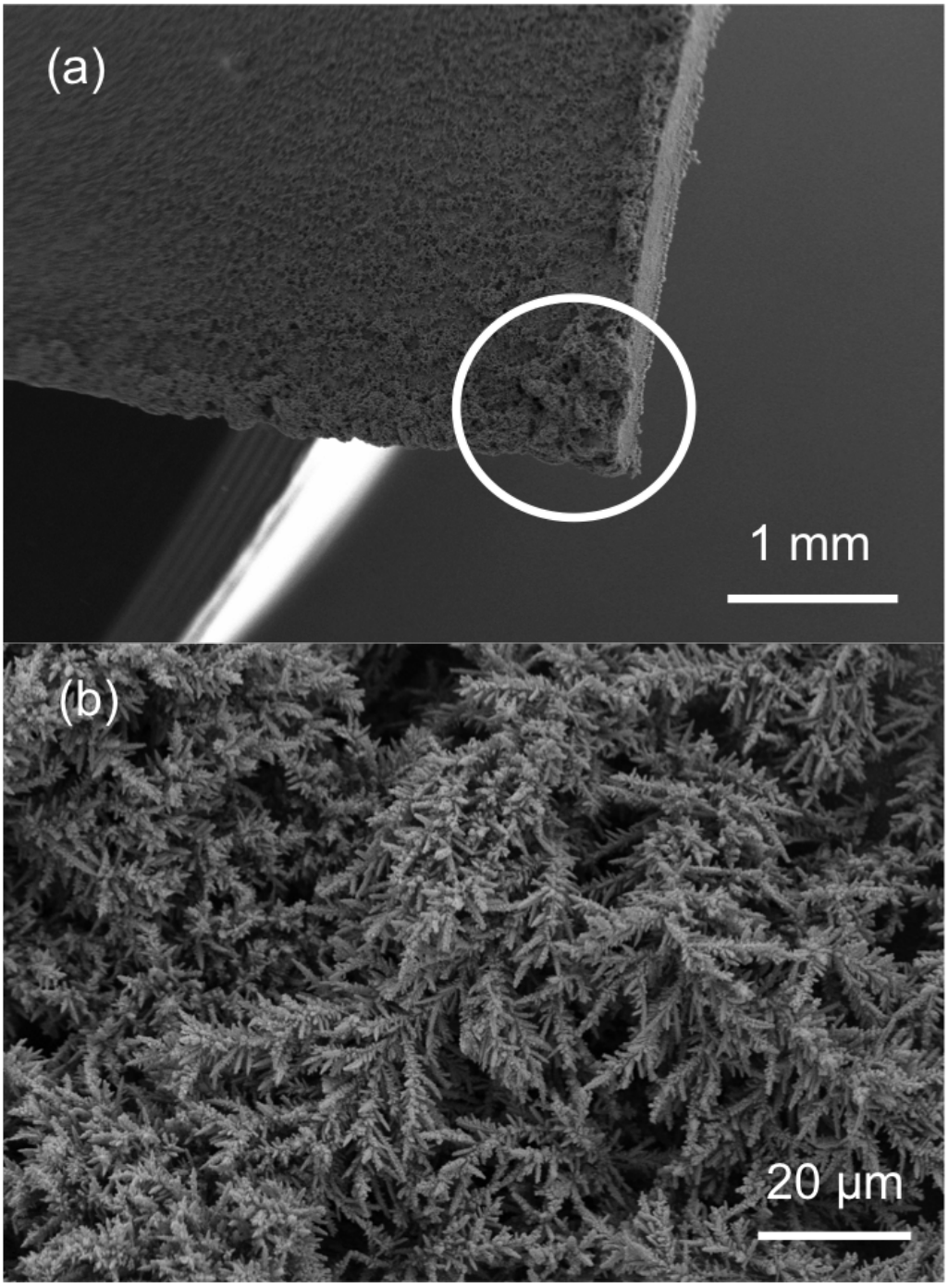

FIGURE 3.6

FIGURE 3.6: SEMs magnified at (a) 22x and (b) 1300x show that the concentration of electric fields at edges can impact the growth of dendrites. A white circle encloses the region of the chip of interest. Here, the bottom edge of the Au film experienced the growth of delicate and thinly branched crystals.

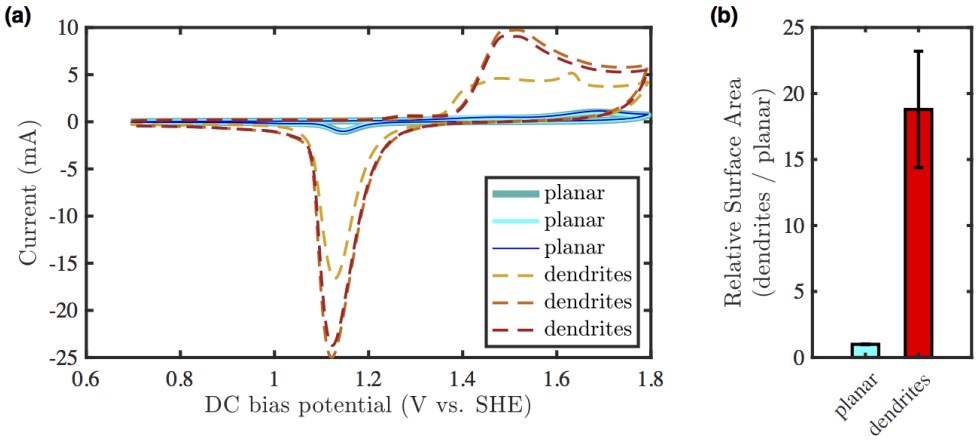
(a)
10
5
0
-5
-10
-15
-20
-25
Current (mA)
0.6
0.8
1
1.2
1.4
1.6
1.8
DC bias potential (V vs. SHE)
planar
planar
planar
dendrites
dendrites
dendrites
(b)
25
20
15
10
5
0
Relative Surface Area
(dendrites / planar)
planar
dendrites

FIGURE 3.7

FIGURE 3.7: Cyclic voltammetry performed on dendrites and planar (flat film) gold to determine differences in surface area. (a) Overlaid CVs of 500 mM sulfuric acid on each nanostructure show the dendrite array has a significantly higher surface area relative to the planar electrode. X axis represents DV bias potential; Y axis represents current. (b) The average relative surface area of 3 of the dendrite chips was calculated by normalizing relative to results from 3 planar electrodes. Scale bars represent the standard deviation.

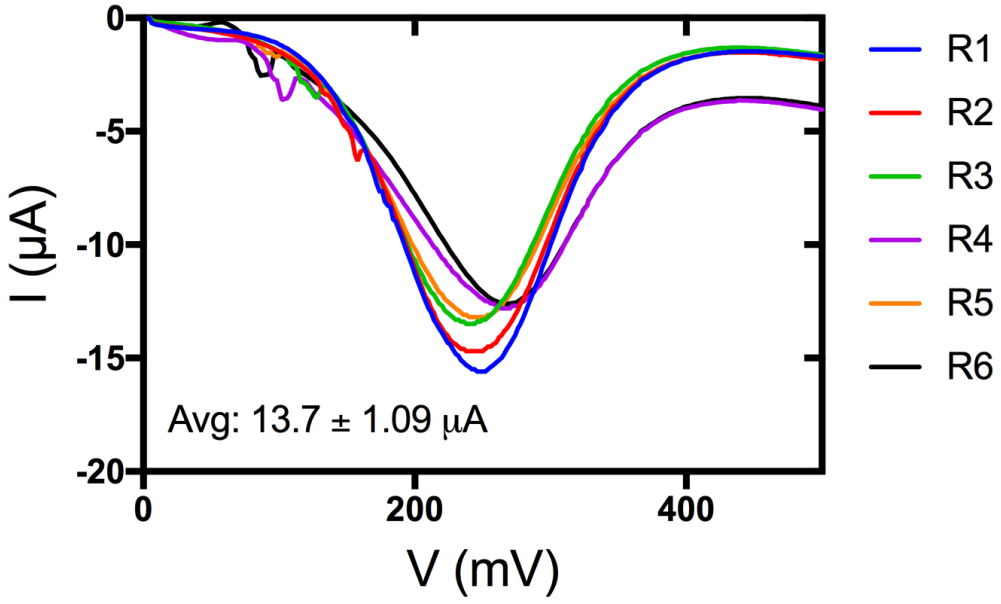

FIGURE 3.8

FIGURE 3.8: Raw FCA oxidation peaks for 6 trials on one dendritic sensing array. Average represents the average peak current achieved in each run, and error is the standard deviation of this peak current.

3.4 Dendrite surface modification

We first attempted to functionalize dendrites with a thiolated protein G, which specifically binds the Fc region of antibodies. Due to the affinity of antibodies to bind to gold, extensive blocking methods proved insufficient to prevent non-specific binding to either the gold electrode or free protein G sites, resulting in large 4-AP redox peaks that were unrelated to analyte concentration (in the μA range, dwarfing true nA sized specific peak currents) (Fig. 3.9). Blocking strategies included the use of BSA, milk, fetal bovine serum (FBS), and a high concentration of nonspecific IgG. None were successful in reliably blocking the gold electrode from binding secondary and tertiary ELISA antibodies. Ultimately, it was speculated that the amount of gold surface area in use was too great to reliably and consistently block, and the strategy of covering the WE with a layer of polymer was conceived.

A galvanostatic method of deposition was first compared against a potentiostatic one on a planar electrode to determine the best method for PCEPy electrogeneration. The galvanostatic deposition was undertaken at 0.25 mA/cm^2 for 2 min in a solution of 10 mM 2-cyano-ethylpyrrole in 0.1 M $NaClO_4$ acting as an electrolyte. For the potentiostatic method, a controlled potential of 800 mV was applied for 100-120 s in the same monomer solution. Generation of a PCEPy film can be confirmed optically, as a change in the electrode surface to a darker brown color (Fig. 3.10a). However, in order to not disturb the electrode surface after PCEPy film generation, wells were not removed until each assay was fully

complete. To assess the success of electrogeneration before biofunctionalization, a DPV of a monomer-free solution of $NaClO_4$ was performed. A peak around -400 mV is indicative of a film of PCEPy. Arrays that did not produce this peak were subjected to a second round of PCEPy deposition. PCEPy oxidation measurements taken on 3 different dendrite chips show that despite variations in dendrite crystal growth, a similar amount of PCEPy is deposited (Fig. 3.10b).

While the galvanostatic method initially seemed more promising, due to well-defined PCEPy oxidation peaks (Fig. 3.11a), this polymer film did not appear to function well for the on-chip ELISA protocol, as evidenced by small, misshapen 4-AP oxidation peaks (Fig. 3.11b). In contrast, the potentiostatic method, while demonstrating broader, less-defined PCEPy oxidation peaks (3.11c), gave much larger and more well defined 4-AP oxidation peaks after an on-chip ELISA (3.11d).

In order to confirm that antibodies tethered to the gold surface were responsible for 4-AP oxidation peaks obtained in an ELISA, and not, for example, antibodies attached to the well (which should be fully blocked), gold nanoparticles were conjugated to the tertiary ELISA antibody. A PCEPy modified electrode was incubated with primary anti-CTX Ab. A high concentration (10 μg $mL^{-}1$) of CTX was applied for 1 h at room temperature, to ensure thorough CTX binding to the capture antibody. A secondary anti-CTX antibody was applied for an hour and washed, followed by the application of the AuNP-tagged tertiary antibody, which was allowed to incubate for 1 h at room temperature. The chip

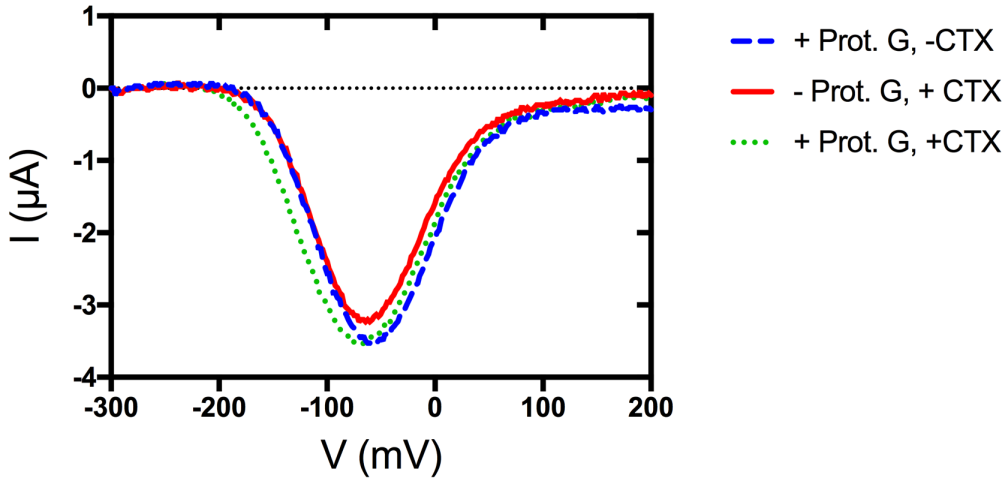
1
0
-1
-2
-3
-4
I (µA)
-300
-200
-100
0
100
200
V (mV)
+ Prot. G, -CTX
- Prot. G, + CTX
+ Prot. G, +CTX

FIGURE 3.9

FIGURE 3.9: Initial studies for on-chip antibody tethering involved the generation of a thiolated protein G self-assembled monolayer on a bare Au substrate. This method resulted in non-specific peak currents that were the same magnitude of specific peaks. This persisted despite the exploration of numerous blocking methods. X axis represents potential; Y axis represents current.

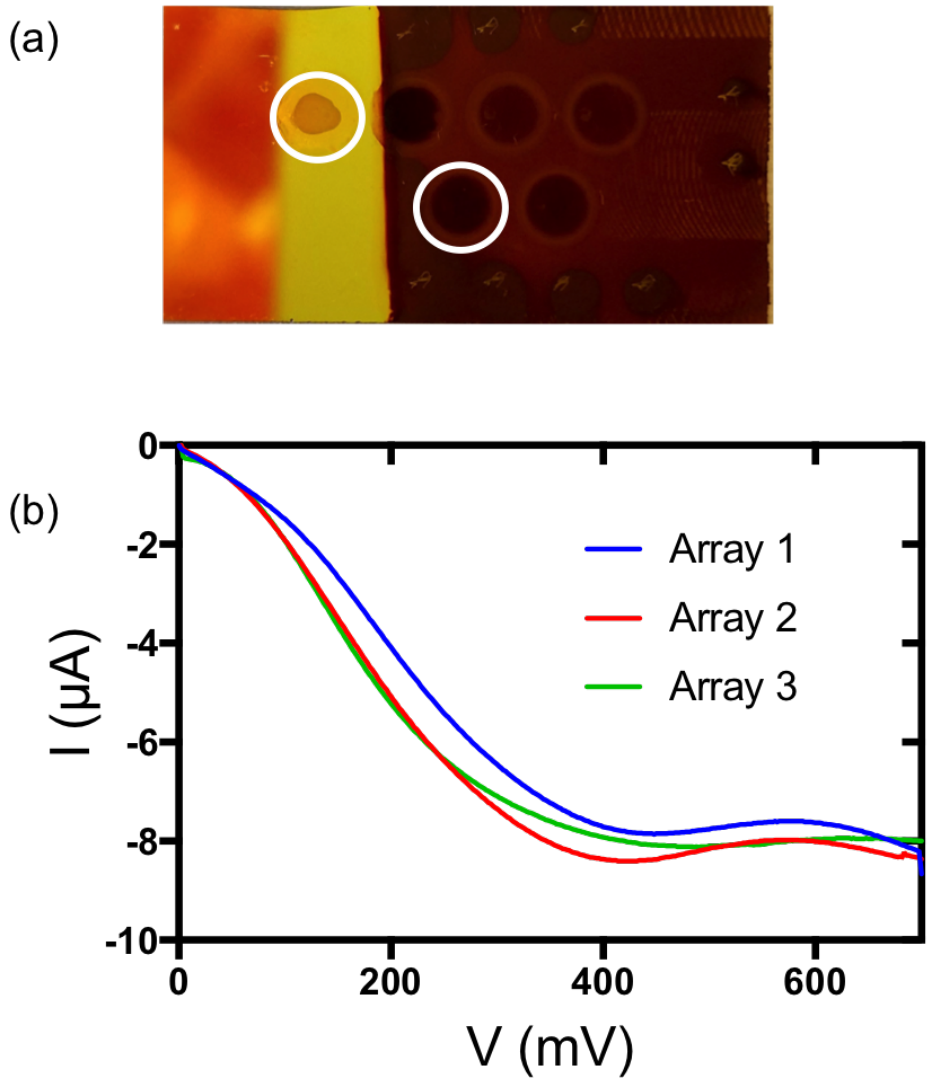

FIGURE 3.10

FIGURE 3.10: (a) Generation of a PCEPy film can be confirmed visually as a change from yellow to brown on bare gold (right) or to a darker shade of brown on dendrites (left). White circles encompass regions of PCEPy deposition. (b) After PCEPy film electrogeneration, a monomer-free aqueous solution of $NaClO_4$ was applied to three separate arrays on the same dendritic chip. A peak around 400 mV is in agreement with published values for the oxidation potential of cyanoethylpyrrole. X axis represents potential; Y axis represents current.

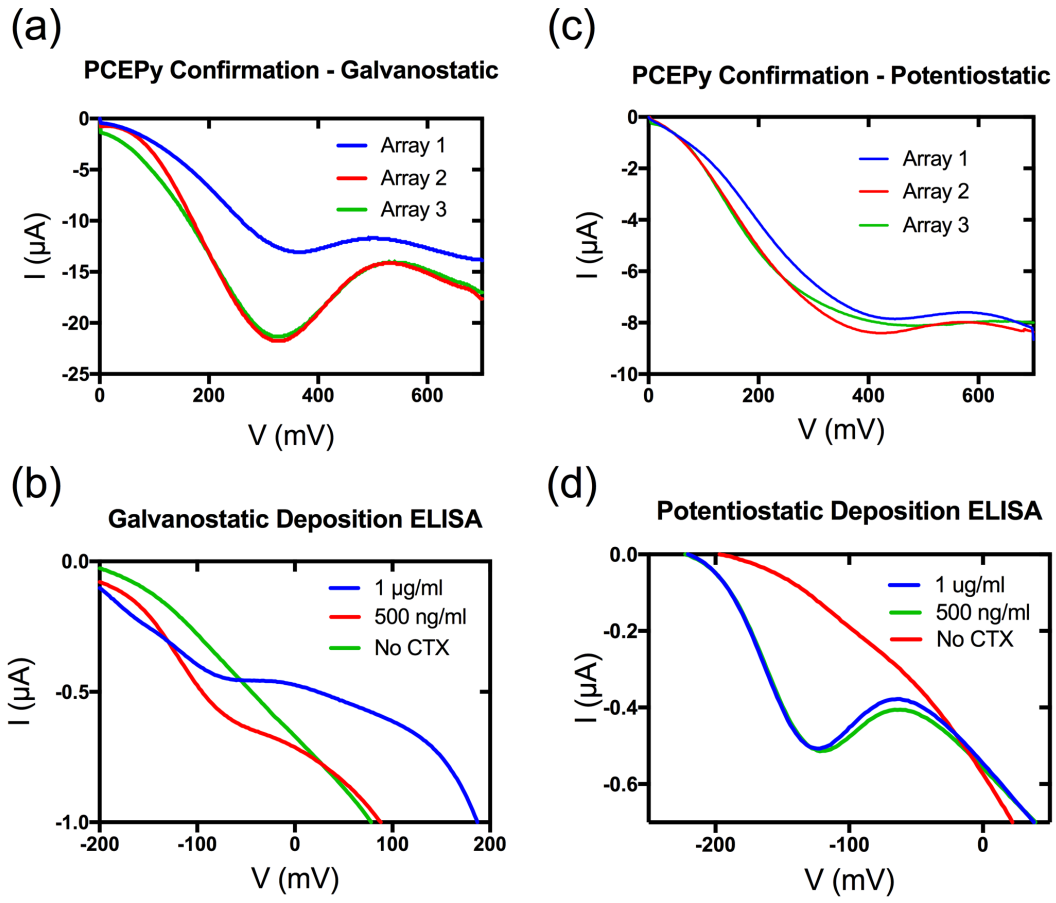
(a)
PCEPy Confirmation - Galvanostatic
Array 1
Array 2
Array 3
I (µA)
V (mV)
(c)
PCEPy Confirmation - Potentiostatic
Array 1
Array 2
Array 3
I (µA)
V (mV)
(b)
Galvanostatic Deposition ELISA
1 µg/ml
500 ng/ml
No CTX
I (µA)
V (mV)
(d)
Potentiostatic Deposition ELISA
1 ug/ml
500 ng/ml
No CTX
I (µA)
V (mV)

FIGURE 3.11

FIGURE 3.11: Electrochemical comparisons of 2 methods of PCEPy electropolymerization on planar Au electrodes. (a) Galvanostatic (constant current) deposition resulted in well-defined PCEPy oxidation peaks, but (b) poorly formed 4-AP redox peaks. (c) A potentiostatic (constant voltage) method gave broader PCEPy oxidation peaks, but (d) much more well-defined 4-AP redox peaks. All X axes represent potential; all Y axes represent current.

was removed from its housing, rinsed thoroughly with TBS and allowed to air dry over night. The chip was then imaged *via* SEM for the presence of nanoparticles ~40 nm in diameter (Fig. 3.12). Positive confirmation of AuNPs on the dendrite surface indicated that all components of the full sandwich ELISA had been successfully tethered to the chip. It is also indicative of the strength of the electrostatic interaction between the primary capture antibody and the PCPEy film, which by the final imaging had undergone 15 washing steps.

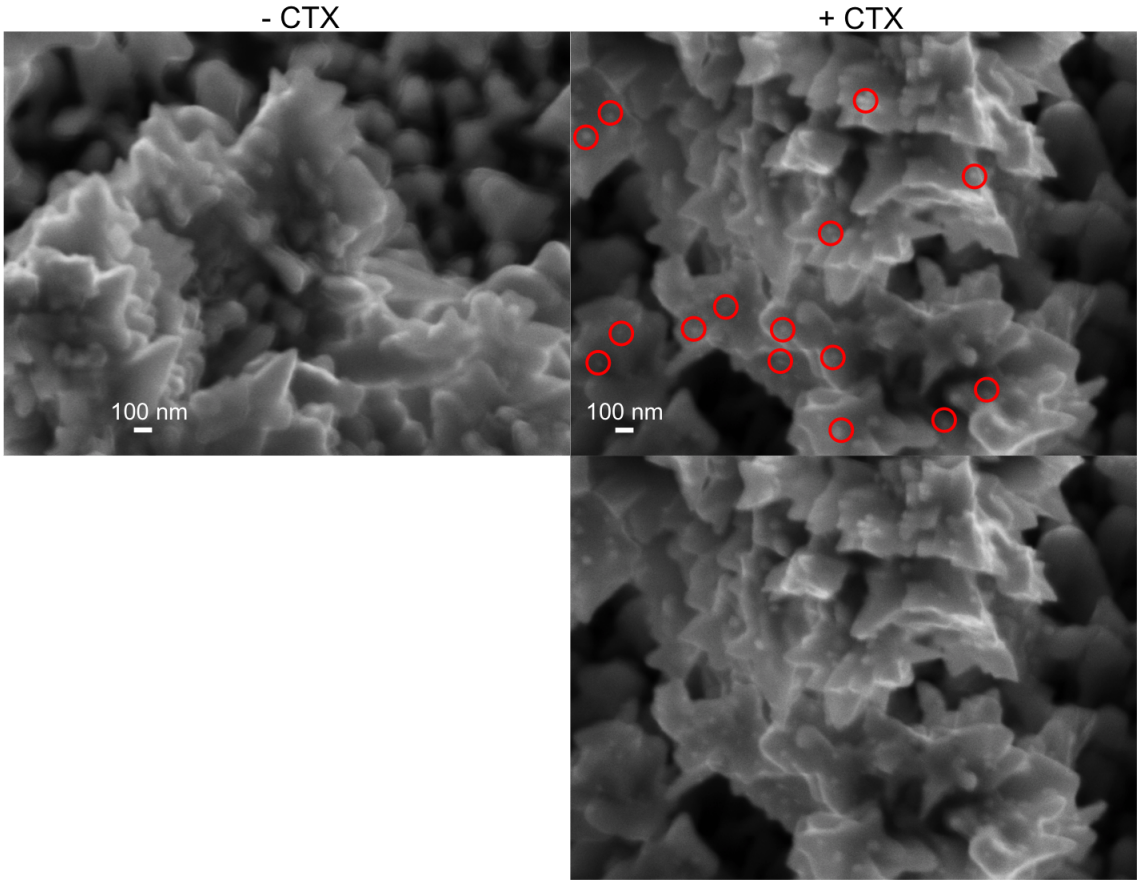

FIGURE 3.12

FIGURE 3.12: 40 nm AuNPs are conjugated to the tertiary ELISA antibody. After the ELISA was performed (+ or - CTX), chips were dried and imaged. Images are magnified at 40,000x. The test condition, +CTX, is shown in duplicate, with red circles enclosing numerous (but not all) gold nanoparticles on the dendrite surface, for better visualization.

3.5 Functionalization for electrochemical sensing

3.5.1 Planar Electrode LOC

Proof-of-concept of a PCEPy facilitated LOC ELISA assay was first examined on a planar gold-coated electrode. This is because a flat Au electrode represents one of the simplest electrode architectures that can be used. More complex architectures, such as dendrites, must justify additional fabrication steps with an improvements in sensing capabilities. Otherwise, if more complex architectures do not confer sensing advantages, there is not any reason to put effort into fabricating them in lieu of a simple planar Au electrode.

A flat Au film electrode was prepared as described previously, with 10 nm Ti and 120 nm Au deposited on a Si wafer. The wafer was then diced into chips 15x15 mm in size. P200 pipette tips were cut to ~1 cm in height. The manufactured end was glued to the chip using a two part epoxy and allowed to cure overnight, creating individual wells (~19 mm^2) on the same chip, isolated from each other (Fig. 3.13).

The planar electrode was coated in a PCEPy film, functionalized with 1 mg mL^{-1} of capture antibody, and then incubated with one of several concentrations of CTX (0.5 ng mL^{-1} - 500 ng mL^{-1}). The ELISA protocol was performed as described previously (*142*). The chip was connected to a Gamry Reference 1000 potentiostat using a three electrode system for analysis. In this method, the 4-AP

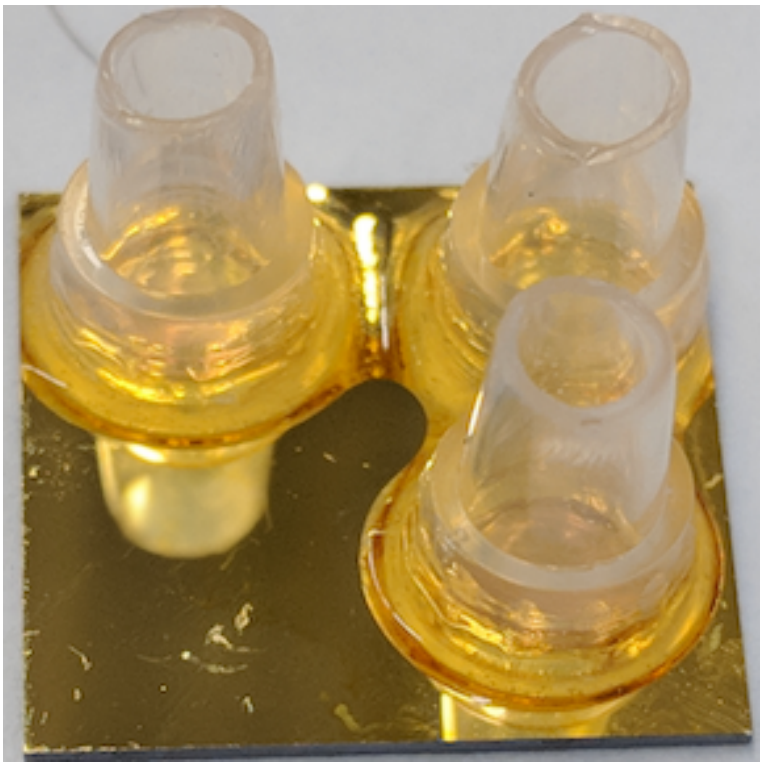

FIGURE 3.13

FIGURE 3.13: A 10 nm/120 nm Ti/Au chip is divided into 3 sensing regions using pipette tips. Tips were adhered to the surface with a 2 part epoxy by their manufactured end to ensure a tight seal. CE and RE wires were inserted into the well, with the gold surface acting as the WE.

generated in the process was oxidized on the same planar gold surface where it was generated, which is a step towards LOC sensing. A representative example titration of different concentrations of CTX detected by the planar gold electrode is shown (Fig. 3.14), where the magnitude of redox peak of 4-AP at -100 mV is proportional to the amount of CTX in the sample. It should be noted that minor deviations from -100 mV are seen for the peak currents, which may be attributed to a slight voltage drift likely caused by the use of a pseudo-reference electrode. Briefly, a pseudo-reference electrode is when an oxide layer is created on a bare silver wire, making it Ag/AgCl. A RE should have a stable and well-known electrode potential, but pseudo-REs experience unstable potentials, which can result in voltage drift (*160*–*162*). It was necessary to use a pseudo-RE in these studies due to the small size of the wells.

An ELISA of each CTX concentration was repeated in triplicate, and the average peak current was plotted against concentration (Fig. 3.15). The lowest detectable concentration of CTX on the planar sensor was 100 ng mL^{-1}, which is not comparable to currently available diagnostic methods such as a standard ELISA, which can detect at 1 ng mL^{-1}.

3.5.2 Dendritic electrode LOC

Given the low sensitivity of the planar chip, the same protocol was then applied to a dendritic gold sensor. We speculated that the increase in surface area afforded by the dendrites would provide a higher sensitivity due to an increase in

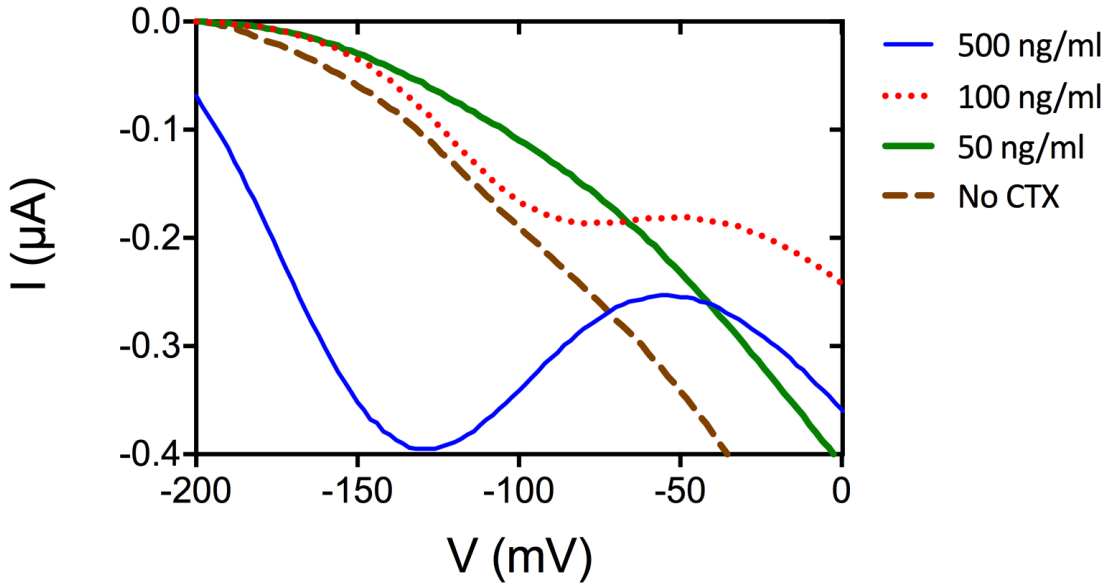
0.0
-0.1
-0.2
-0.3
-0.4
I (µA)
-200
-150
-100
-50
0
V (mV)
500 ng/ml
100 ng/ml
50 ng/ml
No CTX

FIGURE 3.14

FIGURE 3.14: DPV signals from representative CTX dose titrations on planar electrodes. DPVs were baselined at -200 mV to elucidate the true peak current. CTX concentrations ranging from 0.5 ng mL^{-1} to 500 ng mL^{-1} were examined. Note that deviations in peak redox potential from -100 mV were likely due to the use of a pseudo-reference electrode, which may have caused some minor voltage drift. X axis represents potential; Y axis represents current.

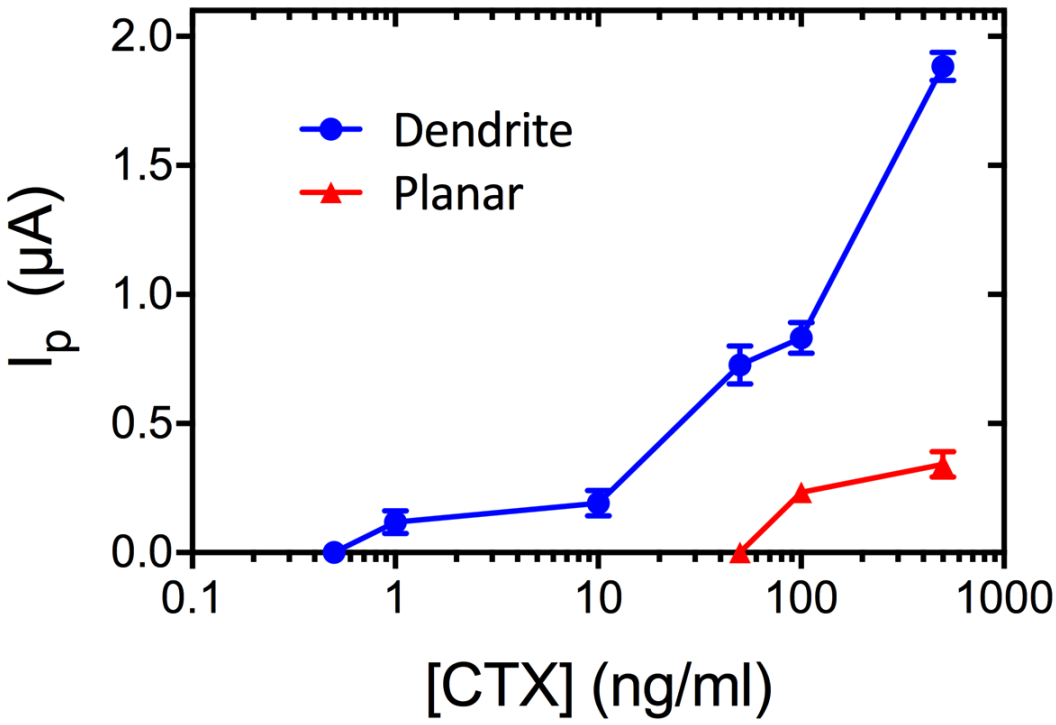

FIGURE 3.15

FIGURE 3.15: Measurements of each concentration of CTX were taken in triplicate. Peak current was plotted against concentration of CTX to compare planar (circle) and dendritic (triangle) sensor performance. Error bars represent the standard deviation in peak current of 3 runs. X axis is CTX concentration; Y axis is peak current.

the number of antibodies tethered near to the chip surface. Removable wells of ~4 mm^2 in area were used, creating 7 sensing regions on an individual chip in order to minimize the effects of surface area variability that we have previously observed (see Fig. 3.7). To ensure that the PCEPy coating did not drastically negatively affect the sensing capacity of the dendrites, FCA measurements were taken pre- and post-PCPEPy modification. As shown in Fig 3.16, while the PCEPy coating does augment both the peak current and the shape of the oxidation peak to a certain degree, the chip is still functional, and the redox peak is still present and prominent. This indicates that the PCEPy coated chips can be used for the on-chip ELISA with theoretically very little deterioration in signal resulting from the polymer film.

Again, sensing regions were connected to a potentiostat, with a CE and RE dipped into the well of interest for measurement. DPV signals from CTX dose titrations (0.5 ng mL^{-1} – 500 ng mL^{-1}) were measured, with a representative titration curve shown in Fig. 3.17. Measurements were performed in triplicate, both on different chips and on different arrays on the same chip. Peak current data was aggregated, as was shown in Fig. 3.15. Despite the known variability within and between dendrite chips which results from the random nature of the crystallization, peak currents for the ELISA were not highly variable. Additionally, the dendritic ELISA-on-chip assay achieved a higher sensitivity than its planar counterpart, detecting at 1 ng mL^{-1} of CTX over a smaller footprint (~4 mm^2 *vs.* ~19 mm^2), with a signal-to-noise ratio of 2.6 for this lowest concentration.

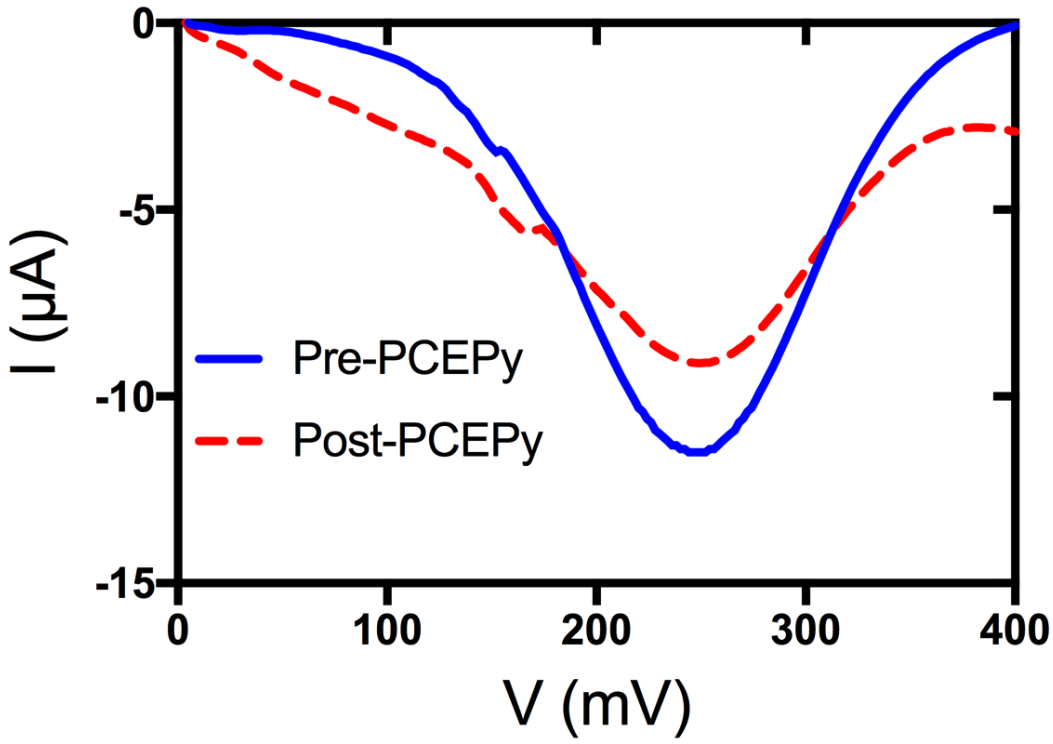

FIGURE 3.16

FIGURE 3.16: FCA measurements were taken before and after modifying a dendritic electrode with a PCEPy film. The coating did not affect the oxidation potential, and only minimally affected the peak current magnitude. X axis represents potential; Y axis represents current.

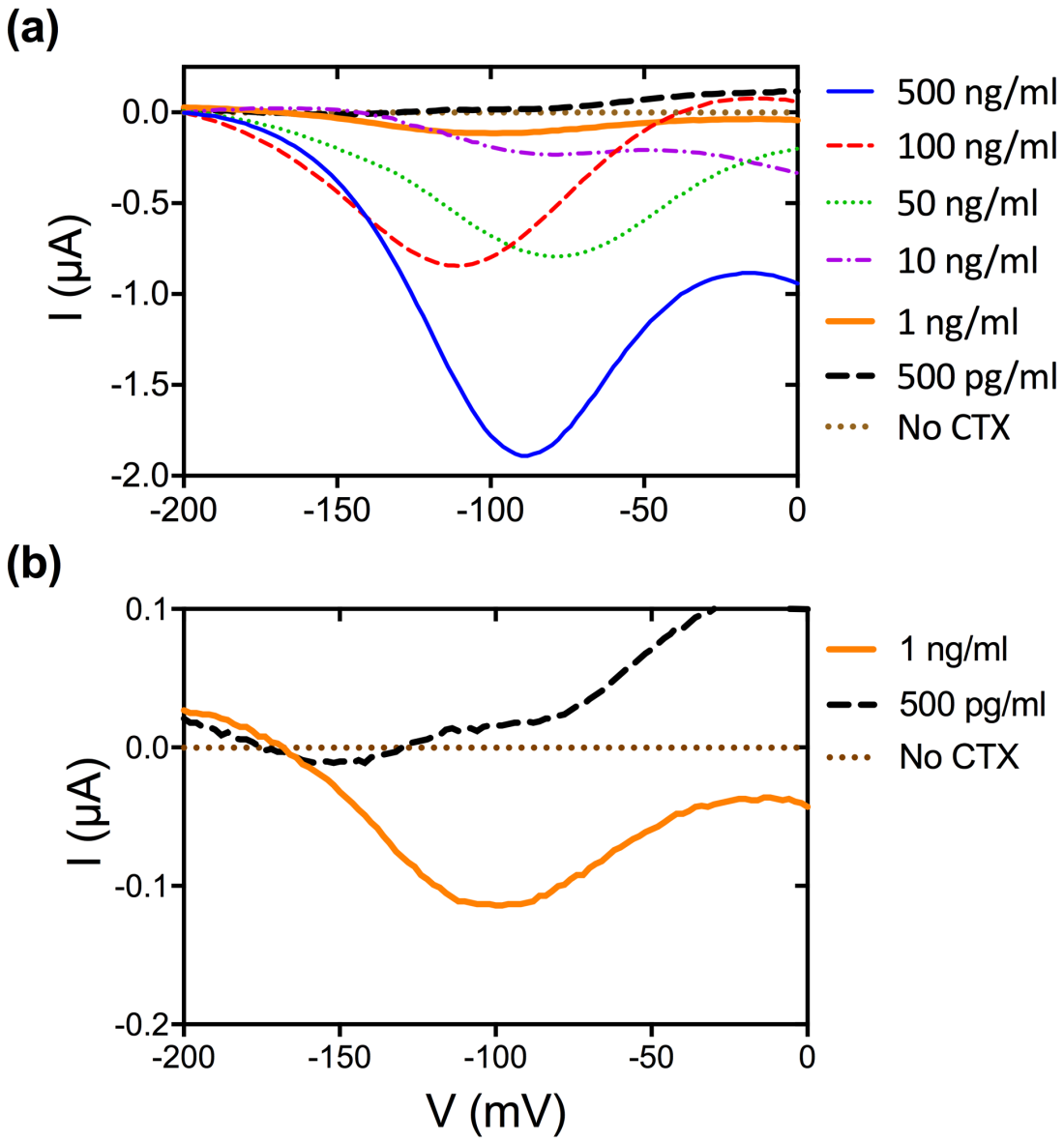
(a)
0.0
-0.5
-1.0
-1.5
-2.0
I (μA)
-200
-150
-100
-50
0
500 ng/ml
100 ng/ml
50 ng/ml
10 ng/ml
1 ng/ml
500 pg/ml
No CTX
(b)
0.1
0.0
-0.1
-0.2
I (μA)
-200
-150
-100
-50
0
V (mV)
1 ng/ml
500 pg/ml
No CTX

FIGURE 3.17

FIGURE 3.17: DPV signals from representative CTX dose titrations on dendritic electrodes. DPVs were baselined at -200 mV to elucidate the true peak current. (a) CTX concentrations ranging from 0.5 ng mL^{-1} to 500 ng mL^{-1} were examined. Note that deviations in peak redox potential from -100 mV were likely due to the use of a pseudo-reference electrode, which may have caused some minor voltage drift. (b) Low concentrations are shown separately to better illustrate the 4-AP redox peak at 1 μ g/ml. X axis represents potential; Y axis represents current.

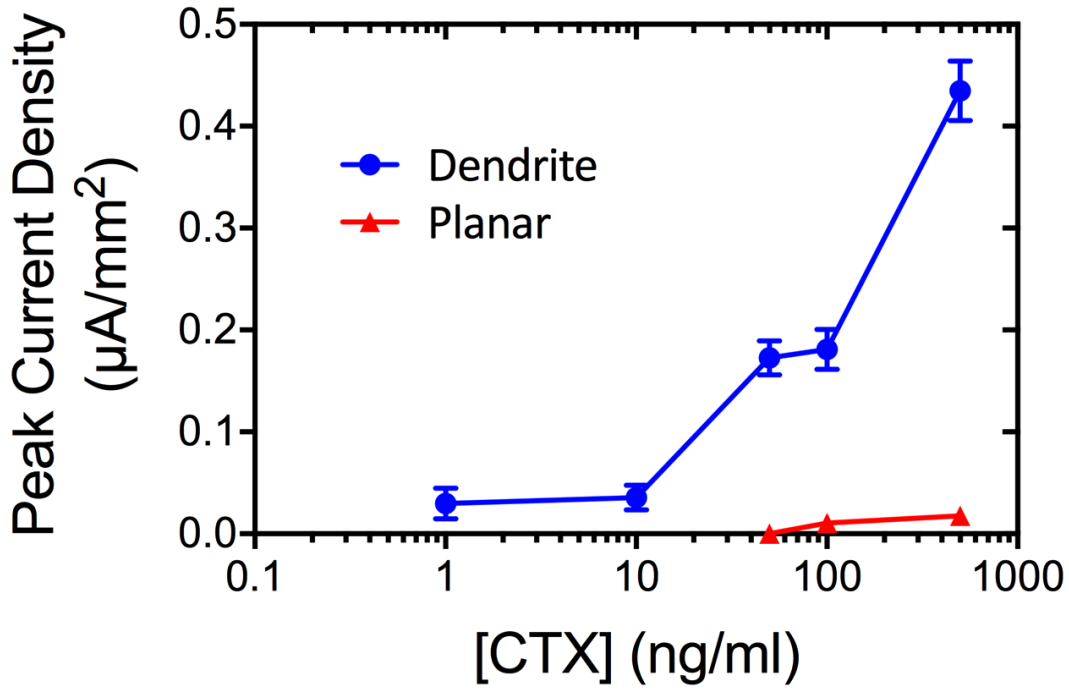
Peak Current Density
(μA/mm²)
0.5
0.4
0.3
0.2
0.1
0.0
Dendrite
Planar
0.1
1
10
100
1000
[CTX] (ng/ml)

FIGURE 3.18

FIGURE 3.18: Current density was used as a measure of the true sensing improvement afforded by the dendritic chips. Peak current was divided by the footprint area of the sensing region of each chip, and plotted against the concentration of CTX. Dendrite (circle) peak current density was compared against planar (triangle). Error bars represent standard deviation of the peak current of 3 tests. X axis is CTX concentration; Y axis is peak current density.

To normalize by footprint surface area, current density was used as a final means of comparing the planar and dendritic sensors (Fig. 3.18). Current density is the peak current at a specific concentration, divided by the footprint of the sensing region. The superiority of the dendritic array is better highlighted in this comparison, with dendrites on average demonstrating 18-25 times the current density of planar gold. This is in good agreement with the increase in surface area demonstrated in Fig. 3.7. Additionally, enhanced electric fields at sharp corners, of which the dendrites have many, may also be responsible for some of the increase in performance over the planar electrode.

Optical ELISAs remain one of the best methods of specifically and sensitively identifying cholera cases. Thus, the electrochemical performance of the dendrites was finally compared against the sensitivity of a standard optical ELISA using the same series of antibodies (Fig. 3.19). The dendritic LOC ELISA and a standard optical ELISA both demonstrate a limit of detection of 1 ng mL^{-1} of cholera toxin. However, the dendritic array affords several advantages over a full optical ELISA, which make it more amenable to POC use. The optical ELISA is not highly portable, and requires laboratory infrastructure. So while highly sensitive and specific, it is a test not available to most people affected by cholera infections.

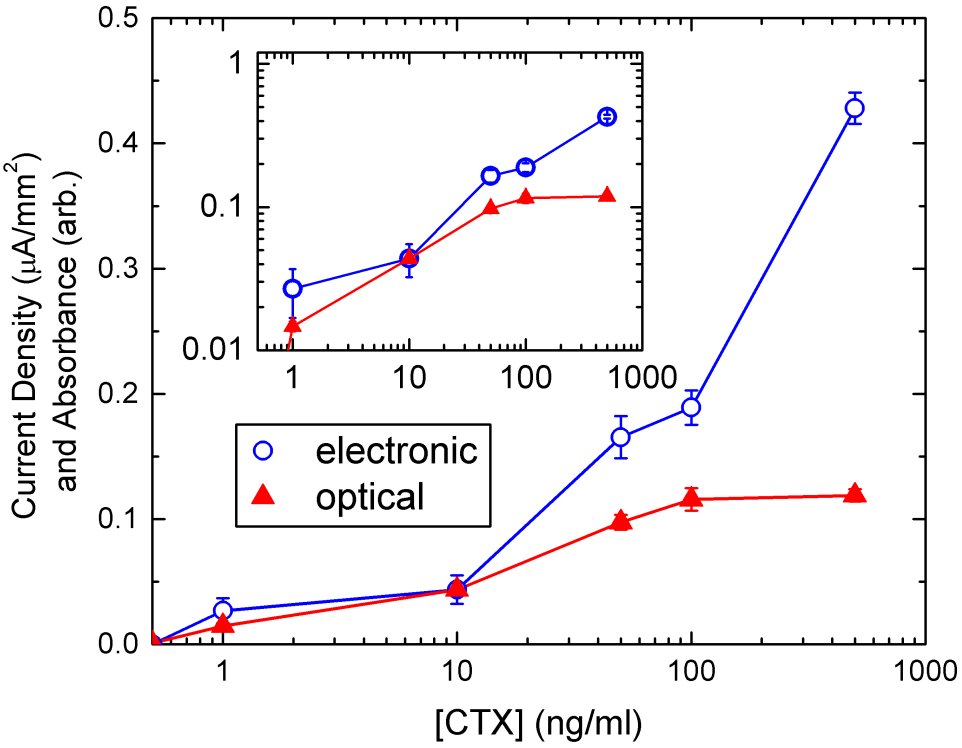
Current Density (μA/mm²)
and Absorbance (arb.)
[CTX] (ng/ml)
electronic
optical
0.0
0.1
0.2
0.3
0.4
0.5
1
10
100
1000
0.01
0.1
1

FIGURE 3.19

FIGURE 3.19: A log-linear (inset: log-log) comparison of dendrite LOC performance (circle) and a standard optical ELISA (triangle). Error bars represent the standard deviation of 3 trials for each CTX concentration on each platform. X axis is CTX concentration; Y axis is peak current density (dendrites) or absorbance at λ=600 nm (optical).

3.6 Future directions

This novel biosensing platform is able to exceed the sensitivity of a simpler planar electrode, and is able to match the diagnostic sensitivity of a standard optical ELISA. However, in its current iteration, the washing and reagent application steps would not be ideal for POC use. Further work dictates the development a microfluidic chip housing, as well as software to interpret electrochemical results for the end user.

Additionally, more extensive and controlled dendritic growth may be achieved using a pillared gold substrate, rather than a planar one. Previous work has shown that in this setup, dendrites will grow out from the sharp pillar tip (Fig. 3.20). Better control of dendrite growth may result in a more finely tuned chip, with less variability from sample to sample.

It should also be noted that the method of tethering the antibodies to the surface is *via* electrostatic interactions, which are susceptible to changes in pH. To overcome issues caused by the pH of a sample, other conductive polymers should be explored, especially those which can be modified in order to create covalent bonds with biomolecules (*163*). This would include polymers with terminal reactive groups like NH_3 and COOH. For example, Hernandez, *et. al.* deposited a pyrrole film onto glassy-carbon electrodes, which they then functionalized to include nitro groups, which were later reduced to amine groups. A carbodiimide reaction linked their protein of interest to the amine group via carboxyl

functionalities on surface amino acids (*116*). Others have used polypyrrole films functionalized with avadin, which were able to tether biotinylated antibodies to the surface (*144*). While both methods will create a more stable bond than the electrostatic interactions utilized in the study undertaken in this thesis, they also represent additional preparation steps. Increases in fabrication complexity must be justified with increases in POC functionality, but it is an avenue worth exploring, especially for its potential to decrease primary antibody incubation time (which is currently 48 hours for electrostatic interactions).

Moving forward, applications of this LOC setup are not limited to cholera detection. Any biomarker for which there are effective antibodies commercially available could be conceivably detected using this protocol. Further work may include examining its efficacy in detecting other infectious disease biomarkers, such as lipoarabinomannan, a putative biomarker for tuberculosis (*164*), or perhaps for biomarkers of some cancers (*157*, *165*).

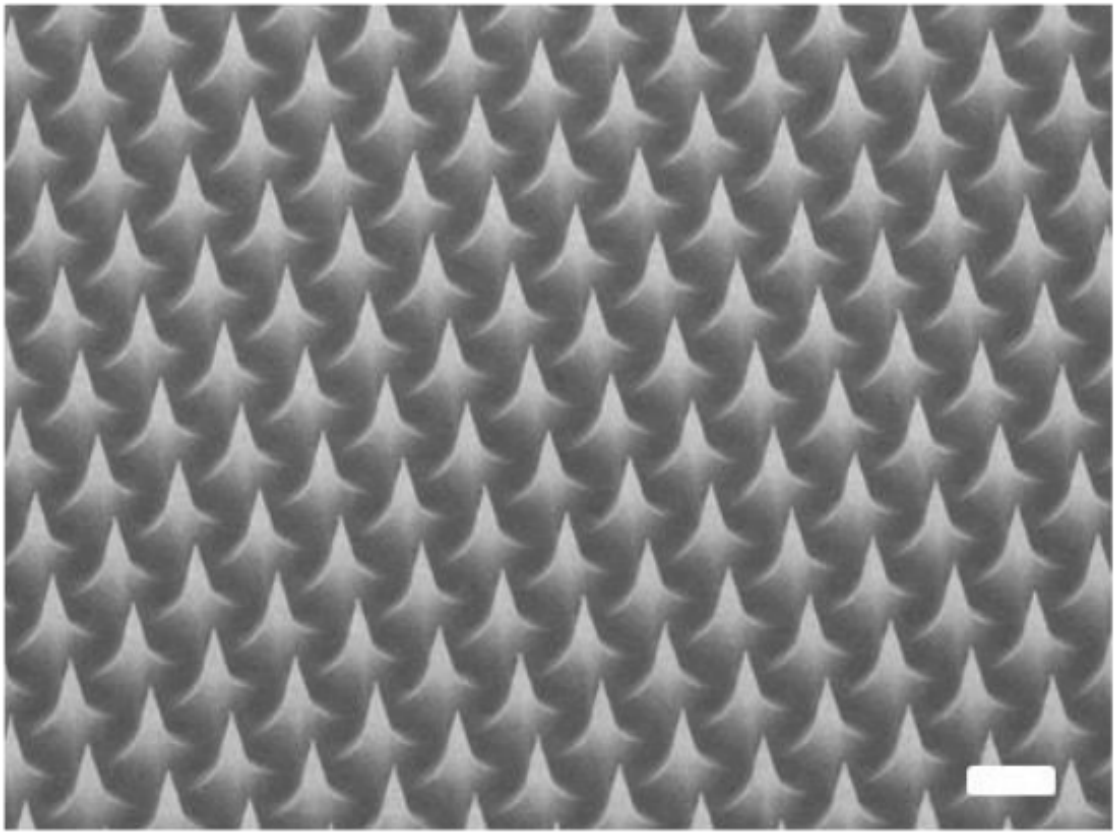

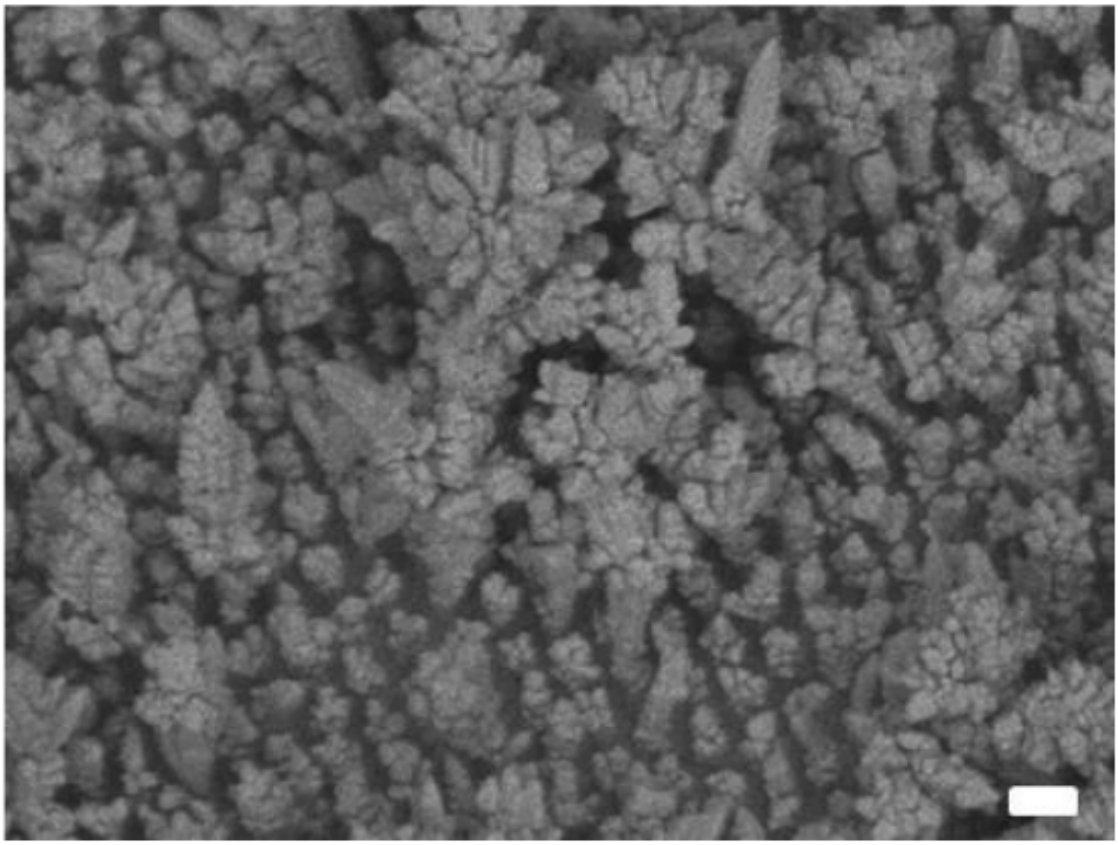

FIGURE 3.20: Dendrites grown on a pillared gold substrate. Scale bar represents 1 μm. Dendrites grow preferentially from the tip of the sharp Au pillars. Image adapted from reference (**archibald_novel_nodate**).

3.7 Summary

Utilizing DENA, gold dendrites grown from a planar gold substrate were fabricated. These dendritic gold sensors demonstrated ~18x the surface area of a planar gold electrode of the same footprint. It was speculated that this increase in surface area would result in a better sensing device, especially for the development of a LOC, where all sensing reagents would be tethered in proximity to the electrode surface.

To facilitate tethering of recognition elements to the sensor, the gold surface was modified with a conductive polypyrrole film. This polymer was able to electrostatically interact with OH groups on the primary capture antibody for a sandwich ELISA. A full ELISA was then completed on-chip, and the resulting redox product, 4-AP, was oxidized to give a peak proportional to the amount of analyte in the sample. Dendrites demonstrated a sensitivity 2 orders of magnitude greater than a planar counterpart. Thus, additional fabrication steps necessary to create a dendritic sensor are justified.

To demonstrate the real-world utility of the dendrite sensor, its performance was also compared against a standard optical ELISA. The dendrites were able to match the sensitivity of this assay (1 ng mL^{-1}). This is important as it shows that decreasing the sensing area did not result in a loss of sensitivity.

This dendritic sensor holds the potential to meet the A.S.S.U.R.E.D. diagnostic demands of low cost, portability, and user-friendliness, while still maintaining the sensitivity and specificity afforded by a standard ELISA. It is therefore a viable substrate for further development into a LOC device, for real-world utility in POC diagnosis.

Chapter 4

Extended Core Nanocoax

4.1 Introduction

Lab-on-a-chip electrochemical biosensing is limited largely by a lack of appropriate surface architectures. Signal transduction and overall sensor performance is dictated by the electrode design, and so simplistic structures such as planar gold may not be sufficient to maintain high sensitivity when the platform is miniaturized (*68*, *166*, *167*). One strategy to overcome this limitation, as discussed in chapter 3, is to simply increase surface area, thereby increasing the number of biological events happening in proximity to the electrode. An alternative and perhaps more promising strategy involves decreasing the gap between electrodes to the nanoscale, termed nanogap electrodes (*168*, *169*). Nanogap electrodes display significantly different behavior compared to their macroscopic counterparts, which can afford advantages in an ultrasensitive sensing capacity, such as increased redox cycling (discussed in section 4.4.2) (*127*, *170*, *171*).

A nanogap-based surface architecture, the nanocoax, was previously reported which was able to both transmit visible light (*172*, *173*), and detect volatile organic compounds (VOCs) (*174*). This nanocoaxial architecture has also been used as an optrode for neurophysiology (*175*). Given the high sensitivity demonstrated by the coaxes, it was theorized that they may also hold promise as a platform for biosensing. Indeed, a first-generation nanocoax (Fig. 4.1), fabricated using a facile nanoimprint lithography (NIL) process, was utilized for proof-of-concept cholera detection using an off-chip strategy. This first generation nanocoax was limited in true LOC utility because the nanoscale gap between the working and counter electrodes did not allow for biofunctionalization of the gold core. This was due to difficulties with reagent transport to the electrode surface, likely caused by surface tension that was observed with increasingly smaller nanogaps (**archibald_novel_nodate**). Additionally, once a reagent was applied to the this sensing platform, it was extremely difficult, if not impossible, to remove without the use of ethanol. For LOC, ethanol washing would disrupt the biofunctionalized surface, meaning that this architecture was not well-suited to further development as a POC diagnostic device. In order to overcome this limitation, the gold core of the nanocoax was extended above the chrome shield. This retains the nanocoaxial architecture with nanoscale proximity of the electrodes, but also creates an unobstructed WE gold surface for biofunctionalization which allows for simple reagent exchange. This new generation of nanocoax was called the extended core coax (ECC) (Fig. 4.2). We believe that these features will allow not only for true LOC detection, but will also be amenable to the creation of user-friendly POC flow-through devices, since reagent entry into the

nanogap is not necessary.

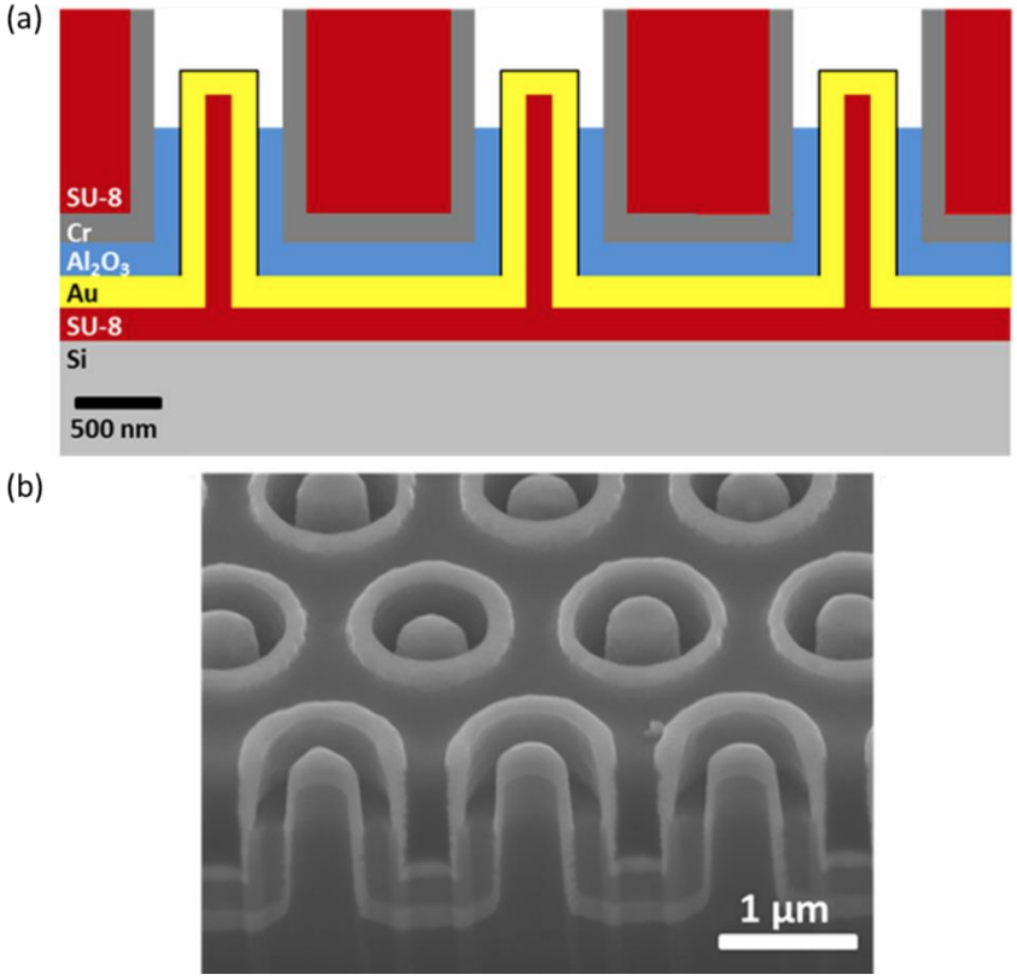

FIGURE 4.1

FIGURE 4.1: (a) A schematic representation of a first generation nanocoax (non-ECC), which was fabricated *via* a nanoimprint lithography process which created SU-8 pillars (red), followed by metal deposition steps (Gold (Au): yellow; alumina (Al_2O_3): blue; chrome (Cr): gray). The WE of the first generation was nested within the CE, with a nanoscale gap separating them. (b) A cross-section of nanocoaxes imaged by SEM, which shows all metal layers. Image from reference (**archibald_novel_nodate**)

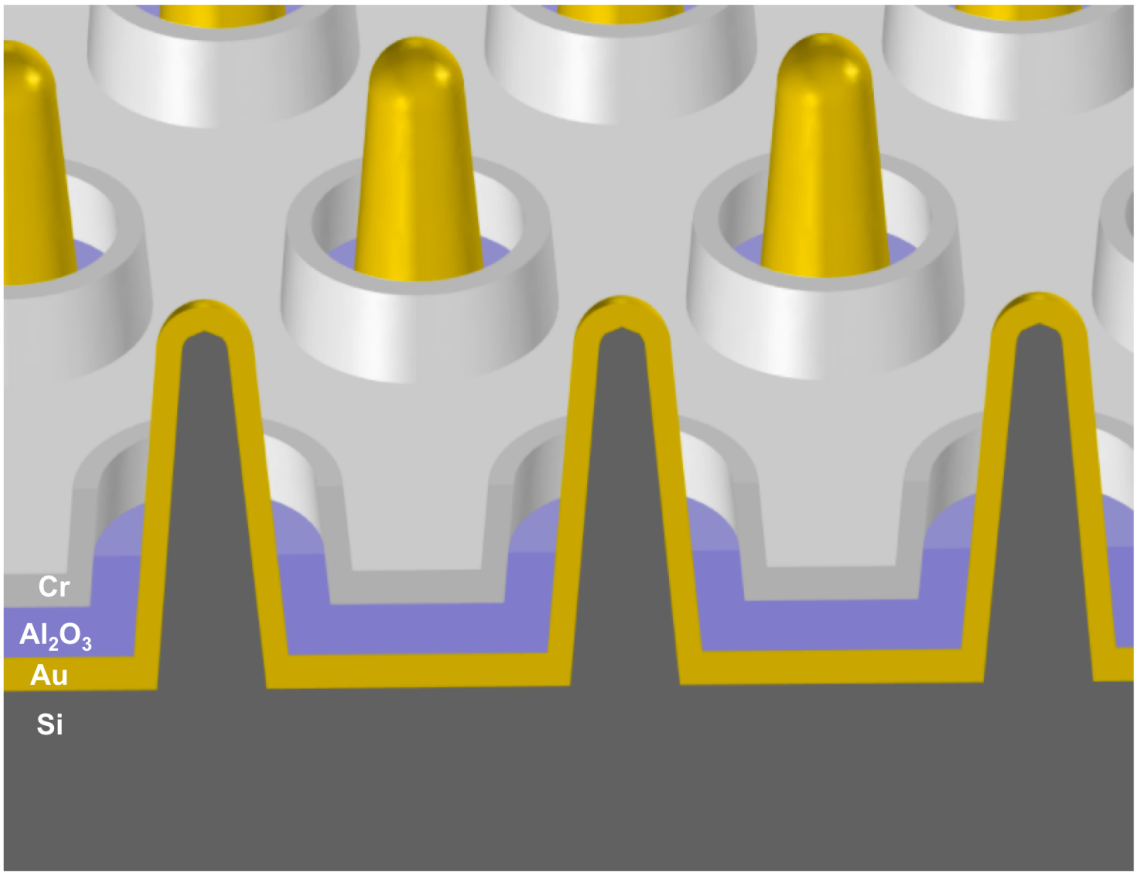

FIGURE 4.2

FIGURE 4.2: A schematic illustration of an ECC chip showing coaxes in cross-section. Ti/Au (yellow) is deposited over Si pillars (dark gray). A dielectric layer of alumina is deposited (blue), followed by Cr (light gray). The extended core is created using metal etching steps. (Image courtesy of Luke D'Imperio.)

4.2 Aim of Study

Here, the ECC was first characterized and optimized, in order to demonstrate that it was potentially a viable alternative to the first generation nanocoax (non-ECC). Several iterations of the ECC architecture were fabricated, with FCA redox as the benchmark assay for electrochemical performance. ECCs were then biofunctionalized using a thiolated protein G. Protein G will specifically bind the Fc region of an antibody and was used to tether a primary anti-CTX antibody to the ECC WE. This antibody was used to capture cholera toxin, after which ELISA was performed directly on-chip. The final antibody of the ELISA was conjugated to ALP, which generates 4-AP when the substrate pAPP is added. The ECC chip was then used to oxidize the 4-AP, where resulting redox peaks were expected to be proportional to the concentration of CTX in the sample.

4.3 Fabrication and optimization

Silicon pillar chips 16x30 mm^2 in size were thoroughly cleaned for metal deposition. A 3:1:H_2SO_4:H_2O_2 *piranha* cleaning mixture was prepared. The WE was formed by coating Si pillars with an adhesion layer of Ti (10 nm) followed by 120 nm of Au, *via* sputtering deposition (Fig. 4.3a and b). Gold was chosen as the WE metal due to its biocompatibility, amenability to biofunctionalization, and relative inertness (*176*, *177*). Given the small size of the electrode and the nm scale thickness, using gold does not drastically increase the price of producing an ECC chip, though other cheaper metals, such as Cr, could also feasibly be

used for the WE depending on experimental needs. A 200 nm dielectric layer of Al_2O_3 was deposited *via* atomic layer deposition (ALD) to separate the WE and CE (Fig. 4.3c). To serve as the CE, ~110 nm of Cr was deposited by sputtering (Fig. 4.3d). To form the extended core, the Cr outer metal was first lowered using a Cr specific etchant, exposing the Al_2O_3 layer (Fig 4.3e). The dielectric was then etched (Fig. 4.3f), and electrode heights were confirmed with SEM (Fig. 4.4). Further Cr and Al_2O_3 etching was done to yield varied heights of the dielectric and shield according to experimental needs.

All arrays had a base area of 0.049 mm^2 (Fig 4.5). Arrays were isolated from each other for electrochemical measurements using a removable well system held to the chip by pressure (as was used for dendrite chips and described previously). This ensured that no portion of the chip was damaged by epoxy, and allowed for facile washing of the chip after use to examine re-usability.

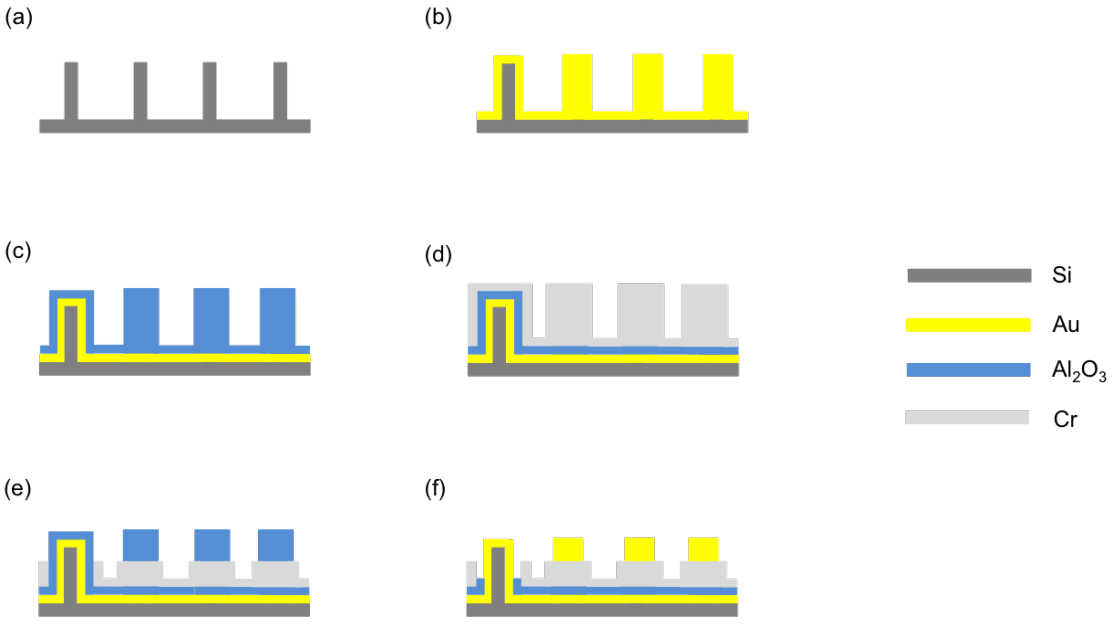

FIGURE 4.3

FIGURE 4.3: A schematic illustration of the fabrication steps involved in ECC production. One nanocoax is illustrated in cross-section. (a) Base pillar silicon (Si) substrate. (b) Inner metal coating of gold (Au) to form WE (Ti not shown). (c) Dielectric alumina (Al_2O_3) deposition. (d) Outer metal coating of chrome (Cr) to form shield. (e) Outer metal etching to lower shield height. (f) Dielectric etching to reveal gold core.

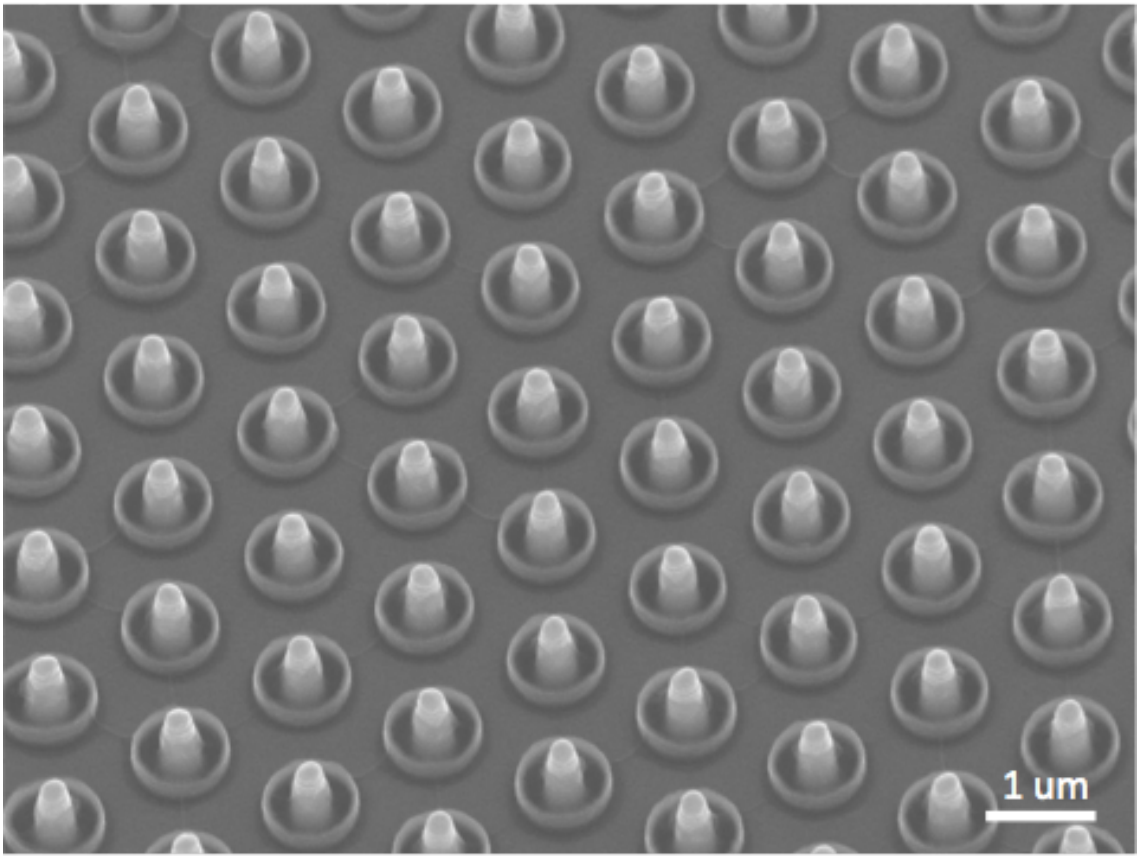

FIGURE 4.4

FIGURE 4.4: SEM of a finished ECC of the final iteration. Coaxes have an annulus thickness of 200 nm, and a core comprised of Au extended ~200 nm above the Cr shield. SEM image taken at a 30° tilt

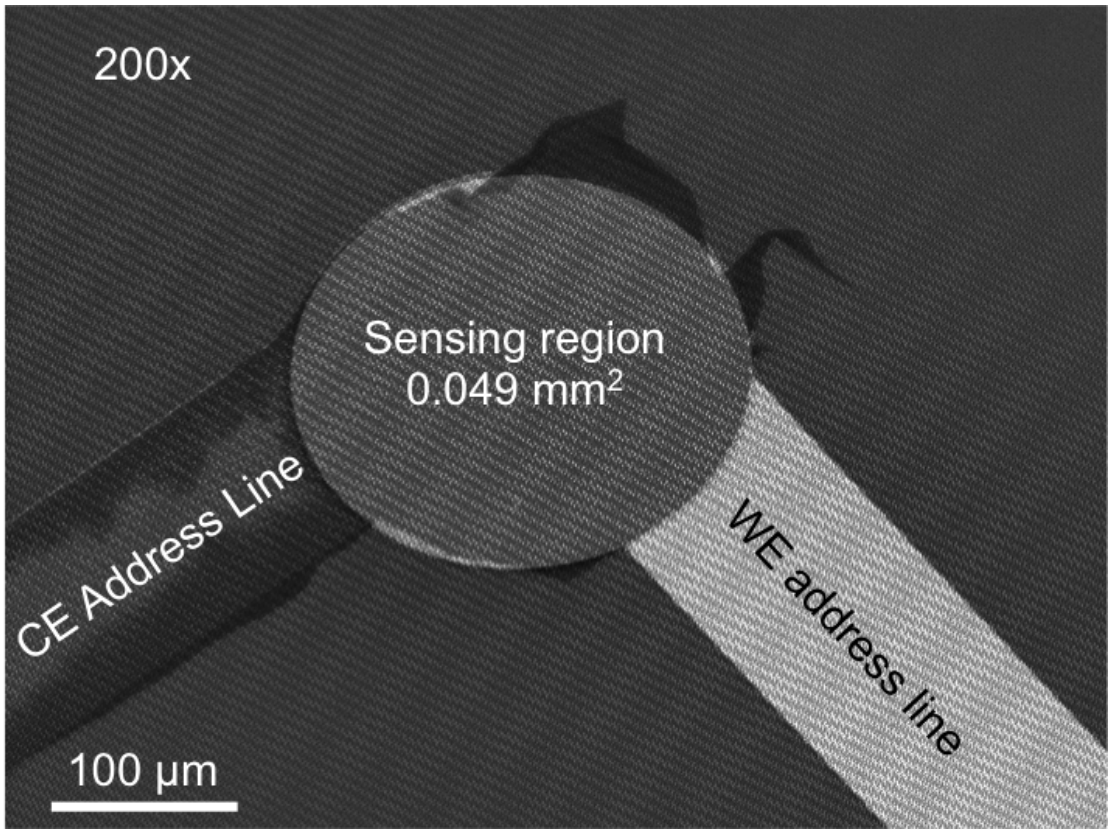
200x
Sensing region
0.049 mm²
CE Address Line
WE address line
100 µm

FIGURE 4.5

FIGURE 4.5: An SEM of a single sensing array, showing Cr and Au address lines to the CE and WE, respectively. Each completed ECC chip contains 7 of these arrays, which function independently of each other.

4.3.1 Nanoimprint lithography

In previous work, the non-extended core nanocoax was prepared on an SU-8 pillar array fabricated by NIL. Briefly, NIL involves making a stamp from a Si master, that is used to shape SU-8 photoresist into pillars, which are then hard baked and later overlaid with metals (*178*–*180*). We first attempted to use NIL to generate base substrates for ECC fabrication, due to a low supply of available Si pillar arrays (Fig. 4.6). However, whereas the previous coaxial iteration underwent a mechanical polishing step in order to expose the WE, ECC fabrication requires chemical etching to produce the extended core. The NIL process resulted in base pillars that were slightly shorter than the Si master, and additionally varied in the degree by which they were shorter. As detailed in the materials and methods, formation of the extended core required first an extremely short UV exposure (~1 s) of a photoresist layer which covers the chip surface after Cr deposition (Fig. 4.7a and b). After exposure, only the very top of the Cr layer on the ECCs was available, leaving the rest of the chip protected from the etchant by the photoresist. When the pillar heights varied, the short UV exposure time was not sufficient to consistently expose the entire chip. This left large swaths of individual nanocoaxes covered in photoresist and unavailable for etching (Fig. 4.7c). As a result, chips produced with NIL were largely nonfunctional, and those that did function were low-sensitivity. For this reason, further work was performed on Si pillar chips only.

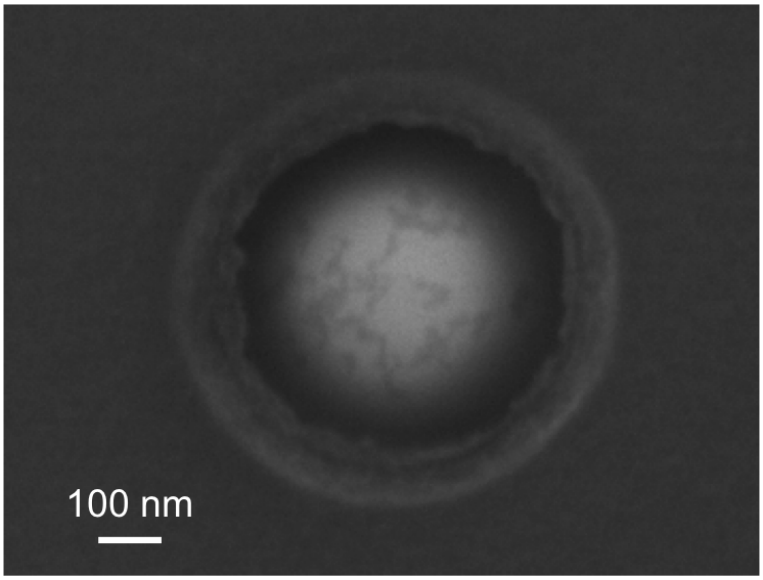

FIGURE 4.6

FIGURE 4.6: ECCs formed from a NIL process were not amenable to electrochemical measurements. SEMs show that cores are low aspect ratio, and their surfaces are imperfect and cracked.

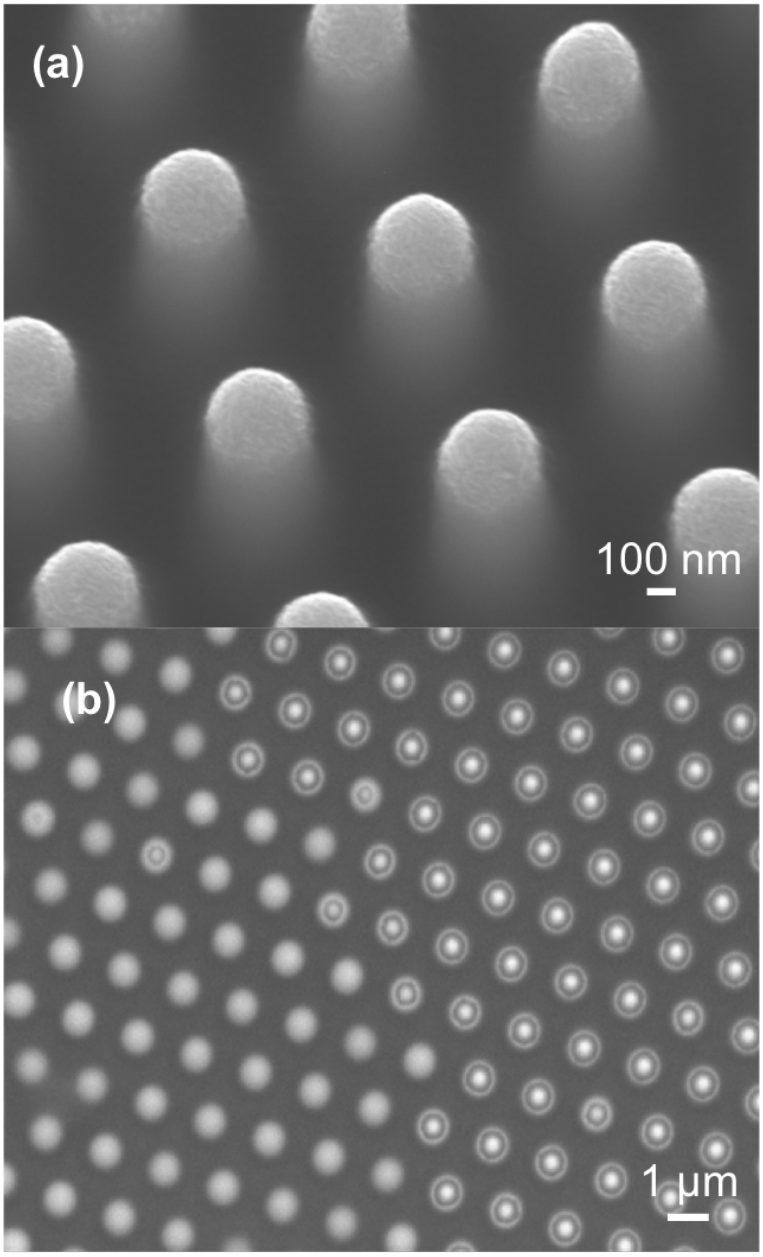

FIGURE 4.7

FIGURE 4.7: (a) The opening of the Cr tops after a UV flood exposure. Features below the top are obscured by the layer of photoresist that was not developed away. Only this topmost part of the coax will be exposed to etchants. (b) The effects of NIL on the final nanocoax. Large areas were not opened up for etching due to height differences in the base substrate. This is visible as fully white circles (left of image), rather than two concentric circles which would indicate a separate core and shield had formed.

4.3.2 Optimization on Si substrates

To optimize the ECC fabrication on Si pillars, chips underwent several changes in architecture, ranging from the shape of the extended core (dictated by Si pillar shape), to the height of the CE and dielectric layers relative to the core. The effects of all changes were measured by FCA redox and compared against the non-ECC, in order to confirm that the changes contributed to either an increase in sensing abilities, or at a minimum that they did not have a detrimental effect on sensitivity. FCA is a commonly used redox species in electrochemical sensing, which has been highly characterized (*181*).

Previous work characterized the ideal thickness for the annulus gap, which is the dielectric layer between the WE and CE (*127*). In order to be a nanogap electrode and allow for high sensitivity, the WE and CE must be in nanoscale proximity. However, previous non-ECC iterations fabricated with small annulus gaps (50-100 nm) experienced issues with liquid exchange and limitations in washing steps, which was likely due to surface tension. Non-ECC chips with sub-100 nm annulus gaps also experienced low manufacturing yield, likely because of shorting caused by the size of the gap. Because ethanol washes were required to fully rinse the non-ECC nanogap (which limits biofunctionalization by denaturing proteins and disrupting interactions (*182*)), and because of a need for high manufacturing yield, an annulus gap of 200 nm was used for all ECC chips.

The first version of the ECC was built on very sharp Si pillars (Fig. 4.8a). These chips showed a high level of sensitivity to FCA redox (Fig. 4.8b), with their current density demonstrating about a 2-fold increase over the best-recorded performance of the non-ECC. The Si pillar substrates on which these chips were fabricated were not available for further manufacture, but due to the availability of other types of Si pillars (Fig. 4.9), we instead explored ECC fabrication on new substrates (Fig 4.10). Since small changes at the nanoscale can result in large effects on function, we speculated that using Si pillars of different shapes may result in chips with different behaviors. Ultimately, the decision to move forward with a specific nanocoax shape was made based on a combination of FCA redox data, electrochemical consistency within and between arrays, and substrate availability. More specifically, a 1 μA current threshold was chosen as the lower signal limit in response to FCA redox, in order to compete with the electrochemical performance of the non-ECC. The NIL fabricated chips and many of the cylindrical Si substrate arrays fell below this threshold, and additionally demonstrated inconsistency in measurements of FCA redox, and were not used. A conical core shape was chosen for further optimization (Fig. 4.9a), and was used to explore how the amount of shielded or unshielded WE may affect sensitivity. Iterations were fabricated with a tall dielectric layer (Fig. 4.11), tall CE shield (Fig. 4.12a), and finally a shortened CE shield and dielectric (Fig. 4.12b), relative to the core height.

These latter chips, which were comprised of nanocoaxes with a lowered shield and dielectric layer, and a somewhat conical extended core with abundant gold

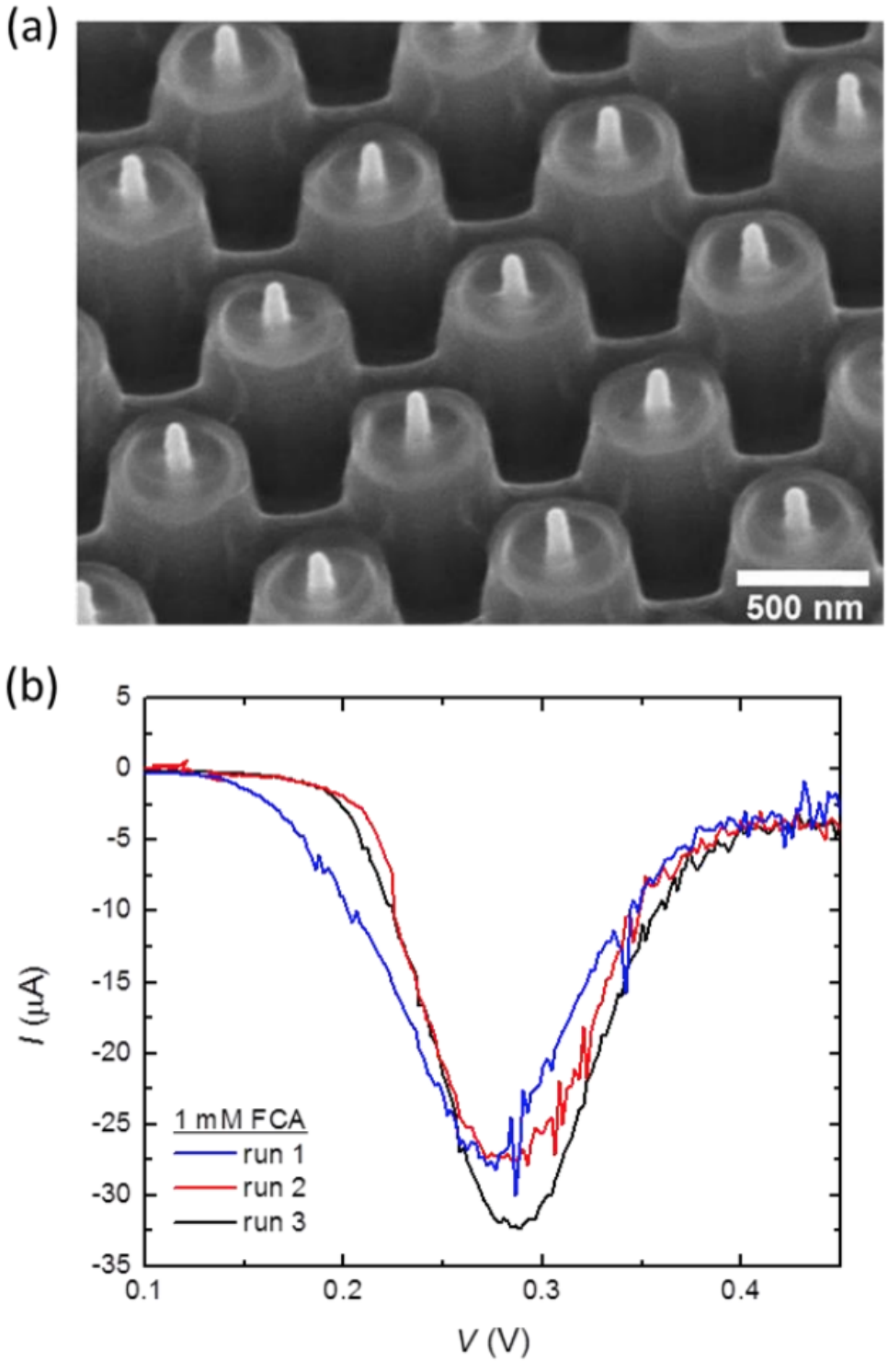
(a)
500 nm
(b)
5
0
-5
-10
-15
-20
-25
-30
-35
I (μA)
0.1
0.2
0.3
0.4
V (V)
1 mM FCA
run 1
run 2
run 3

FIGURE 4.8

FIGURE 4.8: (a)The first ECC chips were built on sharp Si pillars. (b) They demonstrated a high level of sensitivity to FCA redox. Data represent 3 independent FCA redox trials on the same ECC array. Image from reference (**archibald_novel_nodate**). X axis is potential; Y axis is current.

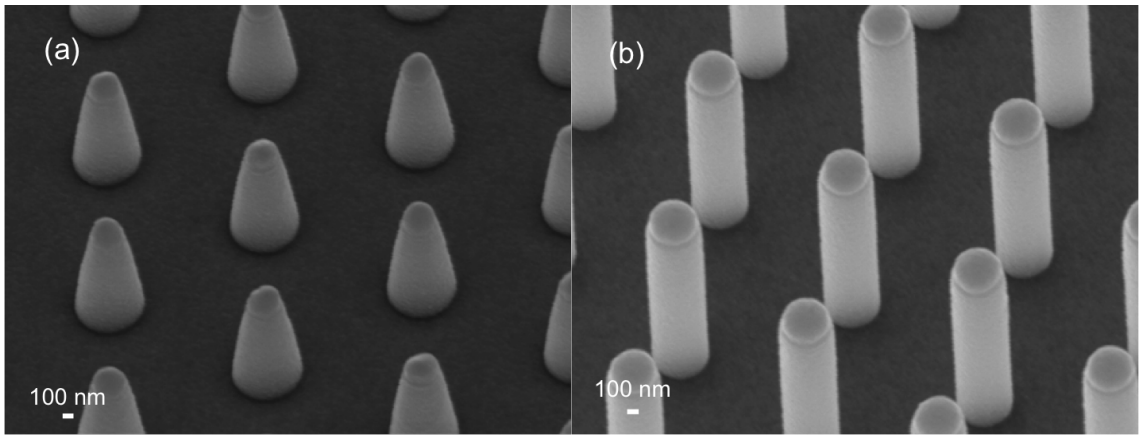

FIGURE 4.9

FIGURE 4.9: Several types of Si base pillar substrates were available. FCA results, in addition to the availability of chips, dictated the shape used for final testing. Slightly conical-shaped Si pillars (a) were chosen for further work. Cylindrical pillars (b) did not provide the electrochemical consistency necessary for further use. SEM images taken at 30° tilt. Si substrates were imaged with a layer of Au deposited for ease of visualization.

surface area available for biofunctionalization, were chosen as the final ECC architecture. Each chip was comprised of 7 individually addressed sensing arrays, which each contained ~30,000 individual nanocoaxes, connected in parallel (Fig. 4.13).

Some issues with the ECC fabrication process which could affect chip function should be noted. For example, at the perimeter of many sensing regions, there was sometimes a strand of partially-connected material remaining (Fig. 4.14a). This may arise from the photolithography process, specifically with the thin layer of LOR resist used prior to SU-8 (*183*). We additionally experienced a problem with crosslinking of the photoresist caused by SEM imaging (Fig. 4.14b), which caused this photoresist to not develop away, and ultimately prevented the formation of ECCs in crosslinked regions.

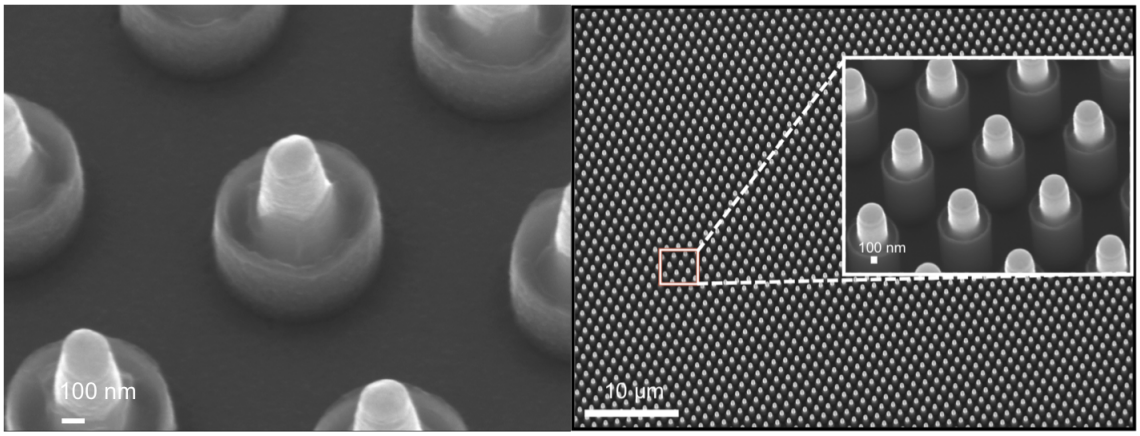

FIGURE 4.10

FIGURE 4.10: Two examples of finished ECC nanocoaxes built on a conical (left) or cylindrical (right) Si base, imaged by SEM. Conical cores were ultimately chosen for further development.

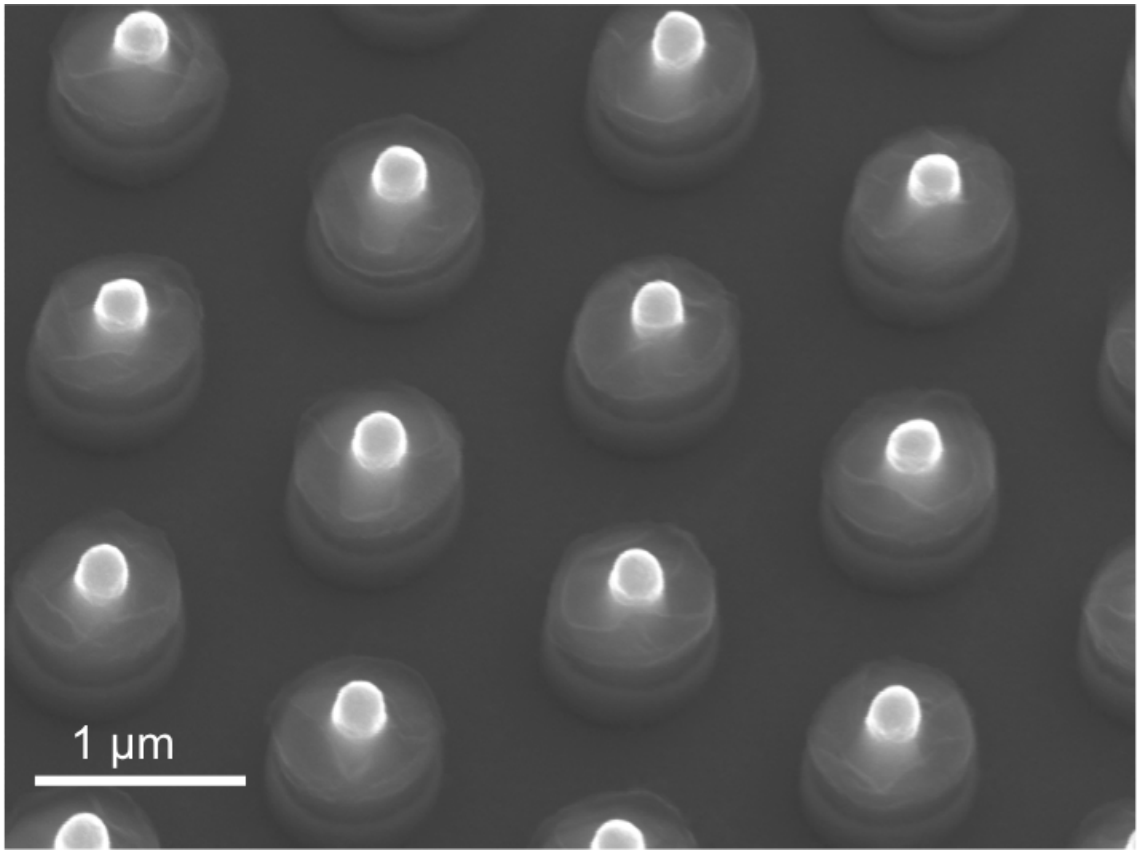

FIGURE 4.11

FIGURE 4.11: An experimental iteration of the ECC, imaged by SEM at a 30° tilt. These devices were fabricated with a lowered Cr shield, but the dielectric layer was not significantly etched, leaving it to cover much of the core. It was believed that inconsistencies in electrochemical performance of chips was due shorting issues caused by the shield and core touching on some of the nanocoaxes in the array. Due to the sheer number of individual coaxes in an array (~30,000) and the number of arrays (7), we could not rule this out with a simple visual assessment. This iteration was created to prevent any chance of shield and core coming into contact.

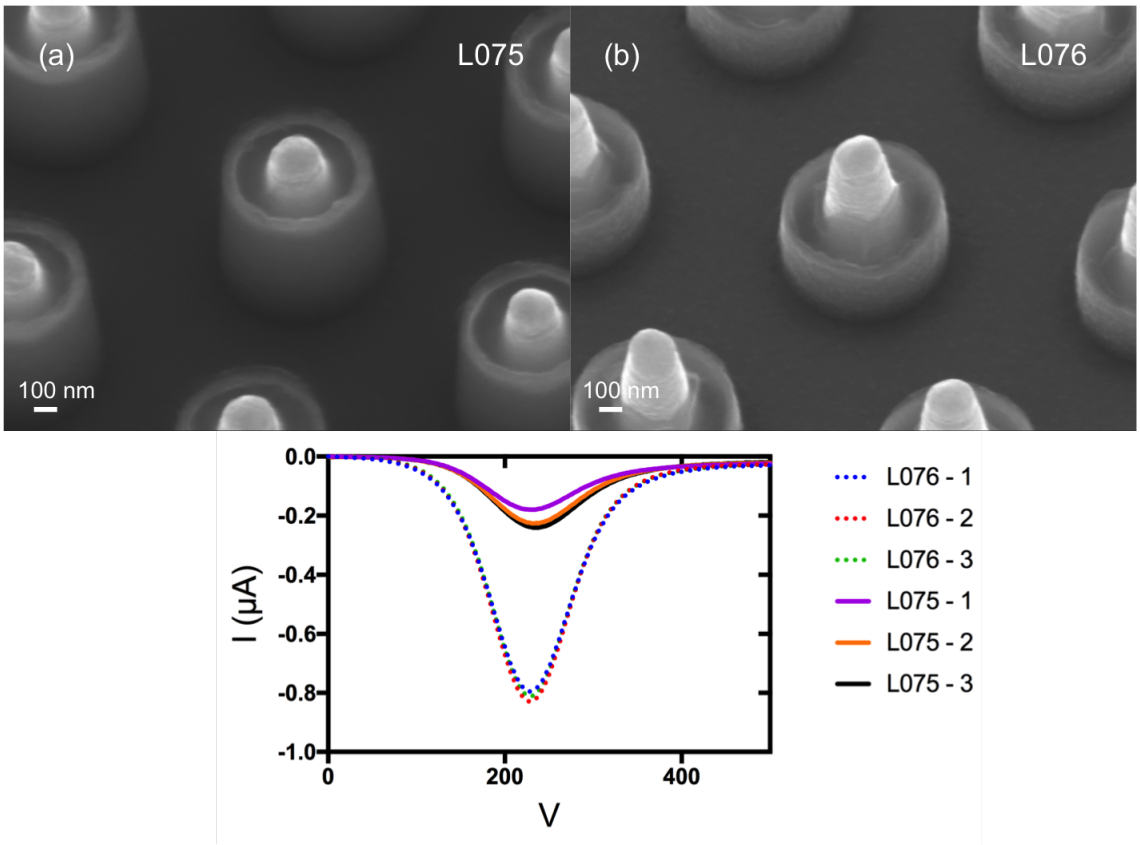
(a)
L075
100 nm
(b)
L076
100 nm
0.0
-0.2
-0.4
-0.6
-0.8
-1.0
I (μA)
0
200
400
V
L076 - 1
L076 - 2
L076 - 3
L075 - 1
L075 - 2
L075 - 3

FIGURE 4.12

FIGURE 4.12: SEMs show nanocoaxes built on the same conical Si substrate, with different shield heights. (a) Chip L075 with high shield. (b) Chip L076 with low shield. FCA data run in triplicate on a representative array from each chip is shown below. X axis is potential; Y axis is current.

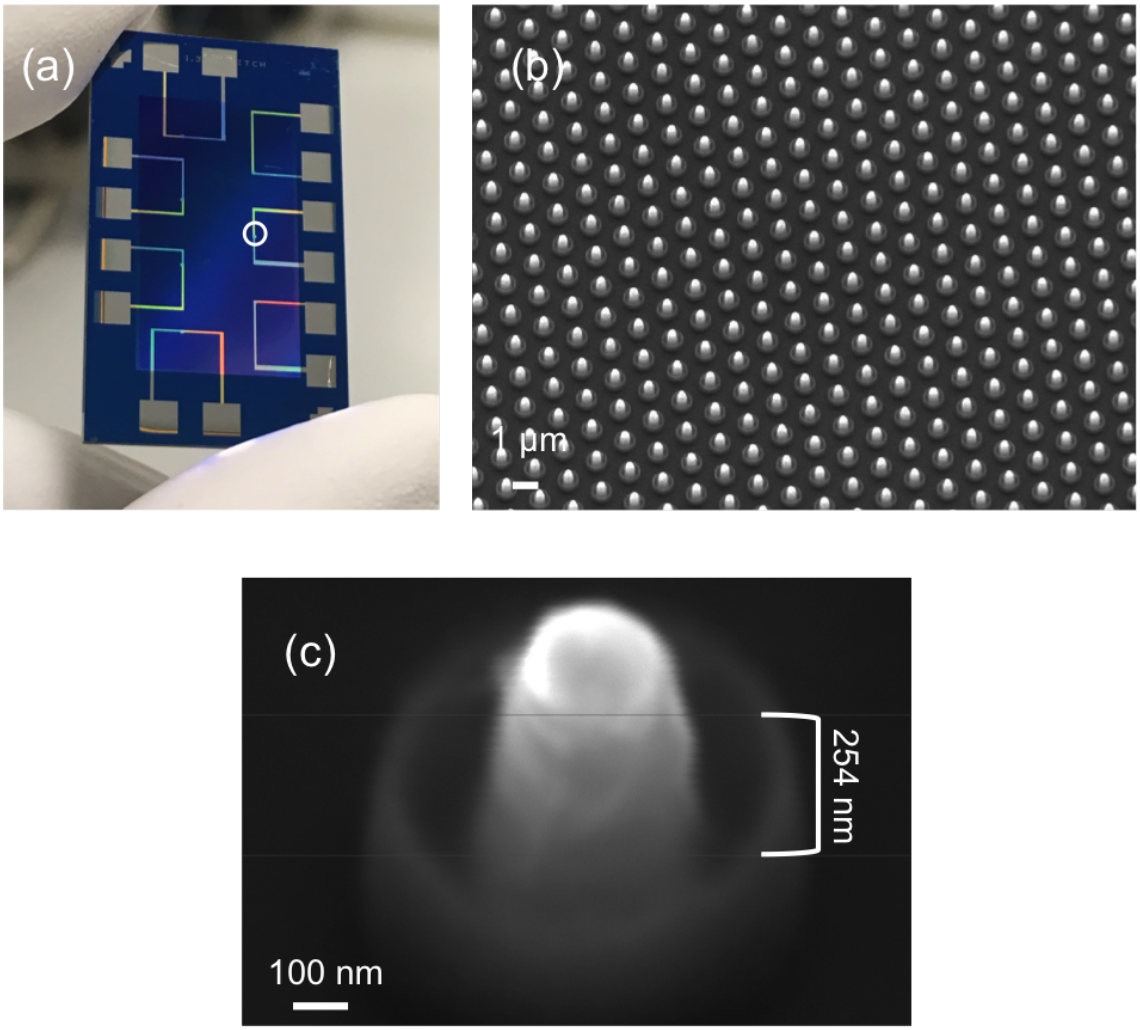

FIGURE 4.13

FIGURE 4.13: The finalized ECC architecture represents an array of vertically oriented nanocoaxes with lowered shield and dielectric layers relative to the extended gold core. (a) Each chip is comprised of 7 individually addressed sensing regions, (b) which each contain ~30,000 individual nanocoaxes connected in parallel (image magnified 5,000x). (c) Bracket indicates that the gold core extends ~200 nm above the shield (image magnified 100,000x).

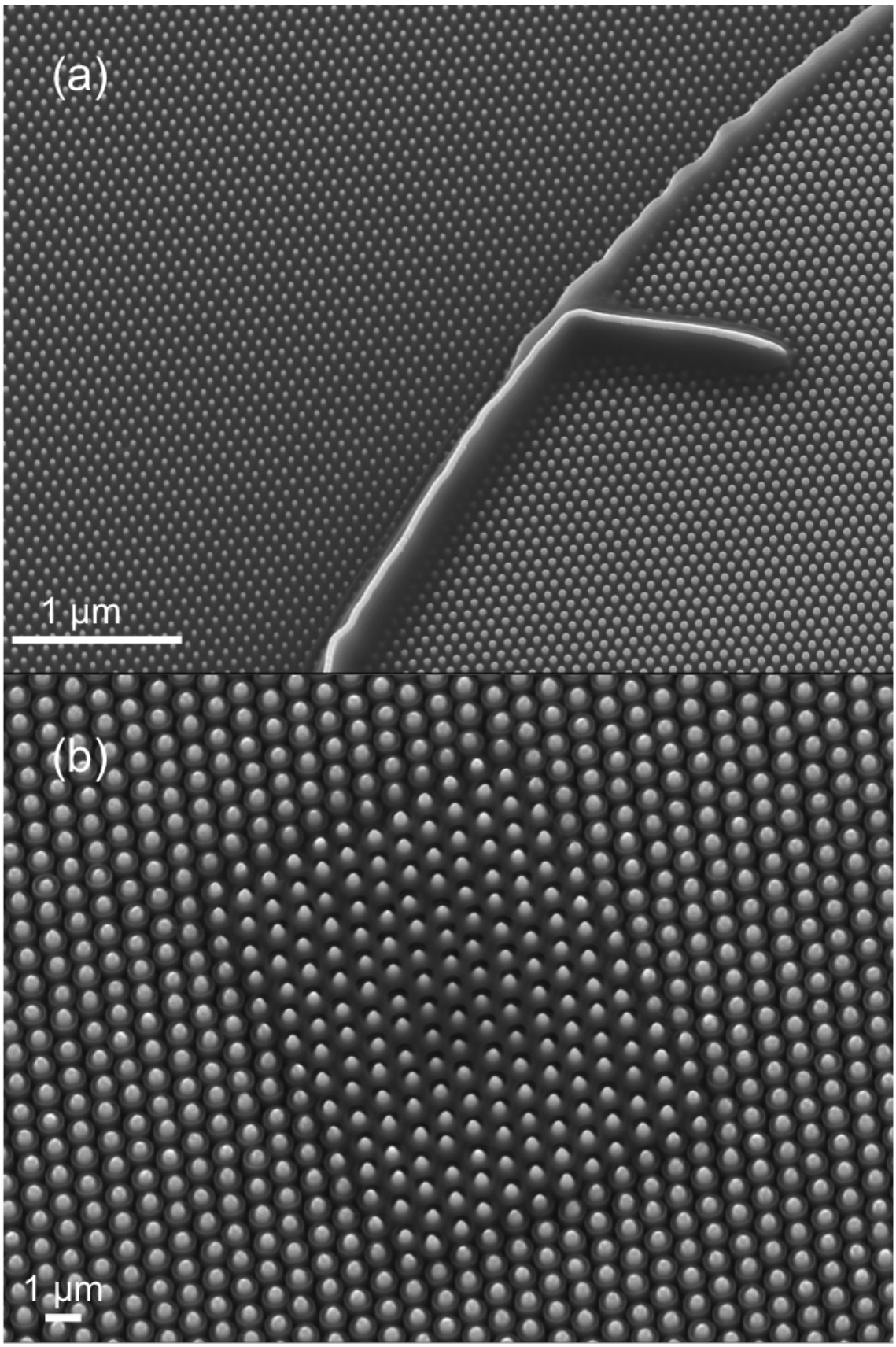

FIGURE 4.14

FIGURE 4.14: SEM images of issues encountered during ECC fabrication. (a) Partially-connected material from the lift-off process remains on the edges of a sensing array. (b) A region of an ECC array which did not form correctly because photoresist was crosslinked and did not develop correctly.

4.4 ECCs for electrochemical sensing

4.4.1 Quality control

Before being used in any biosensing capacity, ECCs underwent three quality control steps: SEM imaging, resistance measurements, and FCA redox testing. SEM imaging confirmed qualitatively that ECCs had been fabricated in the correct shape (lowered CE and dielectric). Resistance between the WE and CE was measured to ensure that arrays were not shorted. Resistances in the GΩ range were considered acceptable for use. It is worth noting that chips with resistances at or below the MΩ range were fabricated which were still functional, which is unusual as this would normally suggest these chips were shorted. Indeed, these low resistance chips actually demonstrated a significant improvement in FCA redox signal over higher resistance chips (Fig. 4.15). This difference may be due to the formation of an oxide layer on the high resistance chips, meaning that the Si substrate may actually be SiO_2. The DC resistivity of SiO_2 is on the order of ~10^{17} Ωcm, while Si is ~10^5 Ωcm (*184*, *185*). It is likely that in the low resistance chips the Si substrate may be contributing to conducting the signal. While these chips appeared to be much more sensitive to FCA redox, they were prone to current overloads and gave highly inconsistent oxidation peaks. For this reason, it was decided to continue to disregard low resistance chips for further work. As a final measure of quality control, FCA oxidation was performed to evaluate both chip current density and consistency. Generally, only arrays demonstrating $\geq$ 1 μA of FCA oxidation current were used for further

experiments. A 1 μA threshold for FCA redox current was chosen based on past electrochemical performance of the non-ECC, with which the ECC must compete. While the non-ECC initially reported extremely high sensitivity to FCA (~80-150 μA mm^2), all chips experienced a degradation in signal in subsequent runs, eventually stabilizing at ~25-30 μA. Thus, given the reduced size of the ECC sensing region *vs.* the non-ECC, a peak of only 1 μA on the ECC gives a current density of ~20 μA/mm^2, which sufficient to surpass the stabilized current density of the non-ECC (~14μA/mm^2). It is also worth noting that the ECC did not experience the signal degradation from one test to the next, which is in itself a significant improvement over the non-ECC.

4.4.2 Electrochemical performance

As stated previously, a nanocoaxial architecture has achieved ultrasensitive detection of VOCs. This was done by measuring a change in capacitance in response to the presence of a gas. This method was not explored for biosensor development, however, due to the generation of an electric double layer which hindered capacitive sensing on the non-ECC. Briefly, a double layer is when ions from a solution are adsorbed onto a substrate (in this case, the electrodes), and then oppositely charged ions from the solution are in turn attracted to the adsorbed ions (*186*). Because of this DPV was chosen as the method of detection for the non-ECC (*142*). DPV is able to suppress capacitive charge by using short pulses of potential (Fig. 4.16), allowing the electrode to discharge between

pulses (*187*). This method was similarly employed for the ECC.

A removable well system was attached to both ECCs and planar controls, and was filled with 60 μl of 1 mM FCA in PBS, pH 7.4. DPV was performed in the potential range of 0-500 mV, with FCA oxidation peak occurring ~300mV. ECCs were compared against non-ECCs and planar electrodes, and Fig. 4.17 illustrates the difference in current density (peak current/area) between each platform. Current density is used as a measure of comparison because even though the planar and ECC chips were measured using identical wells, the active electrode areas are not the same. The sensing region of the ECC (0.049 mm^2) is much smaller than the footprint of the well that encompasses it (~4 mm^2). The ECC sensing region is also smaller than that of the non-ECC (1.8 mm^2). The increase in current density the both nanocoaxial architecures exhibit over planar may be due to the phenomenon of redox cycling. Redox cycling occurs between nanogap electrodes, where a species in oxidized at the WE, then reduced at the CE, where it can then rapidly diffuse back to the WE to be oxidized again (*188*, *189*). Improvement in signal can be obtained by decreasing the size of the annulus gap, which may allow for faster redox cycling (*127*).

The increase in current density that the ECC exhibits over the non-ECC may be explained by the ease of liquid exchange. As stated previously, due to surface tension it was difficult for solution to diffuse to the WE which was situated within the annulus gap. By contrast, ECC WE extends into the solution, and so it may be easier for FCA molecules to move from the bulk solution to the electrode

surface to be oxidized.

From this comparison, it is clear that both nanocoaxial architectures are better-performing than a simple planar electrode. While the drawbacks of the non-ECC have been discussed above, the ECC is not without its own issues. While ECCs did not experience the significant drop in peak current from run to run that plagued the non-ECC, and indeed were extremely consistent within the same sensing region (Fig. 4.18a), arrays did display significant differences in peak current between sensing regions (Fig. 4.18b). Similarly, ECC chips fabricated within the same batch also demonstrated highly variable peak currents in FCA tests (Fig. 4.19). However, as long as peak currents exceeded the current density threshold of 1 μA, chips were still used. This is because we believed that the highest current achievable in a LOC ELISA would always be much smaller than 1 μA, and thus the variability may not significantly impact these results.

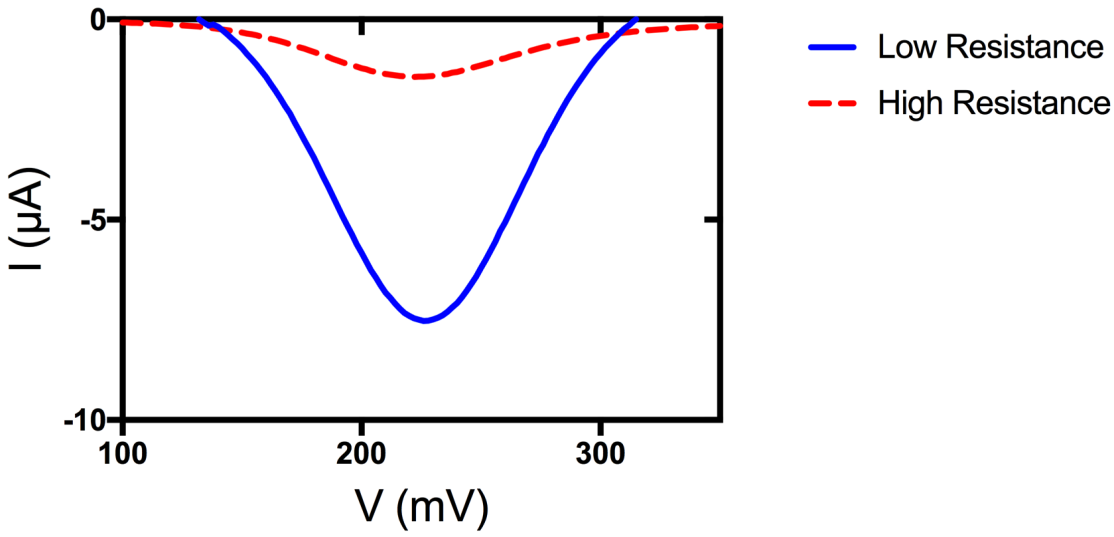

FIGURE 4.15

FIGURE 4.15: Representative FCA oxidation peaks on a chip exhibiting kΩ (low) resistance *vs.* one exhibiting GΩ (high) resistance. Data represent one trial on one array from each chip. X axis represents potential; Y axis represents current.

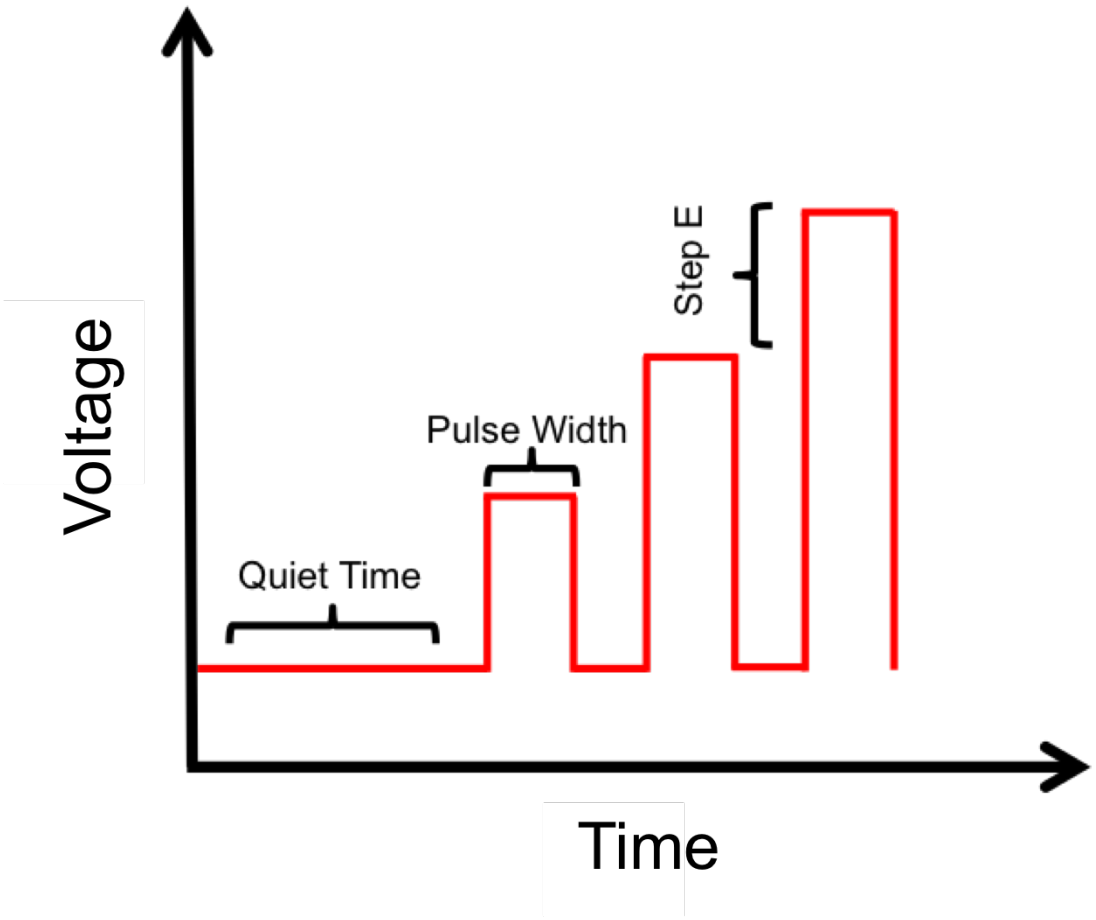

FIGURE 4.16

FIGURE 4.16: Potential waveform used in DPV. Potential is pulsed in increasing increments for short bursts of time. This minimizes the effects of capacitive charging. X axis is time; Y axis is voltage.

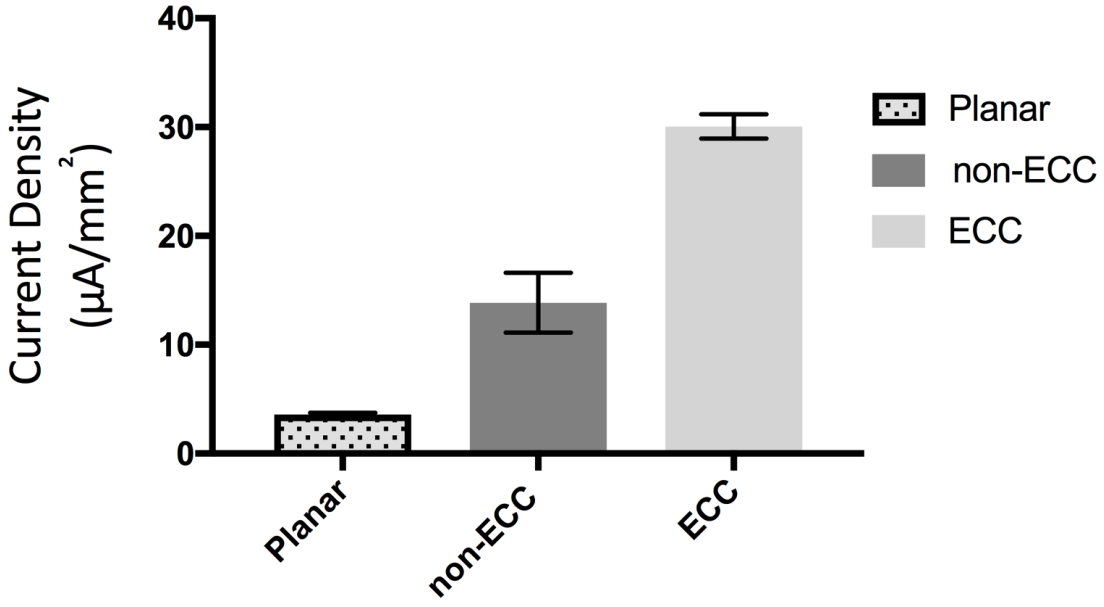
Current Density
(μA/mm²)
40
30
20
10
0
Planar
non-ECC
ECC
Planar
non-ECC
ECC

FIGURE 4.17

FIGURE 4.17: A comparison of average current density achieved in sensing FCA redox between a representative ECC array (three independent runs one one array), a non-ECC array (reported values one array, after stabilization) (*190*), and a planar gold electrode (three independent runs on one array). For the non-ECC, data is reported which excludes the highest FCA current measured on the array, which was achieved on a virgin chip. All trials subsequent to the first run gave a significantly diminished peak current, which may be more indicative of the true sensing capacity of the platform. X axis is sensing platform; Y axis is peak current density.

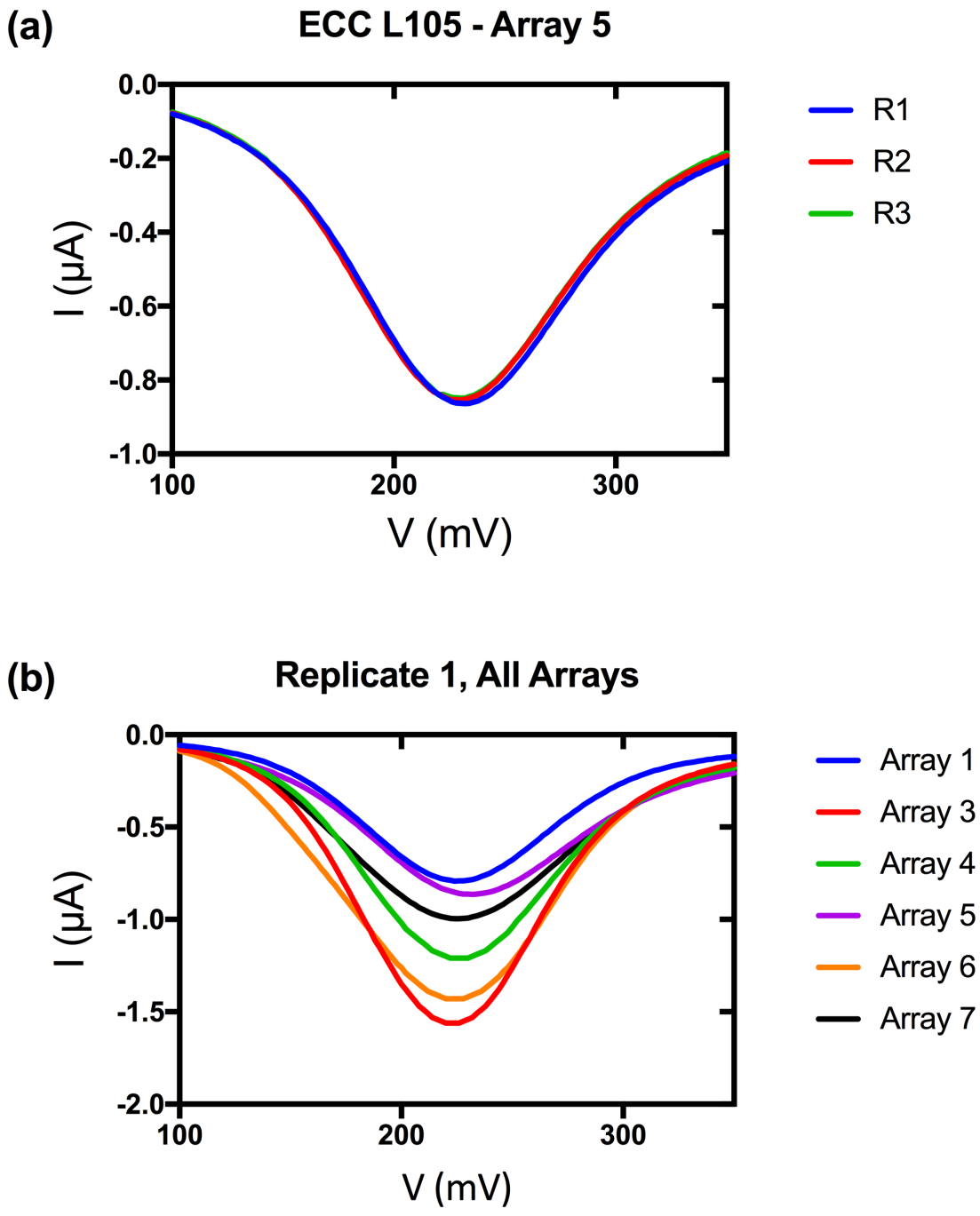
(a)
ECC L105 - Array 5
0.0
-0.2
-0.4
-0.6
-0.8
-1.0
I (µA)
100
200
300
V (mV)
R1
R2
R3
(b)
Replicate 1, All Arrays
0.0
-0.5
-1.0
-1.5
-2.0
I (µA)
100
200
300
V (mV)
Array 1
Array 3
Array 4
Array 5
Array 6
Array 7

FIGURE 4.18

FIGURE 4.18: (a) ECC chips generally demonstrated an extremely high degree of consistency in FCA readings within an array. Data represents 3 trials on the same array on ECC chip L105, run consecutively with no washing step in between. (b) Peak current between different arrays on the same chip varied significantly. Data represent one trial from each array on the same chip. Array 2 is not represented due to shorting issues. X axis is potential; Y axis is current.

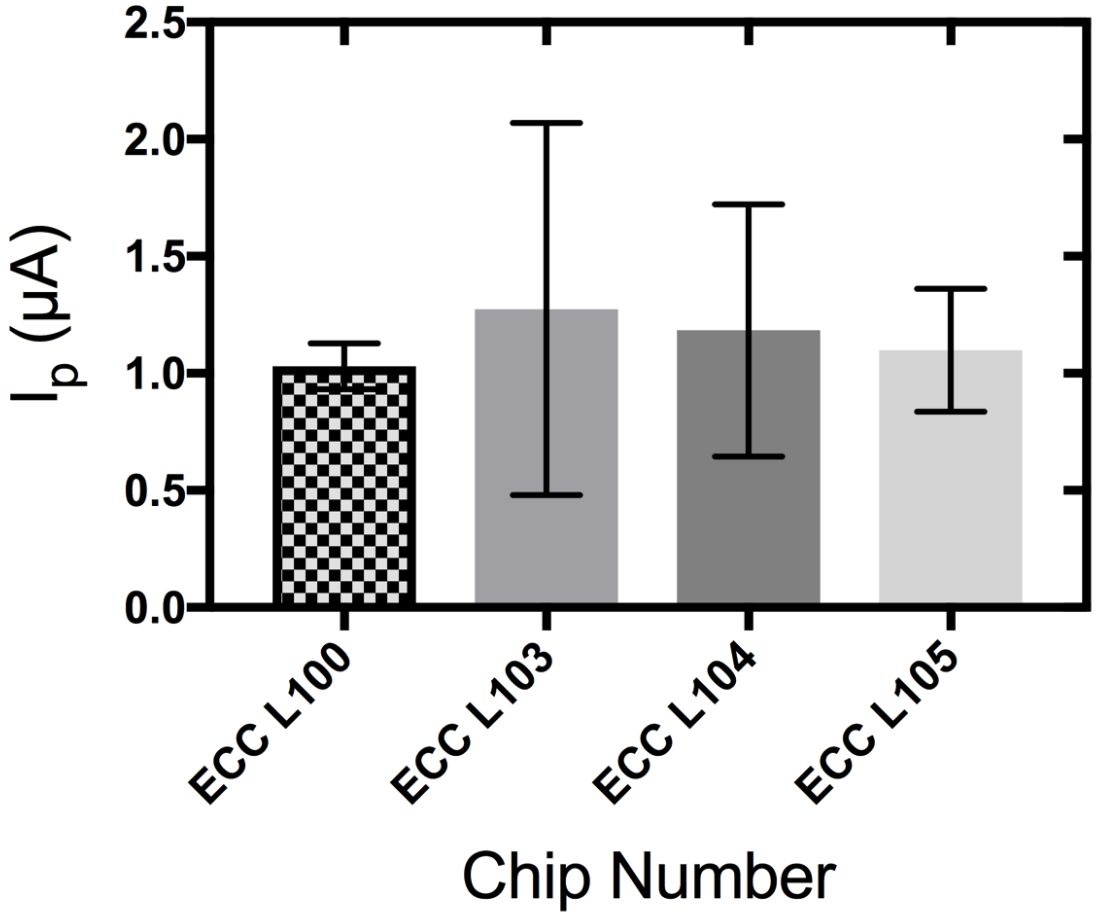
2.5
2.0
1.5
1.0
0.5
0.0
I_p (μA)
ECC L100
ECC L103
ECC L104
ECC L105
Chip Number

FIGURE 4.19

FIGURE 4.19: The variability in FCA peak current of a batch of chips fabricated at the same time. The peak current of all trials on all functional arrays was averaged for each chip. Error bars represent the standard deviation of all peak currents measured on each chip individually. X axis is chip identification number; Y axis is peak current.

4.5 Off-chip biosensing

After fabrication optimization and confirmation of electrochemical function, ECCs were used to measure their biosensing performance compared to the non-ECC. Non-ECCs had previously been used to detect CTX in an off-chip setup; that is, all ELISA steps were performed in a standard 96 well microtiter plate, with only the final redox product applied to the chip surface for detection. This made the non-ECC more of a novel analysis platform than a true LOC.

A titration of ALP was performed to provide a baseline of the biosensing potential of the ECC. Serial dilutions of ALP were made, incubated with 1 mM of the substrate pAPP, and then pipetted on to the ECC chip for electrochemcial analysis (Fig. 4.20). This was done to demonstrate that the ECC is capable of detecting the redox product of an electrochemical ELISA (4-AP), before we moved on to test the full sandwich ELISA. Titration data was taken on a single array to circumvent any issues with the variation between sensing regions. In this assay, an ECC chip was capable of detecting 10 ng mL^{-1} of ALP, confirming the ECC as a viable candidate for further biosensor development.

As a baseline comparison of the non-ECC and the ECC, an off-chip electrochemical ELISA, developed previously, was performed (*142*). CTX was chosen as the biomarker of interest due to its clinical relevance, stability and safety. The off-chip ELISA was performed identically on the ECC as it was on the non-ECC, which in turn was identical to a standard optical ELISA with the exception of

the readout. For the electrochemical ELISA, pAPP was added as the enzymatic substrate as opposed to Bluephos for the optical readout. The ECC off-chip readout showed a comparable level of CTX sensitivity as the non-ECC (Fig. 4.21). Both were able to detect as low as ~1 ng mL^{-1} of CTX. When current density was taken into account, however, the ECC outperformed the non-ECC, as the sensing area of the ECC was significantly smaller than that of the non-ECC (Table 4.1). Thus, if the ECC were scaled up from 0.049 mm^2 to 1.8 mm^2 to match the size of the sensing area of the non-ECC, the ECC would measure a higher current in response to 4-AP oxidation.

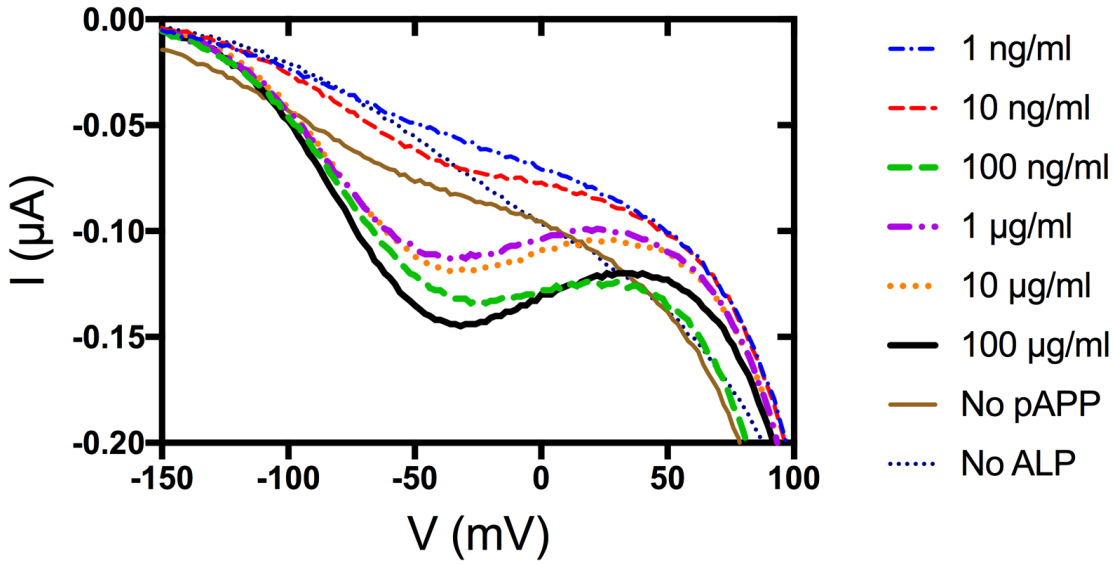
0.00
-0.05
-0.10
-0.15
-0.20
I (µA)
-150
-100
-50
0
50
100
V (mV)
1 ng/ml
10 ng/ml
100 ng/ml
1 µg/ml
10 µg/ml
100 µg/ml
No pAPP
No ALP

FIGURE 4.20

FIGURE 4.20: DPV signals on an ECC array for an ALP titration. Different concentrations of ALP were incubated with pAPP. The redox product 4-AP was oxidized on one array of an ECC chip. DPV signals were subtracted to a baseline at -200 V. A shift in the oxidation potential of 4-AP may be due to the use of a pseudo-reference electrode. X axis is potential, Y axis is current.

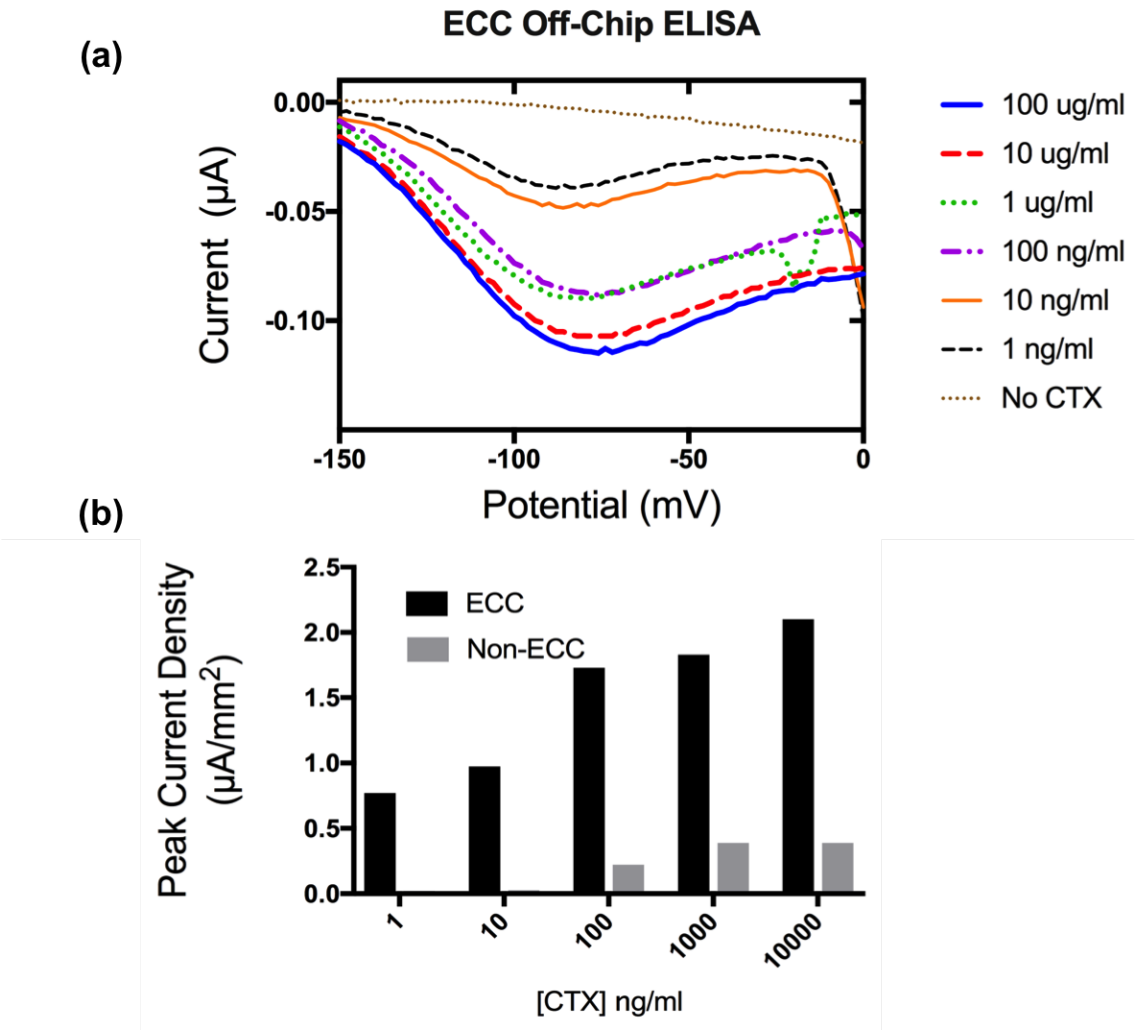
(a)
ECC Off-Chip ELISA
Current (μA)
0.00
-0.05
-0.10
-150
-100
-50
0
Potential (mV)
100 ug/ml
10 ug/ml
1 ug/ml
100 ng/ml
10 ng/ml
1 ng/ml
No CTX
(b)
Peak Current Density (μA/mm²)
2.5
2.0
1.5
1.0
0.5
0.0
ECC
Non-ECC
1
10
100
1000
10000
[CTX] ng/ml

FIGURE 4.21

FIGURE 4.21: (a) An electrochemical ELISA performed off-chip for CTX titrations, and analyzed on the ECC. All measurements were made on the same ECC array to minimize variability. Data were subtracted to a baseline at -200 mV to better elucidate peak currents. Sharp peak seen in the 1 μg/ml data is an artifact, and not relevant to the redox reaction taking place. X axis is potential; Y axis is current. (b) The peak current density at each CTX concentration, as measured on an ECC chip and a non-ECC chip are compared. X axis is CTX concentration; Y axis is peak current density.

4.6 Functionalization of ECCs

Once the ECC proved to have comparative off-chip functionality to the non-ECC, the feasibility of true LOC detection was explored. The ECC was developed primarily to provide structural differences that would overcome sensing limitations of the non-ECC. Namely, the extension of the WE outside of the CE provides a substrate for biosensor development that may not be hindered by surface tension, which will allow for thorough washing and subsequent biofunctionalization.

The PCEPy protocol described in chapter 3 was first implemented for antibody tethering on the ECC. However, PCEPy oxidation peaks at -400 mV were not detected after polymerization (Fig. 4.22), indicating that PCEPy was likely not electropolymerized, and that subsequent antibody binding was not possible. This is likely because PCEPy will deposit on the WE. In the case of the dendrites, the WE is comprised of the entire chip surface. For ECCs, the WE is only the gold core of each nanocoax. There does not seem to be enough WE available to electropolymerize that would give rise to a redox peak. As an alternative, a protein G protocol was evaluated.

Protein G is a bacterially derived protein with specific affinity for the Fc region of IgGs (*191*, *192*). This protein was modified with a thiol group, in order to facilitate binding with a gold surface (*193*). To provide a visual proof-of-concept of protein G-facilitated antibody tethering, a 1 mg mL^{-1} solution of thiolated

protein G was applied to an ECC chip for 2 h at room temperature, with rocking. It was then thoroughly rinsed with TBS, and incubated for 12 h with ELISA tertiary antibody. This tertiary antibody was conjugated with a 40 nm AuNP to allow for SEM visualization of tethering. The chip was then removed from its well housing, rinsed thoroughly in TBS, and dried with N^2 air. SEM images of a control array (no protein G) and test array (protein G) on the same ECC chip are shown in Fig. 4.23. It should be noted that because it was expected that this process would be damaging to the ECC chip and possibly preclude further use, an older chip with a slightly different architecture was used. Since this assay was purely of a visual nature, results were expected to be representative of the behavior of the ECCs used for electrochemical studies. AuNPs about 40 nm in size are visible surrounding the extended cores of the test array, but not around the cores on the control array. This provided visual proof that the extended gold core is indeed amenable to biofunctionalization, and could feasibly be used for LOC detection of biomarkers using a sandwich ELISA setup.

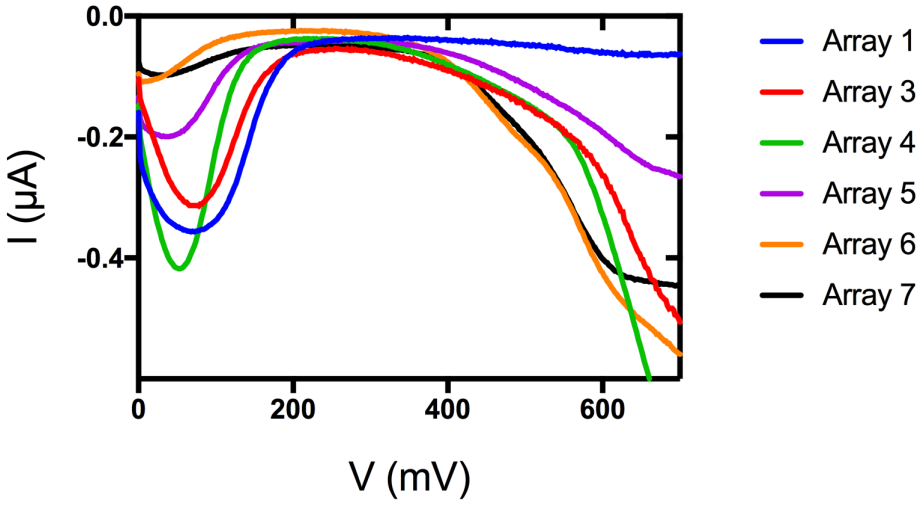
0.0
-0.2
-0.4
I (μA)
0
200
400
600
V (mV)
Array 1
Array 3
Array 4
Array 5
Array 6
Array 7

FIGURE 4.22

FIGURE 4.22: Functionalization facilitated by a PCEPy film was first attempted on the ECCs. Results of PCEPy oxidation are shown for multiple arrays on the same ECC chip, in a solution of $NaClO_4$ containing no monomer. PCEPy oxidation should occur around 400 mV. Measurable PCEPy oxidation peaks were not observed after electropolymerization on any array. Data for array 2 is not shown because of shorting issues. X axis is potential;Y axis is current.

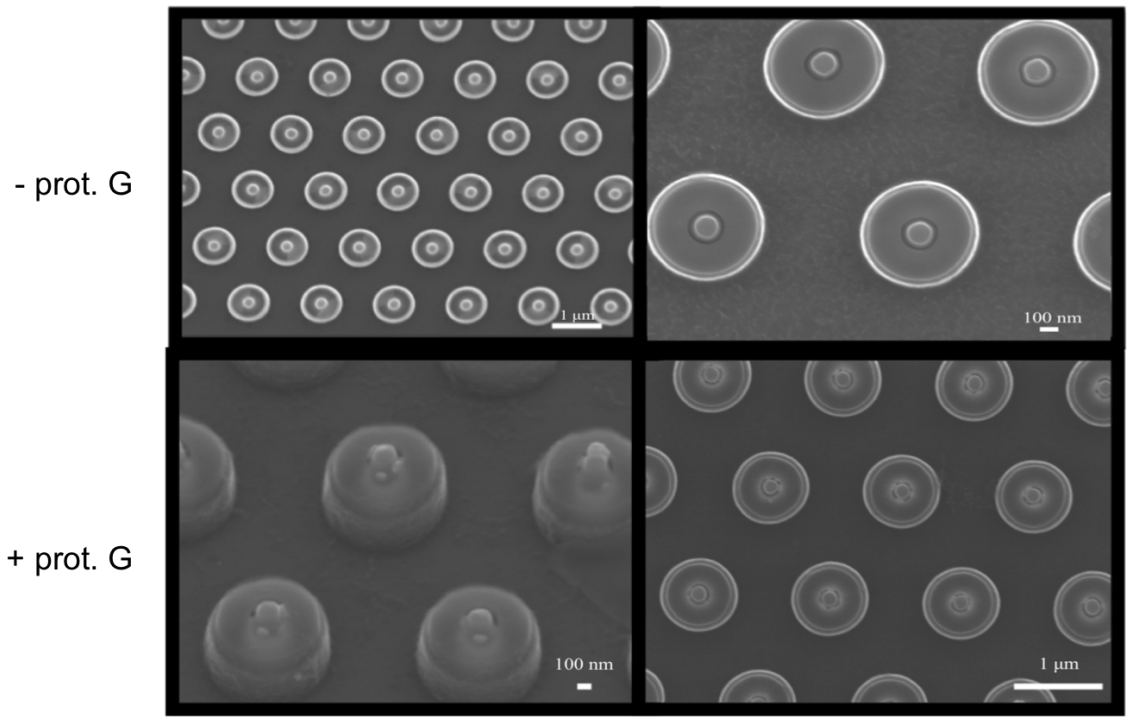

FIGURE 4.23

FIGURE 4.23: SEMs of 2 separate arrays on the same ECC chip, one which was incubated with protein G (+ prot. G) prior to AuNP conjugated antibody application, and one which was not (- prot. G). For each test condition, two images are shown at different magnifications, to provide context. AuNPs of ~40 nm in diameter are visible around the extended cores of the test array, but not the control array. Note that an older iteration of ECC was utilized in this study, but is expected to be representative of the behavior of all ECC chips.

4.7 ECCs as LOC biosensors

To biofunctionalize the ECC toward LOC detection, 1 mg mL^{-1} of thiolated protein G was incubated on-chip for 2 h, and rinsed thoroughly with TBS. A primary ELISA anti-CTX antibody diluted to 1 mg mL^{-1} in HEPES was incubated on the chip for 48 h to allow for thorough binding of the antibody Fc region to the protein G layer. The chip was blocked with 5% BSA and 5% glycerol in TBST for 1 h. The remaining steps of the ELISA procedure, detailed in section 2.7, were performed on-chip, with washes between each. While this work is preliminary, Fig. 4.24 demonstrates preliminary on-chip detection of CTX by a protein G functionalized ECC. The dendritic LOC was capable of a maximum current density of ~0.4 $\mu A/mm^2$; by contrast, these preliminary ECC data demonstrate that the ECC achieved a current density of ~3$\mu A/mm^2$, a 7-fold increase. While more replicates and a full titration are necessary to confirm these findings, from the standpoint of a proof-of-concept, these data are promising.

A final important feature of the ECC as compared to the non-ECC is their amenability to repeated use. The non-ECC chips, as stated previously, demonstrated a signal degradation over the course of several uses. By contrast, ECC chips maintained signal integrity even after repeated use (Fig. 4.25), suggesting that the ECCs, despite their small size, are relatively stable structures. This is important for POC sensing potential, as portable diagnostic tools are typically not stored in ideal conditions. The ECCs chips appear to be able to withstand a large amount of use while maintaining their sensing integrity. For all these reasons, the ECC

represents a significant improvement over the non-ECC architecture, and is a promising architecture for further development toward POC cholera detection.

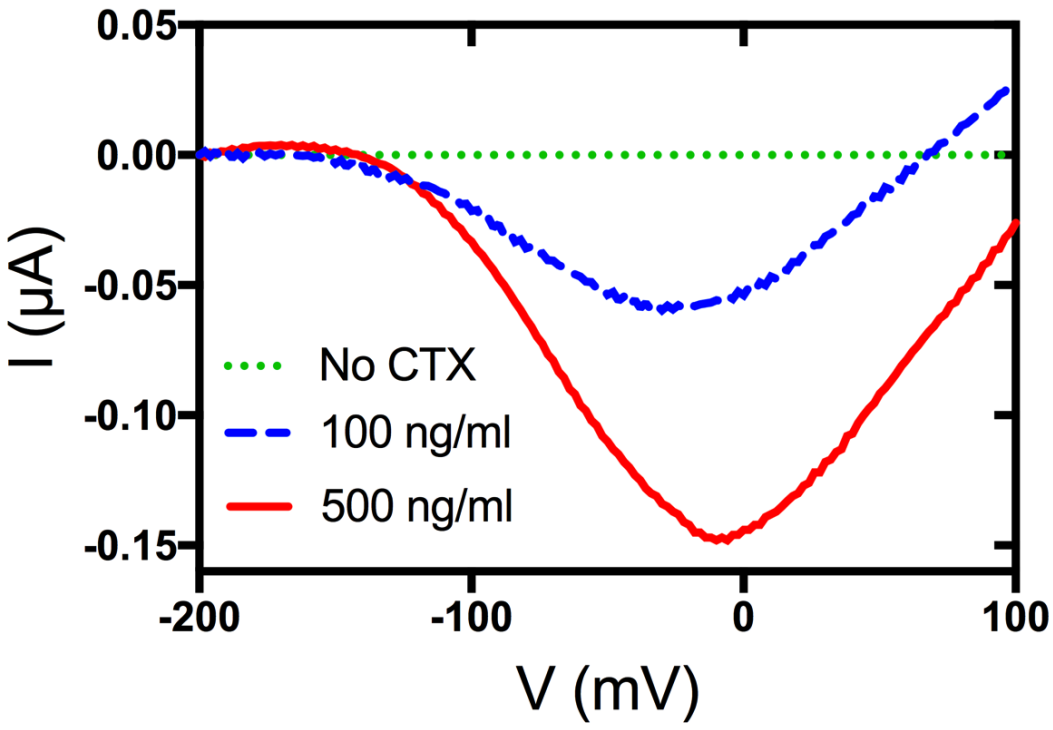
0.05
0.00
-0.05
-0.10
-0.15
I (μA)
No CTX
100 ng/ml
500 ng/ml
-200
-100
0
100
V (mV)

FIGURE 4.24

FIGURE 4.24: Preliminary data suggests a potential for ECCs to be used for LOC deteciton of CTX, using protein G to tether antibodies to the sensor surface. Each trial was performed on a separate array on the same ECC chip. Data represents one trial for each condition. Data were subtracted to a baseline at -200 mV to better elucidate peak current. X axis is potential; Y axis is current.

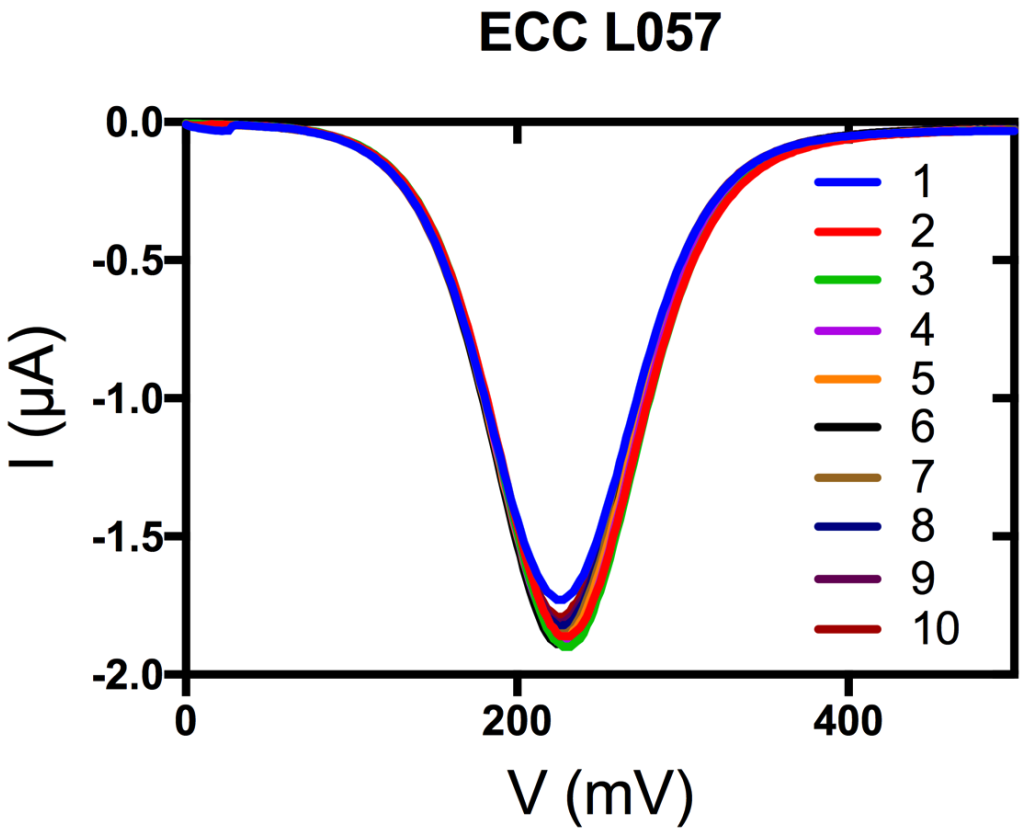

FIGURE 4.25

FIGURE 4.25: Results of multiple FCA oxidation tests run on one array of ECC chip L057. No washing steps were utilized in between trials. X axis is potential; Y axis is current.

4.8 Future directions

We have demonstrated that the ECC architecture is a viable and promising alternative to a first generation, non-ECC nanocoaxial architecture. However, there are still several hurdles preventing the realization of the ECC as a true LOC for POC diagnosis. The labor-intensive nature of chip fabrication, as well as chip variability and failure rate, has precluded us from completing on-chip detection of a full range of CTX concentrations. Once this is done, the performance of the ECC should be compared to that of a standard optical ELISA, to ensure that it has conferred some sensing advantage. However, given the advantages afforded by the ECC, namely its potential for multiplexed biomarker detection on a highly portable platform, a small decrease in sensitivity may still be acceptable in light of other features. Future directions may also include examining more Si pillar shapes. For example, given the tendency for electric fields to concentrate around sharp edges, and given the performance of the very first ECC iteration which was built upon sharp pillars, it may be worth examining the use of a sharp, high aspect ratio Si pillar array fabricated in-house using the Bosch process (or reactive ion etching) (Fig. 4.27).

Aside from this, in its current iteration, the detection platform is not yet portable or user friendly. It is necessary for all reagents to be pipetted on to the chip, and for the user to manually wash after each step. Such a setup is not acceptable for A.S.S.U.R.E.D. diagnostics, which dictate as little end-user participation as possible. To overcome this, the next step is to develop a microfluidic channel

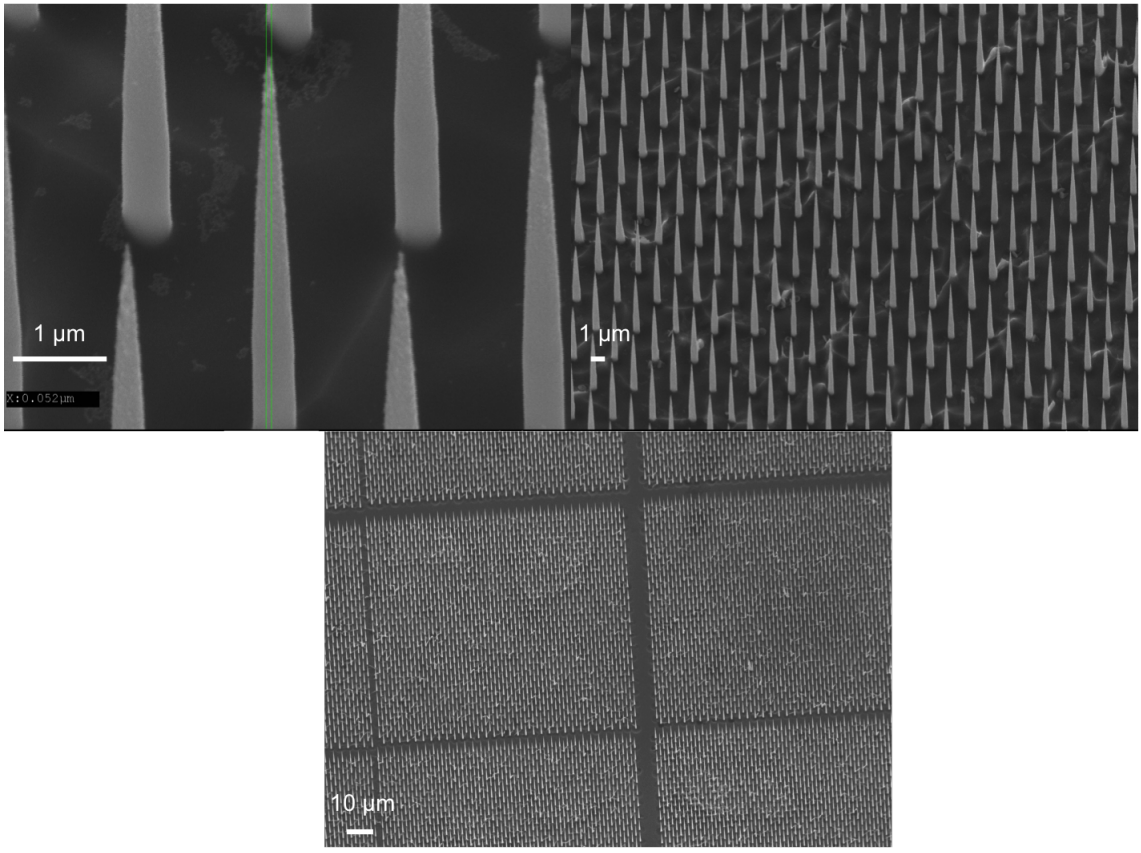

FIGURE 4.26

FIGURE 4.26: Very sharp, high aspect ratio Si pillars fabricated by reactive ion etching represent a potential substrate for further ECC development. These pillars more closely resemble the Si substrate used to manufacture the first ECC iteration, whose sensing capabilities have not yet been recapitulated. (Images courtesy of Jeffrey Naughton)

system that integrates with the chip. Such a system would have wells for each reagent and wash buffer. Ideally, the end user would only have to add sample to begin the diagnostic test. Also problematic is the use of a desktop computer and a full-sized potentiostat for the electrochemical analysis. In order to make the analysis portable, a miniaturized platform built around a smart phone is necessary.

Integration of the ECC with a portable, smart phone-based user interface, and a low-participation microfluidic system has the potential to make the ECC a powerful tool for POC cholera diagnostics. Additionally, the affinity of protein G for any IgG means that the assay can be used to detect any biomarkers for which antibodies are available. This opens up the possibility for detection of numerous other diseases of poverty.

4.9 Summary

Nanocoaxial-based sensing devices were fabricated with surface features meant to overcome previous limitations. The WE core of the nanocoax was extended outside of the CE shield, in order to make the surface available for biofunctionalization. Additionally, the nanoscale gap between the WE and CE was maintained, which was previously shown to confer sensing advantages to nanocoaxes (*127*). These new ECC chips were compared to the standard set by the non-ECC in terms of electrical performance and off-chip sensing abilities. The ECC demonstrated the ability to detect 4-AP, the end product of an electrochemical ELISA. Further, it was able to match the sensitivity towards CTX in an off-chip setup set by the non-ECC, of 1 ng mL^{-1}. This detection limit is comparable to a standard optical ELISA.

The ECC had numerous advantages over the non-ECC, however, which allowed for improved sensing features. The ECC did not experience any signal degradation in between uses, which the non-ECC experienced to a significant degree (~150 μA to ~25 μA). Additionally, the ECC demonstrated amenability toward biofunctionalization using a thiolated protein G to tether a primary ELISA antibody. This biofunctionalization strategy was employed to obtain preliminary data suggesting that the ECC is a more sensitive LOC than a simpler dendritic gold or planar gold architecture, based on current density.

With further development, including the manufacture of more sophisticated chip

housing which incorporates microfluidics and a portable analysis system, the ECC is an attractive candidate for LOC detection of infectious disease biomarkers which may meet A.S.S.U.R.E.D. diagnostics.

Chapter 5

Discussion and concluding remarks

POC use of a standard optical ELISA is limited by the necessity for non-portable, complex instrumentation, which requires a centralized diagnostic facility and trained personnel to perform. Previous work established an electrochemical ELISA assay which was able to match an optical ELISA with regards to CTX detection limit in an off-chip format. That is, the optical and the electrochemical ELISA were both performed in a microtiter plate, with the electrochemical product 4-AP later added to a nanocoaxial array for redox. Architectural features of this nanocoax limited its use to only off-chip applications. In this work, two other architectures, the gold dendrite array, and the extended core nanocoax, were explored for their utility as LOC sensors for the detection of CTX with an electrochemical ELISA. By performing the assay on a miniaturized on-chip platform, these nanoarchitectures hold the potential to be highly portable, low-cost and user-friendly alternatives to an optical ELISA, while maintaining a comparable diagnostic sensitivity. Due to these advantages, both gold dendrites and the ECC are promising candidates for further development into fully integrated LOC

biosensors. A summary of cholera detection by the various methods employed in this thesis is shown in table 5.1.

TABLE 5.1: CTX detection methods

Detection method	**Sensing Area (mm^2)**	**Detection Limit (ng/mL)**
Optical	320	1
Planar LOC	19	100
Dendrite LOC	4	1
Non-ECC off chip	1.8	2
ECC off-chip	0.049	1

5.1 Dendrites

In this study, we sought to improve upon the sensitivity of a simple planar gold architecture by increasing its surface area. This was accomplished through the growth of nanostructured gold crystals on a planar gold electrode using a facile, one-step method called DENA. Our results represent the first use of a gold dendrite architecture functionalized with conductive polymer (PCEPy) for the electrochemical immunodetection of CTX. This novel platform eliminates the necessity for expensive and sophisticated optical instrumentation frequently required for state-of-the-art diagnostics. Moreover, it represents a significant reduction in reagent consumption, especially when compared to a standard optical ELISA. While a standard ELISA in a microtiter plate requires 100 μl of each antibody, here we have been able to reduce that to ~30 μl, with the potential to reduce further to the nL range with a more sophisticated chip housing incorporating microfluidic channels. As a result, the cost of this protocol per assay is lower compared to an optical ELISA. Additionally, the small size of the electrode and its simple electrochemical readout allows the device to maintain a high degree of portability. Its low power needs (in the μW range) means that analysis can be performed using a smart phone. This opens up the possibility for the creation of a user-friendly interface, which lessens the impact of human error in misdiagnoses.

While these chips did not have nanoscale proximity of the WE and CE, increasing electrode surface area is a frequently employed strategy for maintaining sensitivity on miniaturized platforms (*194*, *195*). This has included the use of high-roughness electrodes (such as highly porous Pt films) (*196*), nanoparticles (*197*), nanotubes (*197*, *198*), and nanorods (*199*), as just a few examples of sensor modifications that result in and increase in effective sensing area without increasing geometric area. In fact, similar to the strategy explored in this thesis, Wang, *et. al.* used a polypyrrole coating on their high-surface area Pt electrode to create a sensitive glucose detector, by immobilizing GOx within the polymer film (*196*). An increase in sensitivity was directly attributable to the increased surface area, which facilitated the capture of a greater number of sensing components on the electrode than would be possible on a planar surface.

DENA in particular has proven to be a popular means of easily increasing sensor surface area. Most DENA studies have focused on explorations of fabrication parameters (*148*, *153*–*155*, *200*), but several proof-of-concept biosensors based on this platform have been reported. Soleymani, *et. al.* have used dendrites to rapidly detect bacterial mRNA (*201*), while Fang, *et. al.* were able to detect cancer biomarkers on a multiplexed nanostructured electrode (*202*). Infectious disease biomarkers have also been detected using dendritic architectures, including HIV and rubella (*158*, *203*).

We have focused our work on the detection of CTX using a dendritic array. A popular method for LOC cholera detection is to exploit the affinity of CTX for

GM1 gangliosides (*9*, *90*, *204–206*). However, antibodies may be more desirable capture elements for POC applications compared to GM1, both because the sialic acid (Neu5Ac) glycosidic linkage is labile (*207*), and thus less amenable to POC deployment, and because the use of GM1 severely limits the scope of use of the sensor to only those toxins which interact with it.

While numerous commercial rapid diagnostic assays have been developed as alternative detection methods for cholera, only a few have been found to hold promise for POC applications (*16*). These diagnostics tend to fall into two categories: agglutination or colorimetric immunoassays. The major drawback of such tests is the possibility for inconclusive results due to their readout mechanism. For example, in their assessment of one such tool, Ley, *et. al.* found that a major source of error came from users misinterpreting the lines on colorimetric assays (*21*). For this reason, we chose to focus on an electrochemical detection method for its ability to directly transduce biological events into a simple electrical readout.

PCEPy was chosen for antibody tethering because use of intrinsically conductive polypyrroles is popular and widespread in biosensing applications (*208*, *209*). Other strategies for tethering antibodies to electrodes for biosensing applications have been reported, including using self-assembled monolayers (*210*, *211*), hydrogels (*212*), coated beads (*9*, *213*) and avadin-strepdavadin binding (*214*). However, the ease and gentle conditions of polypyrrole polymerization, as well as the electroconductive stability of the film, make polypyrrole a more attractive

tool for fabrication of LOC devices with POC utility (*215*). As a result, pyrrole and its derivatives have been used in biosensors ranging from neural probes (*216*), to glucose sensing devices (*217*) and DNA biosensors (*218*). When combined with antibodies as a biorecognition element, N-substituted polypyrroles with terminal cyano groups (such as PCEPy) have been utilized to construct immunosensors via electrostatic (*102*) and electrochemically-directed (*103*) tethering of antibodies to the surface of gold electrodes. In both cases, interactions between antibody OH groups and the terminal CN group of the polymer film were used to tether the antibody to the electrode surface. This afforded a higher level of control over the antibody orientation than would be possible on a bare gold substrate, which is important in order to preserve the availability of the antigen-sensing region for analyte recognition.

5.2 Extended core nanocoax

We report progress on a novel nanoarchitecture, the extended core nanocoax (ECC) that has applicability for the detection of biomarkers as a LOC device. This work sought to improve upon a non-ECC nanocoax for the detection of CTX. The architecture represents a vertically oriented nanocoax comprised of a gold inner metal core that extends ~200 nm above a chrome outer metal shield, separated by a dielectric annulus. Each ECC chip contains 7 discrete sensing arrays, 0.049 mm^2 in size, containing ~30,000 nanoscale coaxes connected in

parallel. The non-ECC demonstrated a detection limit of 2 ng mL^{-1} of CTX using an off-chip setup. This sensitivity compares favorably to the standard optical ELISA used in clinical settings. The ECC matches this limit, but additionally offers the benefit of biofunctionalization on the extended gold core.

The ECC is a nanogap biosensor device. Nanogap devices provide attractive prospects for the development of ultrasensitive diagnostic tools, and much attention has been given to those based on field-effect (FET), impedance, or capacitive sensing, where entrapped biomolecules will cause a change the electrical behavior between the electrodes (*219*, *220*) . In this study, we have used an amperometric method in order to exploit a unique electrical behavior of nanogap electrodes, wherein the nanoscale proximity of the WE and CE in these devices potentially allows for increases in sensitivity through the phenomenon of redox cycling. Redox cycling has proven to be an efficient amplification strategy when dealing with redox active molecules, especially when these molecules are in a low concentration (*221*). For example, redox cycling has been an important strategy for detecting the oxidation of neurotransmitter molecules contained within vesicles (*188*). Exploiting this phenomenon relies on the development of architectures that miniaturize and closely integrate electrodes. We therefore have developed the ECC as a nanogap sensor which enhances redox activity through the nanoscale proximity of a working and counter electrode.

Alkaline phosphatase (ALP) is an extremely common reporter for amplified biomolecule detection (*222*–*225*). As such, ALP has also found use in nanogap

electrode systems because of its high turnover frequency and high reaction selectivity (*226*). For example, Hall, *et. al.* fabricated a nanogap-based transducer array utilizing an ALP reporter as a novel DNA sequencing platform (*227*). ALP was similarly employed in our studies.

ECC fabrication aimed to address architectural demands dictated by the electrochemical performance of the non-ECC. Briefly, electrochemical function of the non-ECC was reliant on fluids entering the annulus gap between the WE and the CE. The size of this gap presented several issues, including difficulties in fluid exchange and in diffusion of reagents. For LOC utility, it is necessary to be able to biofunctionalize the chip surface, which requires numerous reagent and wash buffer applications. As a result, the non-ECC did not possess LOC potential, and was relegated to off-chip detection. By contrast, the ECC maintains the nanocoaxial architecture, and thus also maintains the nanoscale proximity of the WE and CE, but the WE has been extended ~200 nm above the CE, and the depth of the annulus gap has been lessened. It was anticipated that these features would decrease the surface tension which we believe prevented fluid exchange, while additionally providing significantly more gold surface area for potential biofunctionalization (*228*, *229*).

Indeed, the ECC demonstrated several performance advantages over the non-ECC. First, we showed that the ECC demonstrated a higher degree of consistency in response to FCA redox than its predecessor. Its electrochemical performance was also superior to the non-ECC when comparing current density; that

is, the ECC can detect more current over a smaller area than the non-ECC. The ECC has proven to be more robust than the non-ECC, by demonstrating a high degree of re-usability and maintaining electrochemical integrity over repeated use. In a comparison of off-chip ELISA results, the ECC matches the detection limit of the non-ECC, which is comparable to a standard optical ELISA. Finally, we were able to obtain visual and preliminary electrochemical data suggesting that the extended gold core is amenable to functionalization with antibodies using a thiolated protein G as an intermediate tethering protein. Protein G was chosen due to its ability to correctly orient antibodies with their Fab away from the sensor surface, because of an affinity to bind the Fc. Taken together, this data makes a strong argument for the use of ECC chips as LOC detectors of infectious disease biomarkers. Further development, including improvements towards portability and automation, could produce a device capable of meeting POC demands.

5.3 A.S.S.U.R.E.D. diagnostics

For both platforms to find utility as fully realized POC devices, it is necessary to address the A.S.S.U.R.E.D. concerns set forth by the WHO (*230*). We believe that the surface architectures and assays detailed herein are capable of meeting most of the needs dictated by the unique environment of low-resource locations, which is created by a limitations in funding, infrastructure, and/or trained personnel. In regards to cholera specifically, all of these factors play a large part

in its endemic presence in over 50 countries, in addition to its frequent reemergence as an epidemic. Limited sanitation infrastructure leads to contaminated drinking water, which is consumed by people who are frequently malnourished, allowing cholera to survive the stomach to colonize the intestines. Widespread infection and numerous deaths weakens the workforce, contributing to poverty, which hinders infrastructure improvements. For endemic countries, being locked in this cycle has allowed one outbreak of cholera to persist for close to 60 years (*231*).

The WHO criteria for affordability puts a constraint of $500.00 per machine used, and $10.00 per test. Despite the use of gold in both the dendritic array and the ECC, the largest cost associated with their manufacture is manpower. It is conceivable that scaling up the fabrication process would allow for this $10 target to be met. We propose that analysis be performed with the use of a smartphone, which are increasingly common even in resource-limited settings, which would fall well beneath the threshold of $500.00.

As detailed herein, the dendritic array is capable of matching a popular diagnostic standard, the optical ELISA, for sensitivity toward CTX (sensing at 1 ng mL^{-1}). Specificity is measured in regards to correctly identifying individuals who are disease-free, which would necessitate clinical samples to accurately assess (*232*). For the purposes of our study, our assays showed high specificity towards samples of CTX diluted in a BSA containing buffer.

In regards to user-friendliness, the WHO suggests that it take no more than 1 to 2 days to train personnel to use a device. While that is not possible in the current iteration of our assays, we propose to develop a user-friendly interface based on a smartphone which could guide users through a testing procedure. Additionally, the electrical readout afforded by the electrochemical assay we have developed would give simple results, uncomplicated by optical interpretations. We believe this will reduce diagnostic error which result from human involvement.

Demands for rapidity and robustness are that tests take no more than 30 minutes, utilize a minimum amount of consumables (*i.e.* pipette tips), and have a shelf life of a year. Given the necessity for thorough antibody binding, an ELISA is not capable of meeting this timing demand. It is conceivable that the sandwich ELISA used in our assay could be reduced to 2 antibodies, which would cut an hour from analysis time. In its current iteration, many consumables in the form of pipette tips are necessary. Moving forward, a microfluidics system would eliminate most or all of this waste, making the only consumable the chip itself. Shelf life has not yet been examined for either functionalized dendrites or functionalized ECCs. However, both chips are physically very robust, and able to maintain function despite abundant handling and prolonged storage (longer than a year).

Equipment-free means that a device should be compact, battery-powered (allowing for on-site analysis and easy handling), and disposable. Chips are not

fabricated with any toxic components, and so would not present an issue for disposal. As stated previously, the electrochemical ELISA represents an assay with low power needs. It is entirely possible for all necessary power to be provided through a smartphone USB port. The potentiostat can be likewise be replaced with either a hand-held potentiostat (*233*), or even more portable, a commercially available potentiostat module (*234*). This also contributes to the last WHO demand, which is for a device to be deliverable (*i.e.* portable and hand-held).

5.4 Future scope

To be amenable to real-world deployment, a number of issues must be addressed for each sensing platform. For dendrites, the first is the highly variable nature of dendrite growth, which can result in inconsistencies in peak current chip-to-chip. We believe that growing dendrites on a pillar array, or indeed even ECC arrays, may result in more homogeneous crystal formation. This may be due to both the concentration of electric fields at sharp edges, as well as the fact that the tip of a pillar array would extend into the $HAuCl_4$ solution, meaning crystals will preferentially form there faster. From there, we can optimize the deposition time to isolate crystal growth largely to the core. A dendritic ECC chip may even represent a significantly more sensitive device, by combining the nanoscale proximity of the WE and the CE with an increase in surface area.

The process of reagent application and washing must also be addressed. In its

current iteration, all steps must be done by hand, which is far too laborious to have true POC utility. A microfluidic channel system should be fabricated which allows for analysis with just sample application, such as that fabricated by Numthuam, *et. al.*, which was similarly used for an electrochemical ELISA (*235*). Their work additionally showed that in a microfluidic device, a planar electrode is only exposed to about half as much analyte as a pillar architecture, which makes an argument for the utility of a dendritic electrode in such a setup.

Finally, a strategy towards either drastically reducing primary antibody tethering time, or alternatively preserving pre-tethered antibodies should be explored. As the protocol currently stands, a chip requires 48 hours of primary antibody incubation for sufficient electrostatic bonding to occur. If this step were to be hypothetically completed in manufacture, the chip must be kept wet and refrigerated until it reaches the end user, which is not a desirable feature for a POC tool as the WHO suggests tools not need to maintain a cold chain. Instead, embedding antibodies within the pyrrole matrix can be explored, which has been used for immobilizing sensing components (*114*, *236*). This method is not without its own drawbacks, such as a lack of directed orientation of antibodies, which can impact sensitivity. Antibody could also be stored as a lyophilized state on the sensing region and re-hydrated at the site of the patient. Such a strategy would necessitate a faster binding protocol than the electrostatic one detailed here.

For ECC chips, the drawbacks are nearly identical. The same need for miniaturizing and automating analysis persists, given the similarity of the electrochemical setup. Issues related to manufacturing inconsistencies must be addressed. It is speculated that scaling up the process may aid this aim, as currently ECCs are made stepwise, one at a time. This is likely where chip-to-chip variability issues arise. Intra-chip variabilities remain an issue, whose cause is currently unknown. Further investigation may reveal why arrays within the same chip do not show the same FCA response, and provide an avenue to remedy this problem. Functionalization of ECCs presents the same issue seen in dendrites where the protein must remain wet and refrigerated. However, the protein G tethering protocol only takes 2 hours, and so there is some potential for on-site rehydration as an alternative.

While numerous, these issues are not insurmountable, and indeed have already been overcome by numerous ELISA LOC-type platforms (*31*, *35*, *237*–*239*). Low-cost, POC diagnosis has the potential to be the intervention necessary to achieve the WHO's goal of a 90% reduction in cholera cases in the next decade. With further development, these architectures may be able to provide invaluable quantitative epidemiological data to areas locked in an endless disease cycle.

Bibliography

(*1*) Global Taskforce on Cholera Control. "Ending Cholera: A Global Roadmap to 2030". In: *WHO* (Oct. 2017). URL: http://www.who.int/cholera/publications/global-roadmap/en/ (visited on 07/24/2018).

(*2*) Dalong Hu et al. "Origins of the current seventh cholera pandemic". en. In: *Proceedings of the National Academy of Sciences* (Nov. 2016), p. 201608732. ISSN: 0027-8424, 1091-6490. DOI: 10.1073/pnas.1608732113. URL: http://www.pnas.org/content/early/2016/11/08/1608732113.

(*3*) Justin Lessler et al. "Mapping the burden of cholera in sub-Saharan Africa and implications for control: an analysis of data across geographical scales". English. In: *The Lancet* 391.10133 (May 2018), pp. 1908–1915. ISSN: 0140-6736, 1474-547X. DOI: 10.1016/S0140-6736(17)33050-7. URL: https://www.thelancet.com/journals/lancet/article/PIIS0140-6736(17)33050-7/abstract.

(*4*) Jason B Harris et al. "Cholera". In: *The Lancet* 379.9835 (June 2012), pp. 2466–2476. ISSN: 0140-6736. DOI: 10.1016/S0140-6736(12)

60436-X. URL: http://www.sciencedirect.com/science/article/pii/S014067361260436X.

(*5*) Richard A. Finkelstein. "Cholera, Vibrio cholerae O1 and O139, and Other Pathogenic Vibrios". eng. In: *Medical Microbiology*. Ed. by Samuel Baron. 4th. Galveston (TX): University of Texas Medical Branch at Galveston, 1996. ISBN: 978-0-9631172-1-2. URL: http://www.ncbi.nlm.nih.gov/books/NBK8407/.

(*6*) R. H. Gilman et al. "Decreased gastric acid secretion and bacterial colonization of the stomach in severely malnourished Bangladeshi children". eng. In: *Gastroenterology* 94.6 (June 1988), pp. 1308–1314. ISSN: 0016-5085.

(*7*) Kaushik Bharati and Nirmal K. Ganguly. "Cholera toxin: A paradigm of a multifunctional protein". In: *The Indian Journal of Medical Research* 133.2 (Feb. 2011), pp. 179–187. ISSN: 0971-5916. URL: https://www.ncbi.nlm.nih.gov/pmc/articles/PMC3089049/.

(*8*) David C. Gadsby, Paola Vergani, and László Csanády. "The ABC protein turned chloride channel whose failure causes cystic fibrosis". In: *Nature* 440.7083 (Mar. 2006), pp. 477–483. ISSN: 0028-0836. DOI: 10.1038/nature04712. URL: https://www.ncbi.nlm.nih.gov/pmc/articles/PMC2720541/.

(*9*) Natinan Bunyakul et al. "Cholera toxin subunit B detection in microfluidic devices". eng. In: *Analytical and Bioanalytical Chemistry* 393.1 (Jan. 2009), pp. 177–186. ISSN: 1618-2650. DOI: 10.1007/s00216-008-2364-6.

(*10*) Mohammad Ali et al. “The global burden of cholera”. eng. In: *Bulletin of the World Health Organization* 90.3 (Mar. 2012), 209–218A. ISSN: 1564-0604. DOI: 10.2471/BLT.11.093427.

(*11*) Consuelo Mendoza et al. “Preparing Health Care Workers for a Cholera Epidemic, Dominican Republic, 2010”. In: *Emerging Infectious Diseases* 17.11 (Nov. 2011), pp. 2177–2178. ISSN: 1080-6040. DOI: 10.3201/eid1711.110703. URL: https://www.ncbi.nlm.nih.gov/pmc/articles/PMC3310570/.

(*12*) Geik Yong Ang, Choo Yee Yu, and Yean Yean Chan. *The hurdles in making diagnostics accessible to the bottom billions: can lateral flow immunoassays make a difference?* URL: http://www.kck.usm.my/diagnosticbook/sites/default/files/Chapter_3%2C2_the_hurdles_in_making_accesible_diagnostics.pdf.

(*13*) Hannah Kettler, Karen White, and Sarah Hawkes. *Mapping the landscape of diagnostics for sexually transmitted infections*. 2004. URL: http://www.who.int/tdr/publications/documents/mapping-landscape-sti.pdf.

(*14*) *Diagnosis and Detection | Cholera | CDC*. en-us. May 2018. URL: https://www.cdc.gov/cholera/diagnosis.html.

(*15*) David Mabey et al. “Diagnostics for the developing world”. eng. In: *Nature Reviews. Microbiology* 2.3 (Mar. 2004), pp. 231–240. ISSN: 1740-1526. DOI: 10.1038/nrmicro841.

(*16*) Michal H. Dick et al. "Review of two decades of cholera diagnostics–how far have we really come?" eng. In: *PLoS neglected tropical diseases* 6.10 (2012), e1845. ISSN: 1935-2735. DOI: 10.1371/journal.pntd.0001845.

(*17*) Paul Yager, Gonzalo J. Domingo, and John Gerdes. "Point-of-Care Diagnostics for Global Health". In: *Annual Review of Biomedical Engineering* 10.1 (2008), pp. 107–144. DOI: 10.1146/annurev.bioeng.10.061807.160524. URL: https://doi.org/10.1146/annurev.bioeng.10.061807.160524.

(*18*) Henk L. Smits et al. "Lateral-Flow Assay for Rapid Serodiagnosis of Human Leptospirosis". In: *Clinical and Diagnostic Laboratory Immunology* 8.1 (Jan. 2001), pp. 166–169. ISSN: 1071-412X. DOI: 10.1128/CDLI.8.1.166-169.2001. URL: https://www.ncbi.nlm.nih.gov/pmc/articles/PMC96027/.

(*19*) Geertruida A. Posthuma-Trumpie, Jakob Korf, and Aart van Amerongen. "Lateral flow (immuno)assay: its strengths, weaknesses, opportunities and threats. A literature survey". eng. In: *Analytical and Bioanalytical Chemistry* 393.2 (Jan. 2009), pp. 569–582. ISSN: 1618-2650. DOI: 10.1007/s00216-008-2287-2.

(*20*) Muhammad Sajid, Abdel-Nasser Kawde, and Muhammad Daud. "Designs, formats and applications of lateral flow assay: A literature review". In: *Journal of Saudi Chemical Society* 19.6 (Nov. 2015), pp. 689–705. ISSN: 1319-6103. DOI: 10.1016/j.jscs.2014.09.001.

URL: http://www.sciencedirect.com/science/article/pii/S131961031400129X.

(*21*) Benedikt Ley et al. "Evaluation of a Rapid Dipstick (Crystal VC) for the Diagnosis of Cholera in Zanzibar and a Comparison with Previous Studies". en. In: *PLOS ONE* 7.5 (May 2012), e36930. ISSN: 1932-6203. DOI: 10.1371/journal.pone.0036930. URL: http://journals.plos.org/plosone/article?id=10.1371/journal.pone.0036930.

(*22*) Wilfredo R. Matias et al. "Laboratory evaluation of immunochromatographic rapid diagnostic tests for cholera in Haiti". en. In: *PLOS ONE* 12.11 (Nov. 2017), e0186710. ISSN: 1932-6203. DOI: 10.1371/journal.pone.0186710. URL: http://journals.plos.org/plosone/article?id=10.1371/journal.pone.0186710.

(*23*) David A. Sack. *Learn How to Use the Crystal VC Dipstick Test to Detect Vibrio Cholera in Our New Video | DOVE: Stop Cholera*. Jan. 2017. URL: https://www.stopcholera.org/blog/learn-how-use-crystal-vc-dipstick-test-detect-vibrio-cholera-our-new-video.

(*24*) M. Mkandawire. "From biosensors to lab-on-chip: Developing chip-based biosensors for environmental and clinical applications". In: *2012 5th International Conference on Computers and Devices for Communication (CODEC)*. Dec. 2012, pp. 1–1. DOI: 10.1109/CODEC.2012.6509267.

(*25*) Ruchika Malhotra et al. "Ultrasensitive detection of cancer biomarkers in the clinic by use of a nanostructured microfluidic array". eng. In: *Analytical Chemistry* 84.14 (July 2012), pp. 6249–6255. ISSN: 1520-6882. DOI: 10.1021/ac301392g.

(*26*) Timothy R. Kline et al. "ABO, D Blood Typing and Subtyping Using Plug-Based Microfluidics". In: *Analytical Chemistry* 80.16 (Aug. 2008), pp. 6190–6197. ISSN: 0003-2700. DOI: 10.1021/ac800485q. URL: https://doi.org/10.1021/ac800485q.

(*27*) Lidong Qin et al. "Self-powered microfluidic chips for multiplexed protein assays from whole blood". en. In: *Lab on a Chip* 9.14 (2009), pp. 2016–2020. DOI: 10.1039/B821247C. URL: https://pubs.rsc.org/en/content/articlelanding/2009/lc/b821247c.

(*28*) Vijay Srinivasan, Vamsee K. Pamula, and Richard B. Fair. "An integrated digital microfluidic lab-on-a-chip for clinical diagnostics on human physiological fluids". en. In: *Lab on a Chip* 4.4 (2004), pp. 310–315. DOI: 10.1039/B403341H. URL: https://pubs.rsc.org/en/content/articlelanding/2004/lc/b403341h.

(*29*) Cheuk W. Kan et al. "Isolation and detection of single molecules on paramagnetic beads using sequential fluid flows in microfabricated polymer array assemblies". eng. In: *Lab on a Chip* 12.5 (Mar. 2012), pp. 977–985. ISSN: 1473-0189. DOI: 10.1039/c2lc20744c.

(*30*) Dingbin Liu et al. "Glucose oxidase-catalyzed growth of gold nanoparticles enables quantitative detection of attomolar cancer biomarkers". eng.

In: *Analytical Chemistry* 86.12 (June 2014), pp. 5800–5806. ISSN: 1520-6882. DOI: 10.1021/ac500478g.

(*31*) Jeong-Yeol Yoon et al. "Lab-on-a-Chip Pathogen Sensors for Food Safety". en. In: *Sensors* 12.8 (Aug. 2012), pp. 10713–10741. DOI: 10.3390/s120810713. URL: http://www.mdpi.com/1424-8220/12/8/10713.

(*32*) Christos Kokkinos, Anastasios Economou, and Ioannis Raptis. "Microfabricated disposable lab-on-a-chip sensors with integrated bismuth microelectrode arrays for voltammetric determination of trace metals". In: *Analytica Chimica Acta* 710 (Jan. 2012), pp. 1–8. ISSN: 0003-2670. DOI: 10.1016/j.aca.2011.10.048. URL: http://www.sciencedirect.com/science/article/pii/S0003267011014280.

(*33*) Am Jang et al. "State-of-the-art lab chip sensors for environmental water monitoring". en. In: *Measurement Science and Technology* 22.3 (2011), p. 032001. ISSN: 0957-0233. DOI: 10.1088/0957-0233/22/3/032001. URL: http://stacks.iop.org/0957-0233/22/i=3/a=032001.

(*34*) Petra S. Dittrich, Kaoru Tachikawa, and Andreas Manz. "Micro total analysis systems. Latest advancements and trends". eng. In: *Analytical Chemistry* 78.12 (June 2006), pp. 3887–3908. ISSN: 0003-2700. DOI: 10.1021/ac0605602.

(*35*) Curtis D. Chin, Vincent Linder, and Samuel K. Sia. "Lab-on-a-chip devices for global health: Past studies and future opportunities". en. In: *Lab on a Chip* 7.1 (Dec. 2006), pp. 41–57. ISSN: 1473-0189. DOI: 10.

1039/B611455E. URL: https://pubs.rsc.org/en/content/articlelanding/2007/lc/b611455e.

(*36*) Angel Rios, Mohammed Zougagh, and Monica Avila. "Miniaturization through lab-on-a-chip: Utopia or reality for routine laboratories? A review". In: *Analytica Chimica Acta* 740 (Aug. 2012), pp. 1–11. ISSN: 0003-2670. DOI: 10.1016/j.aca.2012.06.024. URL: http://www.sciencedirect.com/science/article/pii/S0003267012008926.

(*37*) Darwin R. Reyes et al. "Micro Total Analysis Systems. 1. Introduction, Theory, and Technology". In: *Analytical Chemistry* 74.12 (June 2002), pp. 2623–2636. ISSN: 0003-2700. DOI: 10.1021/ac0202435. URL: https://doi.org/10.1021/ac0202435.

(*38*) George M. Whitesides. *The origins and the future of microfluidics*. en. Special Features. July 2006. DOI: 10.1038/nature05058. URL: https://www.nature.com/articles/nature05058.

(*39*) Elodie Sollier et al. "Rapid prototyping polymers for microfluidic devices and high pressure injections". en. In: *Lab on a Chip* 11.22 (2011), pp. 3752–3765. DOI: 10.1039/C1LC20514E. URL: https://pubs.rsc.org/en/content/articlelanding/2011/lc/c1lc20514e.

(*40*) Carston Haber. "Microfluidics in commercial applications; an industry perspective". en. In: *Lab on a Chip* 6.9 (2006), pp. 1118–1121. DOI: 10.1039/B610250F. URL: https://pubs.rsc.org/en/content/articlelanding/2006/lc/b610250f.

(*41*) Richard S. Gaster, Drew A. Hall, and Shan X. Wang. "nanoLAB: An ultraportable, handheld diagnostic laboratory for global health". en. In: *Lab on a Chip* 11.5 (Mar. 2011), pp. 950–956. ISSN: 1473-0189. DOI: 10.1039/C0LC00534G. URL: https://pubs.rsc.org/en/content/articlelanding/2011/lc/c0lc00534g.

(*42*) Arjan Floris et al. "A prefilled, ready-to-use electrophoresis based lab-on-a-chip device for monitoring lithium in blood". en. In: *Lab on a Chip* 10.14 (2010), pp. 1799–1806. DOI: 10.1039/C003899G. URL: https://pubs.rsc.org/en/content/articlelanding/2010/lc/c003899g.

(*43*) Beom Seok Lee et al. "Fully integrated lab-on-a-disc for simultaneous analysis of biochemistry and immunoassay from whole blood". en. In: *Lab on a Chip* 11.1 (2011), pp. 70–78. DOI: 10.1039/C0LC00205D. URL: https://pubs.rsc.org/en/content/articlelanding/2011/lc/c0lc00205d.

(*44*) C. H. Ahn et al. "Disposable smart lab on a chip for point-of-care clinical diagnostics". In: *Proceedings of the IEEE* 92.1 (Jan. 2004), pp. 154–173. ISSN: 0018-9219. DOI: 10.1109/JPROC.2003.820548.

(*45*) Christian Kellner et al. "Automated microsystem for electrochemical detection of cancer markers". eng. In: *Electrophoresis* 32.8 (Apr. 2011), pp. 926–930. ISSN: 1522-2683. DOI: 10.1002/elps.201000667.

(*46*) Michelle L. Kovarik et al. "Micro Total Analysis Systems for Cell Biology and Biochemical Assays". In: *Analytical Chemistry* 84.2 (Jan.

2012), pp. 516–540. ISSN: 0003-2700. DOI: 10.1021/ac202611x. URL: https://doi.org/10.1021/ac202611x.

(*47*) Mazher-Iqbal Mohammed and Marc P. Y. Desmulliez. "Lab-on-a-chip based immunosensor principles and technologies for the detection of cardiac biomarkers : a review". en. In: *Lab on a Chip* 11.4 (2011), pp. 569–595. DOI: 10.1039/C0LC00204F. URL: https://pubs.rsc.org/en/content/articlelanding/2011/lc/c0lc00204f.

(*48*) W. C. Chan and S. Nie. "Quantum dot bioconjugates for ultrasensitive nonisotopic detection". eng. In: *Science (New York, N.Y.)* 281.5385 (Sept. 1998), pp. 2016–2018. ISSN: 0036-8075.

(*49*) Jesse V. Jokerst et al. "Nano-bio-chips for high performance multiplexed protein detection: Determinations of cancer biomarkers in serum and saliva using quantum dot bioconjugate labels". In: *Biosensors and Bioelectronics* 24.12 (Aug. 2009), pp. 3622–3629. ISSN: 0956-5663. DOI: 10.1016/j.bios.2009.05.026. URL: http://www.sciencedirect.com/science/article/pii/S095656630900284X.

(*50*) *Quantum Dots Explained: What they are and why they're awesome*. en-US. Feb. 2014. URL: https://www.trustedreviews.com/opinion/quantum-dots-explained-what-they-are-and-why-they-re-awesome-2916068.

(*51*) *Quantum Dots*. en-US. URL: http://www.nanosysinc.com/what-we-do/quantum-dots/.

(*52*) Mei Hu et al. "Ultrasensitive, Multiplexed Detection of Cancer Biomarkers Directly in Serum by Using a Quantum Dot-Based Microfluidic Protein Chip". In: *ACS Nano* 4.1 (Jan. 2010), pp. 488–494. ISSN: 1936-0851. DOI: 10.1021/nn901404h. URL: https://doi.org/10.1021/nn901404h.

(*53*) *The Pros and Cons of Quantum Dots*. URL: https://www.brighthubengineering.com/manufacturing-technology/89345-quantum-dots-advantages-and-disadvantages/.

(*54*) Da-Shin Wang and Shih-Kang Fan. "Microfluidic Surface Plasmon Resonance Sensors: From Principles to Point-of-Care Applications". In: *Sensors (Basel, Switzerland)* 16.8 (July 2016). ISSN: 1424-8220. DOI: 10.3390/s16081175. URL: https://www.ncbi.nlm.nih.gov/pmc/articles/PMC5017341/.

(*55*) X. D. Hoa, A. G. Kirk, and M. Tabrizian. "Towards integrated and sensitive surface plasmon resonance biosensors: A review of recent progress". In: *Biosensors and Bioelectronics* 23.2 (Sept. 2007), pp. 151–160. ISSN: 0956-5663. DOI: 10.1016/j.bios.2007.07.001. URL: http://www.sciencedirect.com/science/article/pii/S0956566307002710.

(*56*) Susie Eustis and Mostafa A. el-Sayed. "Why gold nanoparticles are more precious than pretty gold: noble metal surface plasmon resonance and its enhancement of the radiative and nonradiative properties of nanocrystals of different shapes". eng. In: *Chemical Society Reviews* 35.3 (Mar. 2006), pp. 209–217. ISSN: 0306-0012. DOI: 10.1039/b514191e.

(*57*) Weihai Ni et al. “Tailoring longitudinal surface plasmon wavelengths, scattering and absorption cross sections of gold nanorods”. eng. In: *ACS nano* 2.4 (Apr. 2008), pp. 677–686. ISSN: 1936-086X. DOI: 10.1021/nn7003603.

(*58*) A. Bouhelier et al. “Surface plasmon characteristics of tunable photoluminescence in single gold nanorods”. eng. In: *Physical Review Letters* 95.26 (Dec. 2005), p. 267405. ISSN: 0031-9007. DOI: 10.1103/PhysRevLett.95.267405.

(*59*) S. L. Smitha et al. “Studies on surface plasmon resonance and photoluminescence of silver nanoparticles”. eng. In: *Spectrochimica Acta. Part A, Molecular and Biomolecular Spectroscopy* 71.1 (Nov. 2008), pp. 186–190. ISSN: 1386-1425. DOI: 10.1016/j.saa.2007.12.002.

(*60*) General Electric Healthcare Lifescience. *Biacore 8K*. en. URL: https://www.gelifesciences.com/en/pt/shop/protein-analysis/spr-label-free-analysis/systems/biacore-8k-p-05540.

(*61*) Farid E. Ahmed et al. “Surface Plasmon Resonance (SPR) Spectrometry as a Tool to Analyze Nucleic Acid–Protein Interactions in Crude Cellular Extracts”. en. In: *Cancer Genomics - Proteomics* 7.6 (Nov. 2010), pp. 303–309. ISSN: 1109-6535, 1790-6245. URL: http://cgp.iiarjournals.org/content/7/6/303.

(*62*) Elisa Mariotti, Maria Minunni, and Marco Mascini. “Surface plasmon resonance biosensor for genetically modified organisms detection”. In:

Analytica Chimica Acta 453.2 (Feb. 2002), pp. 165–172. ISSN: 0003-2670. DOI: 10.1016/S0003-2670(01)01458-1. URL: http://www.sciencedirect.com/science/article/pii/S0003267001014581.

(*63*) A. Hassani and M. Skorobogatiy. "Design of the microstructured optical fiber-based surface plasmon resonance sensors with enhanced microfluidics". eng. In: *Optics Express* 14.24 (Nov. 2006), pp. 11616–11621. ISSN: 1094-4087.

(*64*) Kuo-Hoong Lee et al. "Microfluidic systems integrated with two-dimensional surface plasmon resonance phase imaging systems for microarray immunoassay". eng. In: *Biosensors & Bioelectronics* 23.4 (Nov. 2007), pp. 466–472. ISSN: 0956-5663. DOI: 10.1016/j.bios.2007.05.007.

(*65*) Onur Tokel et al. "Portable microfluidic integrated plasmonic platform for pathogen detection". eng. In: *Scientific Reports* 5 (Mar. 2015), p. 9152. ISSN: 2045-2322. DOI: 10.1038/srep09152.

(*66*) G. Krishnamoorthy. "Lab-on-a-Chip Surface Plasmon Resonance Biosensor for Multiplex Bioassays". Undefined. In: (Mar. 2010). DOI: 10.3990/1.9789036529952. URL: https://research.utwente.nl/en/publications/lab-on-a-chip-surface-plasmon-resonance-biosensor-for-multiplex-b-2.

(*67*) J. Breault-Turcot et al. "Single chip SPR and fluorescent ELISA assay of prostate specific antigen". eng. In: *Lab on a Chip* 15.23 (Dec. 2015), pp. 4433–4440. ISSN: 1473-0189. DOI: 10.1039/c5lc01045d.

(*68*) Dorothee Grieshaber et al. “Electrochemical Biosensors - Sensor Principles and Architectures”. In: *Sensors (Basel, Switzerland)* 8.3 (Mar. 2008), pp. 1400–1458. ISSN: 1424-8220. URL: https://www.ncbi.nlm.nih.gov/pmc/articles/PMC3663003/.

(*69*) Parikha Mehrotra. “Biosensors and their applications – A review”. In: *Journal of Oral Biology and Craniofacial Research* 6.2 (2016), pp. 153–159. ISSN: 2212-4268. DOI: 10.1016/j.jobcr.2015.12.002. URL: https://www.ncbi.nlm.nih.gov/pmc/articles/PMC4862100/.

(*70*) Jules L. Hammond et al. “Electrochemical biosensors and nanobiosensors”. In: *Essays in Biochemistry* 60.1 (June 2016), pp. 69–80. ISSN: 0071-1365. DOI: 10.1042/EBC20150008. URL: https://www.ncbi.nlm.nih.gov/pmc/articles/PMC4986461/.

(*71*) Nelson R. Stradiotto, Hideko Yamanaka, and Maria Valnice B. Zanoni. “Electrochemical sensors: a powerful tool in analytical chemistry”. In: *Journal of the Brazilian Chemical Society* 14.2 (Apr. 2003), pp. 159–173. ISSN: 0103-5053. DOI: 10.1590/S0103-50532003000200003. URL: http://www.scielo.br/scielo.php?script=sci_abstract&pid=S0103-50532003000200003&lng=en&nrm=iso&tlng=en.

(*72*) S. V. Dzyadevych et al. “Amperometric enzyme biosensors: Past, present and future”. In: *IRBM* 29.2 (Apr. 2008), pp. 171–180. ISSN: 1959-0318. DOI: 10.1016/j.rbmret.2007.11.007. URL: http://www.sciencedirect.com/science/article/pii/S1297956207001258.

(*73*) Eun-Hyung Yoo and Soo-Youn Lee. "Glucose Biosensors: An Overview of Use in Clinical Practice". In: *Sensors (Basel, Switzerland)* 10.5 (May 2010), pp. 4558–4576. ISSN: 1424-8220. DOI: 10.3390/s100504558. URL: https://www.ncbi.nlm.nih.gov/pmc/articles/PMC3292132/.

(*74*) G. G. Guilbault and G. J. Lubrano. "An enzyme electrode for the amperometric determination of glucose". In: *Analytica Chimica Acta* 64.3 (May 1973), pp. 439–455. ISSN: 0003-2670. DOI: 10.1016/S0003-2670(01)82476-4. URL: http://www.sciencedirect.com/science/article/pii/S0003267001824764.

(*75*) Joseph Wang. "Electrochemical Glucose Biosensors - Chemical Reviews". In: *ACS Chemical Reviews* 108.2 (2008), pp. 814–825. URL: https://pubs.acs.org/doi/abs/10.1021/cr068123a.

(*76*) Paul D'Orazio. "Biosensors in clinical chemistry". eng. In: *Clinica Chimica Acta; International Journal of Clinical Chemistry* 334.1-2 (Aug. 2003), pp. 41–69. ISSN: 0009-8981.

(*77*) Michael J. Schoning and Arshak Poghossian. "Recent advances in biologically sensitive field-effect transistors (BioFETs)". eng. In: *The Analyst* 127.9 (Sept. 2002), pp. 1137–1151. ISSN: 0003-2654.

(*78*) Asha Chaubey and B. D. Malhotra. "Mediated biosensors". eng. In: *Biosensors & Bioelectronics* 17.6-7 (June 2002), pp. 441–456. ISSN: 0956-5663.

(*79*) Joseph Wang, Guodong Liu, and M. Rasul Jan. "Ultrasensitive Electrical Biosensing of Proteins and DNA: Carbon-Nanotube Derived Amplification of the Recognition and Transduction Events". In: *Journal of the American Chemical Society* 126.10 (Mar. 2004), pp. 3010–3011. ISSN: 0002-7863. DOI: 10.1021/ja031723w. URL: https://doi.org/10.1021/ja031723w.

(*80*) Pablo Fanjul-Bolado, Maria Begona Gonzalez-Garcia, and Agustin Costa-Garcia. "Flow screen-printed amperometric detection of p-nitrophenol in alkaline phosphatase-based assays". eng. In: *Analytical and Bioanalytical Chemistry* 385.7 (Aug. 2006), pp. 1202–1208. ISSN: 1618-2642. DOI: 10.1007/s00216-006-0367-8.

(*81*) Al-Monsur Jiaul Haque et al. "An Electrochemically Reduced Graphene Oxide-Based Electrochemical Immunosensing Platform for Ultrasensitive Antigen Detection". In: *Analytical Chemistry* 84.4 (Feb. 2012), pp. 1871–1878. ISSN: 0003-2700. DOI: 10.1021/ac202562v. URL: https://doi.org/10.1021/ac202562v.

(*82*) Ruchika Malhotra et al. "Ultrasensitive Electrochemical Immunosensor for Oral Cancer Biomarker IL-6 Using Carbon Nanotube Forest Electrodes and Multilabel Amplification". In: *Analytical Chemistry* 82.8 (Apr. 2010), pp. 3118–3123. ISSN: 0003-2700. DOI: 10.1021/ac902802b. URL: https://doi.org/10.1021/ac902802b.

(*83*) Md. Rajibul Akanda et al. "Optimization of Phosphatase- and Redox Cycling-Based Immunosensors and Its Application to Ultrasensitive Detection of Troponin I". In: *Analytical Chemistry* 83.10 (May 2011), pp. 3926–

3933. ISSN: 0003-2700. DOI: 10.1021/ac200447b. URL: https://doi.org/10.1021/ac200447b.

(*84*) Chenyi Hu et al. "Ag@BSA Core/Shell Microspheres As an Electrochemical Interface for Sensitive Detection of Urinary Retinal-Binding Protein". In: *Analytical Chemistry* 84.23 (Dec. 2012), pp. 10324–10331. ISSN: 0003-2700. DOI: 10.1021/ac3023795. URL: https://doi.org/10.1021/ac3023795.

(*85*) Bill Stanley, Palm Joon Kim, TransDimension et al. *On-The-Go Supplement to the USB 2.0 Specification*. Dec. 2001. URL: http://www.usb.org/developers/onthego/otg1_0.pdf.

(*86*) Peter B. Lillehoj et al. "Rapid electrochemical detection on a mobile phone". en. In: *Lab on a Chip* 13.15 (2013), pp. 2950–2955. DOI: 10.1039/C3LC50306B. URL: https://pubs.rsc.org/en/content/articlelanding/2013/lc/c3lc50306b.

(*87*) Timothy B. Lee. *Android Poised to Dominate the Developing World*. en. URL: https://www.forbes.com/sites/timothylee/2011/08/16/android-poised-to-dominate-the-developing-world/.

(*88*) David Erickson et al. "Smartphone technology can be transformative to the deployment of lab-on-chip diagnostics". en. In: *Lab on a Chip* 14.17 (2014), pp. 3159–3164. DOI: 10.1039/C4LC00142G. URL: https://pubs.rsc.org/en/content/articlelanding/2014/lc/c4lc00142g.

(*89*) Quan Cheng et al. "Functional lipid microstructures immobilized on a gold electrode for voltammetric biosensing of cholera toxin". en. In: *Analyst* 129.4 (2004), pp. 309–314. DOI: 10.1039/B315656G. URL: https://pubs.rsc.org/en/content/articlelanding/2004/an/b315656g.

(*90*) Subramanian Viswanathan et al. "Electrochemical Immunosensor for Cholera Toxin Using Liposomes and Poly(3,4-ethylenedioxythiophene)-Coated Carbon Nanotubes". In: *Analytical Chemistry* 78.4 (Feb. 2006), pp. 1115–1121. ISSN: 0003-2700. DOI: 10.1021/ac051435d. URL: https://doi.org/10.1021/ac051435d.

(*91*) Yingshuai Liu and Chang Ming Li. "Advanced Immobilization and Amplification for High Performance Protein Chips". In: *Analytical Letters* 45.2-3 (Jan. 2012), pp. 130–155. ISSN: 0003-2719. DOI: 10.1080/00032719.2011.633187. URL: https://doi.org/10.1080/00032719.2011.633187.

(*92*) Qiaoling Yu et al. "Technological Development of Antibody Immobilization for Optical Immunoassays: Progress and Prospects". In: *Critical Reviews in Analytical Chemistry* 45.1 (Jan. 2015), pp. 62–75. ISSN: 1040-8347. DOI: 10.1080/10408347.2014.881249. URL: https://doi.org/10.1080/10408347.2014.881249.

(*93*) Zong Dai et al. "Novel amperometric immunosensor for rapid separation-free immunoassay of carcinoembryonic antigen". eng. In: *Journal of Immunological Methods* 287.1-2 (Apr. 2004), pp. 13–20. ISSN: 0022-1759. DOI: 10.1016/j.jim.2004.01.012.

(*94*) Jiehua Lin and Huangxian Ju. “Electrochemical and chemiluminescent immunosensors for tumor markers”. eng. In: *Biosensors & Bioelectronics* 20.8 (Feb. 2005), pp. 1461–1470. ISSN: 0956-5663. DOI: 10.1016/j.bios.2004.05.008.

(*95*) Priyabrata Sarkar et al. “Amperometric biosensors for detection of the prostate cancer marker (PSA)”. eng. In: *International Journal of Pharmaceutics* 238.1-2 (May 2002), pp. 1–9. ISSN: 0378-5173.

(*96*) Yongwon Jung, Jin Young Jeong, and Bong Hyun Chung. “Recent advances in immobilization methods of antibodies on solid supports”. en. In: *Analyst* 133.6 (2008), pp. 697–701. DOI: 10.1039/B800014J. URL: https://pubs.rsc.org/en/content/articlelanding/2008/an/b800014j.

(*97*) Bin Lu, Malcolm R. Smyth, and Richard O’Kennedy. “Tutorial review. Oriented immobilization of antibodies and its applications in immunoassays and immunosensors”. en. In: *Analyst* 121.3 (1996), 29R–32R. DOI: 10.1039/AN996210029R. URL: https://pubs.rsc.org/en/content/articlelanding/1996/an/an996210029r.

(*98*) Rebecca W. Grawe and Thomas A. Knotts. “The effects of tether placement on antibody stability on surfaces”. In: *The Journal of Chemical Physics* 146.21 (June 2017), p. 215102. ISSN: 0021-9606. DOI: 10.1063/1.4983705. URL: https://aip.scitation.org/doi/10.1063/1.4983705.

(*99*) Anke K. Trilling, Jules Beekwilder, and Han Zuilhof. “Antibody orientation on biosensor surfaces: a minireview”. en. In: *Analyst* 138.6 (2013),

pp. 1619–1627. DOI: 10.1039/C2AN36787D. URL: https://pubs.rsc.org/en/content/articlelanding/2013/an/c2an36787d.

(*100*) Won Jun Sung and You Han Bae. "A glucose oxidase electrode based on polypyrrole with polyanion/PEG/enzyme conjugate dopant". eng. In: *Biosensors & Bioelectronics* 18.10 (Sept. 2003), pp. 1231–1239. ISSN: 0956-5663.

(*101*) Yiseul Ryu et al. "Increase in the detection sensitivity of a lateral flow assay for a cardiac marker by oriented immobilization of antibody". en. In: *BioChip Journal* 5.3 (Sept. 2011), p. 193. ISSN: 1976-0280, 2092-7843. DOI: 10.1007/s13206-011-5301-2. URL: https://link.springer.com/article/10.1007/s13206-011-5301-2.

(*102*) O. Ouerghi et al. "Gold electrode functionalized by electropolymerization of a cyano N-substituted pyrrole: application to an impedimetric immunosensor". In: *Journal of Electroanalytical Chemistry* 501.1 (Mar. 2001), pp. 62–69. ISSN: 1572-6657. DOI: 10.1016/S0022-0728(00)00485-X. URL: http://www.sciencedirect.com/science/article/pii/S002207280000485X.

(*103*) Hyun-Ju Um et al. "Electrochemically oriented immobilization of antibody on poly-(2-cyano-ethylpyrrole)-coated gold electrode using a cyclic voltammetry". eng. In: *Talanta* 84.2 (Apr. 2011), pp. 330–334. ISSN: 1873-3573. DOI: 10.1016/j.talanta.2011.01.013.

(*104*) Nicholas G. Welch et al. "Orientation and characterization of immobilized antibodies for improved immunoassays (Review)". In: *Biointerphases* 12.2 (Mar. 2017), p. 02D301. ISSN: 1934-8630. DOI: 10.1116/1.4978435. URL: https://avs.scitation.org/doi/full/10.1116/1.4978435.

(*105*) Shu-Lin Guo et al. "A Fast Universal Immobilization of Immunoglobulin G at 4°C for the Development of Array-based Immunoassays". en. In: *PLOS ONE* 7.12 (Dec. 2012), e51370. ISSN: 1932-6203. DOI: 10.1371/journal.pone.0051370. URL: http://journals.plos.org/plosone/article?id=10.1371/journal.pone.0051370.

(*106*) Masumi Iijima et al. "Nanocapsule-based probe for evaluating the orientation of antibodies immobilized on a solid phase". en. In: *Analyst* 138.12 (2013), pp. 3470–3477. DOI: 10.1039/C3AN00481C. URL: https://pubs.rsc.org/en/content/articlelanding/2013/an/c3an00481c.

(*107*) P. L. Ey, S. J. Prowse, and C. R. Jenkin. "Isolation of pure IgG1, IgG2a and IgG2b immunoglobulins from mouse serum using protein A-Sepharose". In: *Immunochemistry* 15.7 (July 1978), pp. 429–436. ISSN: 0019-2791. DOI: 10.1016/0161-5890(78)90070-6. URL: http://www.sciencedirect.com/science/article/pii/0161589078900706.

(*108*) Paul Peluso et al. "Optimizing antibody immobilization strategies for the construction of protein microarrays". In: *Analytical Biochemistry* 312.2 (Jan. 2003), pp. 113–124. ISSN: 0003-2697. DOI: 10.1016/S0003-

2697(02)00442-6. URL: http://www.sciencedirect.com/science/article/pii/S0003269702004426.

(*109*) Nihan Aydemir, Jenny Malmstrom, and Jadranka Travas-Sejdic. "Conducting polymer based electrochemical biosensors". en. In: *Physical Chemistry Chemical Physics* 18.12 (Mar. 2016), pp. 8264–8277. ISSN: 1463-9084. DOI: 10.1039/C5CP06830D. URL: https://pubs.rsc.org/en/content/articlelanding/2016/cp/c5cp06830d.

(*110*) Minni Singh, Pavan Kumar Kathuroju, and Nagaraju Jampana. "Polypyrrole based amperometric glucose biosensors". In: *Sensors and Actuators B: Chemical* 143.1 (Dec. 2009), pp. 430–443. ISSN: 0925-4005. DOI: 10.1016/j.snb.2009.09.005. URL: http://www.sciencedirect.com/science/article/pii/S0925400509006947.

(*111*) Wolfgang Schuhmann et al. "Electrocatalytic properties of polypyrrole in amperometric electrodes". In: *Biosensors and Bioelectronics* 6.8 (Jan. 1991), pp. 689–697. ISSN: 0956-5663. DOI: 10.1016/0956-5663(91)87023-5. URL: http://www.sciencedirect.com/science/article/pii/0956566391870235.

(*112*) Liliane Coche-Guerente et al. "Controlled electrochemical preparation of enzymatic layers for the design of amperometric biosensors". en. In: *Electroanalysis* 5.8 (Sept. 1993), pp. 647–652. ISSN: 1521-4109. DOI: 10.1002/elan.1140050804. URL: https://onlinelibrary.wiley.com/doi/abs/10.1002/elan.1140050804.

(*113*) Joseph Wang and Mustafa Musameh. "Carbon-nanotubes doped polypyrrole glucose biosensor". In: *Analytica Chimica Acta* 539.1 (May 2005),

pp. 209–213. ISSN: 0003-2670. DOI: 10.1016/j.aca.2005.02.059. URL: http://www.sciencedirect.com/science/article/pii/S0003267005003041.

(*114*) Nicola C. Foulds and Christopher R. Lowe. "Immobilization of glucose oxidase in ferrocene-modified pyrrole polymers". In: *Analytical Chemistry* 60.22 (Nov. 1988), pp. 2473–2478. ISSN: 0003-2700. DOI: 10.1021/ac00173a008. URL: https://doi.org/10.1021/ac00173a008.

(*115*) Itamar Willner et al. "Bioelectrocatalysed reduction of nitrate utilizing polythiophene bipyridinium enzyme electrodes". In: *Bioelectrochemistry and Bioenergetics* 29.1 (Nov. 1992), pp. 29–45. ISSN: 0302-4598. DOI: 10.1016/0302-4598(92)80051-H. URL: http://www.sciencedirect.com/science/article/pii/030245989280051H.

(*116*) Emily C. Hernández et al. "Potentiometric enzyme electrode for urea based on electrochemically prepared polypyrrole membranes". English. In: *Mikrochimica Acta* 121.1-4 (Mar. 1995), pp. 63–72. ISSN: 0026-3672. DOI: 10.1007/BF01248241. URL: https://miami.pure.elsevier.com/en/publications/potentiometric-enzyme-electrode-for-urea-based-on-electrochemical.

(*117*) Shihua Song et al. "Characterization of cytochrome c/alkanethiolate structures prepared by self-assembly on gold". In: *The Journal of Physical Chemistry* 97.24 (June 1993), pp. 6564–6572. ISSN: 0022-3654. DOI: 10.1021/j100126a037. URL: https://doi.org/10.1021/j100126a037.

(*118*) Jose Hodak et al. "Layer-by-Layer Self-Assembly of Glucose Oxidase with a Poly(allylamine)ferrocene Redox Mediator". In: *Langmuir* 13.10 (May 1997), pp. 2708–2716. ISSN: 0743-7463. DOI: 10.1021/la962014h. URL: https://doi.org/10.1021/la962014h.

(*119*) A. F. Diaz et al. "Conducting poly-N-alkylpyrrole polymer films". In: *Journal of Electroanalytical Chemistry and Interfacial Electrochemistry* 133.2 (Feb. 1982), pp. 233–239. ISSN: 0022-0728. DOI: 10.1016/0368-1874(82)85140-X. URL: http://www.sciencedirect.com/science/article/pii/036818748285140X.

(*120*) Saïd Sadki et al. "The mechanisms of pyrrole electropolymerization". en. In: *Chemical Society Reviews* 29.5 (2000), pp. 283–293. DOI: 10.1039/A807124A. URL: https://pubs.rsc.org/en/content/articlelanding/2000/cs/a807124a.

(*121*) Terje A. Skotheim and John Reynolds. *Handbook of Conducting Polymers*. en. CRC Press, Jan. 2007. URL: https://www.crcpress.com/Handbook-of-Conducting-Polymers-2-Volume-Set/Skotheim-Reynolds/p/book/9781574446654.

(*122*) Roger D. van Zee, Gernot S. Pomrenke, and Heather M. Evans. *Nanotechnology - Enabled Sensing:* en. Tech. rep. Fort Belvoir, VA: Defense Technical Information Center, May 2009. DOI: 10.21236/ADA523650. URL: http://www.dtic.mil/docs/citations/ADA523650.

(*123*) Nathaniel L. Rosi and Chad A. Mirkin. "Nanostructures in Biodiagnostics". In: *Chemical Reviews* 105.4 (Apr. 2005), pp. 1547–1562. ISSN:

0009-2665. DOI: 10.1021/cr030067f. URL: https://doi.org/10.1021/cr030067f.

(*124*) *Nanostructures in Biodiagnostics - Chemical Reviews (ACS Publications)*. URL: https://pubs.acs.org/doi/10.1021/cr030067f.

(*125*) NanoInk. *Introduction to Nanoscale Science and Technology: Version 1*. en. NanoInk, May 2010. ISBN: 978-0-9837896-0-4.

(*126*) Niklas Elfstrom et al. "Surface Charge Sensitivity of Silicon Nanowires: Size Dependence". In: *Nano Letters* 7.9 (Sept. 2007), pp. 2608–2612. ISSN: 1530-6984. DOI: 10.1021/nl0709017. URL: https://doi.org/10.1021/nl0709017.

(*127*) Binod Rizal et al. "Nanocoax-Based Electrochemical Sensor". In: *Analytical Chemistry* 85.21 (Nov. 2013), pp. 10040–10044. ISSN: 0003-2700. DOI: 10.1021/ac402441x. URL: https://doi.org/10.1021/ac402441x.

(*128*) Jose M. Pingarron, Paloma Yanez-Sedeno, and Araceli Gonzalez-Cortes. "Gold nanoparticle-based electrochemical biosensors". In: *Electrochimica Acta* 53.19 (Aug. 2008), pp. 5848–5866. ISSN: 0013-4686. DOI: 10.1016/j.electacta.2008.03.005. URL: http://www.sciencedirect.com/science/article/pii/S0013468608003599.

(*129*) W. P. Faulk and G. M. Taylor. "An immunocolloid method for the electron microscope". eng. In: *Immunochemistry* 8.11 (Nov. 1971), pp. 1081–1083. ISSN: 0019-2791.

(*130*) L.A. Dykman and N.G. Khlebtsov. "Gold Nanoparticles in Biology and Medicine: Recent Advances and Prospects". In: *Acta Naturae* 3.2 (2011),

pp. 34–55. ISSN: 2075-8251. URL: https://www.ncbi.nlm.nih.gov/pmc/articles/PMC3347577/.

(*131*) Dianping Tang et al. "New amperometric and potentiometric immunosensors based on gold nanoparticles/tris(2,2'-bipyridyl)cobalt(III) multilayer films for hepatitis B surface antigen determinations". In: *Biosensors and Bioelectronics* 21.4 (Oct. 2005), pp. 539–548. ISSN: 0956-5663. DOI: 10.1016/j.bios.2004.11.024. URL: http://www.sciencedirect.com/science/article/pii/S0956566304005846.

(*132*) Dianping Tang and Jingjing Ren. "Direct and Rapid Detection of Diphtherotoxin via Potentiometric Immunosensor Based on Nanoparticles Mixture and Polyvinyl Butyral as Matrixes". en. In: *Electroanalysis* 17.24 (Dec. 2005), pp. 2208–2216. ISSN: 1521-4109. DOI: 10.1002/elan.200503351. URL: https://onlinelibrary.wiley.com/doi/abs/10.1002/elan.200503351.

(*133*) Dianping Tang et al. "Preparation and application on a kind of immobilization method of anti-diphtheria for potentiometric immunosensor modified colloidal Au and polyvinyl butyral as matrixes". In: *Sensors and Actuators B: Chemical* 104.2 (Jan. 2005), pp. 199–206. ISSN: 0925-4005. DOI: 10.1016/j.snb.2004.04.116. URL: http://www.sciencedirect.com/science/article/pii/S0925400504003089.

(*134*) Zhao-Peng Chen et al. "A sensitive immunosensor using colloidal gold as electrochemical label". In: *Talanta*. Special Issue on China-Japan-Korea Environmental Analysis 72.5 (July 2007), pp. 1800–1804. ISSN:

0039-9140. DOI: 10.1016/j.talanta.2007.02.020. URL: http://www.sciencedirect.com/science/article/pii/S0039914007001476.

(*135*) Fernando Patolsky et al. "Electrical detection of single viruses". en. In: *Proceedings of the National Academy of Sciences* 101.39 (Sept. 2004), pp. 14017–14022. ISSN: 0027-8424, 1091-6490. DOI: 10.1073/pnas.0406159101. URL: http://www.pnas.org/content/101/39/14017.

(*136*) Jinjie Yin et al. "A hydrogen peroxide electrochemical sensor based on silver nanoparticles decorated silicon nanowire arrays". In: *Electrochimica Acta* 56.11 (Apr. 2011), pp. 3884–3889. ISSN: 0013-4686. DOI: 10.1016/j.electacta.2011.02.033. URL: http://www.sciencedirect.com/science/article/pii/S0013468611002453.

(*137*) Gengfeng Zheng et al. "Multiplexed electrical detection of cancer markers with nanowire sensor arrays". en. In: *Nature Biotechnology* 23.10 (Oct. 2005), pp. 1294–1301. ISSN: 1546-1696. DOI: 10.1038/nbt1138. URL: https://www.nature.com/articles/nbt1138.

(*138*) Werner Kern. "The Evolution of Silicon Wafer Cleaning Technology". en. In: *Journal of The Electrochemical Society* 137.6 (June 1990), pp. 1887–1892. ISSN: 0013-4651, 1945-7111. DOI: 10.1149/1.2086825. URL: http://jes.ecsdl.org/content/137/6/1887.

(*139*) *EPIKURE 3140 Curing Agent | EPOXY Curing Agent | Hexion*. en-US. Sept. 2016. URL: https://www.miller-stephenson.com/product/epikure-3140/.

(*140*) Modutek Corporation. *How Piranha Etch is Used in Silicon Wafer Cleaning*. en-US. Dec. 2016. URL: https://www.modutek.com/how-piranha-etch-is-used-in-silicon-wafer-cleaning/.

(*141*) Nathan T. Nesbitt et al. "Au Dendrite Electrocatalysts for CO2 Electrolysis". In: *The Journal of Physical Chemistry C* 122.18 (May 2018), pp. 10006–10016. ISSN: 1932-7447. DOI: 10.1021/acs.jpcc.8b01831. URL: https://doi.org/10.1021/acs.jpcc.8b01831.

(*142*) Michelle M. Archibald et al. "A nanocoaxial-based electrochemical sensor for the detection of cholera toxin". eng. In: *Biosensors & Bioelectronics* 74 (Dec. 2015), pp. 406–410. ISSN: 1873-4235. DOI: 10.1016/j.bios.2015.06.069.

(*143*) Francesco Ricci, Gianluca Adornetto, and Giuseppe Palleschi. "A review of experimental aspects of electrochemical immunosensors". In: *Electrochimica Acta*. ELECTROCHEMICAL SCIENCE AND TECHNOLOGYState of the Art and Future PerspectivesOn the occasion of the International Year of Chemistry (2011) 84 (Dec. 2012), pp. 74–83. ISSN: 0013-4686. DOI: 10.1016/j.electacta.2012.06.033. URL: http://www.sciencedirect.com/science/article/pii/S0013468612009735.

(*144*) Oussama Ouerghi et al. "Electrodeposited Biotinylated Polypyrrole as an Immobilization Method for Impedimetric Immunosensors". In: *Sensors Journal, IEEE* 4 (Nov. 2004), pp. 559–567. DOI: 10.1109/JSEN.2004.832858.

(*145*) Jeremy M. Fowler, Margaret C. Stuart, and Danny K. Y. Wong. "Self-Assembled Layer of Thiolated Protein G as an Immunosensor Scaffold". In: *Analytical Chemistry* 79.1 (Jan. 2007), pp. 350–354. ISSN: 0003-2700. DOI: 10.1021/ac061175f. URL: https://doi.org/10.1021/ac061175f.

(*146*) *Cholera count reaches 500 000 in Yemen*. en. URL: http://www.who.int/news-room/detail/14-08-2017-cholera-count-reaches-500-000-in-yemen.

(*147*) Kristin B. Cederquist and Shana O. Kelley. "Nanostructured biomolecular detectors: pushing performance at the nanoscale". eng. In: *Current Opinion in Chemical Biology* 16.3-4 (Aug. 2012), pp. 415–421. ISSN: 1879-0402. DOI: 10.1016/j.cbpa.2012.04.011.

(*148*) Jason K. Kawasaki and Craig B. Arnold. "Synthesis of Platinum Dendrites and Nanowires Via Directed Electrochemical Nanowire Assembly". In: *Nano Letters* 11.2 (Feb. 2011), pp. 781–785. ISSN: 1530-6984. DOI: 10.1021/nl1039956. URL: https://doi.org/10.1021/nl1039956.

(*149*) Bret N. Flanders. "Directed electrochemical nanowire assembly: precise nanostructure assembly via dendritic solidification". In: *Modern Physics Letters B* 26.01 (Jan. 2012), p. 1130001. ISSN: 0217-9849. DOI: 10.1142/S0217984911300018. URL: https://www.worldscientific.com/doi/abs/10.1142/S0217984911300018.

(*150*) Birol Ozturk, Ishan Talukdar, and Bret N. Flanders. "Directed growth of diameter-tunable nanowires". en. In: *Nanotechnology* 18.36 (2007),

p. 365302. ISSN: 0957-4484. DOI: 10.1088/0957-4484/18/36/365302. URL: http://stacks.iop.org/0957-4484/18/i=36/a=365302.

(*151*) W. W. Mullins and R. F. Sekerka. "Stability of a Planar Interface During Solidification of a Dilute Binary Alloy". In: *Journal of Applied Physics* 35.2 (Feb. 1964), pp. 444–451. ISSN: 0021-8979. DOI: 10.1063/1.1713333. URL: https://aip.scitation.org/doi/10.1063/1.1713333.

(*152*) Chuanding Cheng et al. "Self-assembly of metallic nanowires from aqueous solution". eng. In: *Nano Letters* 5.1 (Jan. 2005), pp. 175–178. ISSN: 1530-6984. DOI: 10.1021/nl048240q.

(*153*) A. Nerowski et al. "Dielectrophoretic Growth of Platinum Nanowires: Concentration and Temperature Dependence of the Growth Velocity". In: *Langmuir* 28.19 (May 2012), pp. 7498–7504. ISSN: 0743-7463. DOI: 10.1021/la300302n. URL: https://doi.org/10.1021/la300302n.

(*154*) Govind Paneru and Bret N. Flanders. "Complete reconfiguration of dendritic gold". en. In: *Nanoscale* 6.2 (Dec. 2013), pp. 833–841. ISSN: 2040-3372. DOI: 10.1039/C3NR04317G. URL: https://pubs.rsc.org/en/content/articlelanding/2014/nr/c3nr04317g.

(*155*) Xiaogang Wen et al. "Dendritic Nanostructures of Silver: Facile Synthesis, Structural Characterizations, and Sensing Applications". In: *Langmuir* 22.10 (May 2006), pp. 4836–4842. ISSN: 0743-7463. DOI: 10.1021/la060267x. URL: https://doi.org/10.1021/la060267x.

(*156*) Md. Harunar Rashid and Tarun K. Mandal. "Synthesis and Catalytic Application of Nanostructured Silver Dendrites". In: *The Journal of Physical Chemistry C* 111.45 (Nov. 2007), pp. 16750–16760. ISSN: 1932-7447. DOI: 10.1021/jp074963x. URL: https://doi.org/10.1021/jp074963x.

(*157*) Jagotamoy Das and Shana O. Kelley. "Protein Detection Using Arrayed Microsensor Chips: Tuning Sensor Footprint to Achieve Ultrasensitive Readout of CA-125 in Serum and Whole Blood". In: *Analytical Chemistry* 83.4 (Feb. 2011), pp. 1167–1172. ISSN: 0003-2700. DOI: 10.1021/ac102917f. URL: https://doi.org/10.1021/ac102917f.

(*158*) Alyajahan Bhimji et al. "Electrochemical enzyme-linked immunosorbent assay featuring proximal reagent generation: detection of human immunodeficiency virus antibodies in clinical samples". eng. In: *Analytical Chemistry* 85.14 (July 2013), pp. 6813–6819. ISSN: 1520-6882. DOI: 10.1021/ac4009429.

(*159*) Junhua Li et al. "High-sensitivity paracetamol sensor based on Pd/graphene oxide nanocomposite as an enhanced electrochemical sensing platform". eng. In: *Biosensors & Bioelectronics* 54 (Apr. 2014), pp. 468–475. ISSN: 1873-4235. DOI: 10.1016/j.bios.2013.11.001.

(*160*) Kelley Hammon. "Overview of Reference Electrodes and Alternative Reference Electrodes". en. In: (2016), p. 12.

(*161*) *Reference Electrodes Influence Electrochemical Measurements*. URL: https://www.gamry.com/application-notes/electrodes-cells/reference-electrodes/.

(*162*) M. Waleed Shinwari et al. “Microfabricated Reference Electrodes and their Biosensing Applications”. en. In: *Sensors* 10.3 (Mar. 2010), pp. 1679–1715. DOI: 10.3390/s100301679. URL: http://www.mdpi.com/1424-8220/10/3/1679.

(*163*) Serge Cosnier and CH Gondran. “Fabrication of biosensors by attachment of biological macromolecules to electropolymerized conducting films”. In: *http://dx.doi.org/10.1051/analusis:1999270558* 27 (Sept. 1999). DOI: 10.1051/analusis:1999270558.

(*164*) Delia Goletti et al. “Tuberculosis Biomarkers: From Diagnosis to Protection”. In: *Infectious Disease Reports* 8.2 (June 2016). ISSN: 2036-7430. DOI: 10.4081/idr.2016.6568. URL: https://www.ncbi.nlm.nih.gov/pmc/articles/PMC4927936/.

(*165*) Adriano Ambrosi, Federico Airo, and Arben Merkoci. “Enhanced gold nanoparticle based ELISA for a breast cancer biomarker”. eng. In: *Analytical Chemistry* 82.3 (Feb. 2010), pp. 1151–1156. ISSN: 1520-6882. DOI: 10.1021/ac902492c.

(*166*) Christopher R. Lowe. “Biosensors”. English. In: *Trends in Biotechnology* 2.3 (May 1984), pp. 59–65. ISSN: 0167-7799, 1879-3096. DOI: 10.1016/0167-7799(84)90011-8. URL: https://www.cell.com/trends/biotechnology/abstract/0167-7799(84)90011-8.

(*167*) Bengt Kasemo. “Biological Surface Science”. In: *Surface Science* 500 (Oct. 1998), pp. 656–677. DOI: 10.1016/S0039-6028(01)01809-X.

(*168*) Tao Li, Wenping Hu, and Daoben Zhu. "Nanogap Electrodes". en. In: *Advanced Materials* 22.2 (Jan. 2010), pp. 286–300. ISSN: 1521-4095. DOI: 10.1002/adma.200900864. URL: https://onlinelibrary.wiley.com/doi/abs/10.1002/adma.200900864.

(*169*) Yudong He et al. "Graphene and graphene oxide nanogap electrodes fabricated by atomic force microscopy nanolithography". In: *Applied Physics Letters* 97.13 (Sept. 2010), p. 133301. ISSN: 0003-6951. DOI: 10.1063/1.3493647. URL: https://aip.scitation.org/doi/full/10.1063/1.3493647.

(*170*) Stephen M. Oja, Marissa Wood, and Bo Zhang. "Nanoscale Electrochemistry". In: *Analytical Chemistry* 85.2 (Jan. 2013), pp. 473–486. ISSN: 0003-2700. DOI: 10.1021/ac3031702. URL: https://doi.org/10.1021/ac3031702.

(*171*) Kanwar Vikas Singh et al. "3D nanogap interdigitated electrode array biosensors". In: *Analytical and Bioanalytical Chemistry* 397.4 (), pp. 1493–1502. URL: https://link.springer.com/article/10.1007%2Fs00216-010-3682-z.

(*172*) J. Rybczynski et al. "Subwavelength waveguide for visible light". In: *Applied Physics Letters* 90.2 (Jan. 2007), p. 021104. ISSN: 0003-6951. DOI: 10.1063/1.2430400. URL: https://aip.scitation.org/doi/10.1063/1.2430400.

(*173*) Juan M. Merlo et al. "Near-field observation of light propagation in nanocoax waveguides". EN. In: *Optics Express* 22.12 (June 2014), pp. 14148–14154. ISSN: 1094-4087. DOI: 10.1364/OE.22.014148. URL:

https://www.osapublishing.org/oe/abstract.cfm?uri=oe-22-12-14148.

(*174*) Huaizhou Zhao et al. "Ultrasensitive Chemical Detection Using a Nanocoax Sensor". In: *ACS Nano* 6.4 (Apr. 2012), pp. 3171–3178. ISSN: 1936-0851. DOI: 10.1021/nn205036e. URL: https://doi.org/10.1021/nn205036e.

(*175*) Jeffrey R. Naughton et al. "Shielded Coaxial Optrode Arrays for Neurophysiology". English. In: *Frontiers in Neuroscience* 10 (2016). ISSN: 1662-453X. DOI: 10.3389/fnins.2016.00252. URL: https://www.frontiersin.org/articles/10.3389/fnins.2016.00252/full.

(*176*) T. R. Tshikhudo, Z. Wang, and M. Brust. "Biocompatible gold nanoparticles". In: *Materials Science and Technology* 20.8 (Aug. 2004), pp. 980–984. ISSN: 0267-0836. DOI: 10.1179/026708304225019849. URL: https://doi.org/10.1179/026708304225019849.

(*177*) Eric T. K. Demann, Pamela S. Stein, and James E. Haubenreich. "Gold as an Implant in Medicine and Dentistry". English. In: *Journal of Long-Term Effects of Medical Implants* 15.6 (2005). ISSN: 1050-6934, 1940-4379. DOI: 10.1615/JLongTermEffMedImplants.v15.i6.100. URL: http://www.dl.begellhouse.com/journals/1bef42082d7a0fdf,56437700108bb47c,6dde54560f83061a.html.

(*178*) Byron D. Gates et al. "New Approaches to Nanofabrication: Molding, Printing, and Other Techniques". In: *Chemical Reviews* 105.4 (Apr.

2005), pp. 1171–1196. ISSN: 0009-2665. DOI: 10.1021/cr030076o. URL: https://doi.org/10.1021/cr030076o.

(*179*) Stephen Y. Chou, Peter R. Krauss, and Preston J. Renstrom. "Imprint Lithography with 25-Nanometer Resolution". en. In: *Science* 272.5258 (Apr. 1996), pp. 85–87. ISSN: 0036-8075, 1095-9203. DOI: 10.1126/science.272.5258.85. URL: http://science.sciencemag.org/content/272/5258/85.

(*180*) C. M. Sotomayor Torresa et al. "Nanoimprint lithography: an alternative nanofabrication approach". In: *Materials Science and Engineering C* 23 (2002), pp. 23–31.

(*181*) Petr Stepnika. *Ferrocenes: Ligands, Materials and Biomolecules*. en-us. Wiley, 2008. ISBN: 978-0-470-03585-6. URL: https://www.wiley.com/en-us/Ferrocenes%3A+Ligands%2C+Materials+and+Biomolecules-p-9780470035856.

(*182*) Theodore T. Herskovits, Barbara Gadegbeku, and Helen Jaillet. "On the Structural Stability and Solvent Denaturation of Proteins I. DENATURATION BY THE ALCOHOLS AND GLYCOLS". en. In: *Journal of Biological Chemistry* 245.10 (May 1970), pp. 2588–2598. ISSN: 0021-9258, 1083-351X. URL: http://www.jbc.org/content/245/10/2588.

(*183*) *PMGI and LOR Resists: FAQs :: MicroChem*. URL: http://www.microchem.com/pmgi-lor_faq.htm.

(*184*) *2.1 Silicon Dioxide Properties*. URL: http://www.iue.tuwien.ac.at/phd/filipovic/node26.html.

(*185*) *Properties of Silicon - El-Cat.com*. URL: https://www.el-cat.com/silicon-properties.htm.

(*186*) *The Electrical Double Layer — Department of Chemical Engineering and Biotechnology*. en. Page. URL: https://www.ceb.cam.ac.uk/research/groups/rg-eme/teaching-notes/the-electrical-double-layer.

(*187*) *Pulse Voltammetric Techniques*. URL: https://www.basinc.com/manuals/EC_epsilon/Techniques/Pulse/pulse.

(*188*) Bernhard Wolfrum et al. "Nanoscale Electrochemical Sensor Arrays: Redox Cycling Amplification in Dual-Electrode Systems". In: *Accounts of Chemical Research* 49.9 (Sept. 2016), pp. 2031–2040. ISSN: 0001-4842. DOI: 10.1021/acs.accounts.6b00333. URL: https://doi.org/10.1021/acs.accounts.6b00333.

(*189*) Henry S. White and Kim McKelvey. "Redox cycling in nanogap electrochemical cells". en. In: *Current Opinion in Electrochemistry* 7 (Jan. 2018), pp. 48–53. ISSN: 2451-9103. DOI: 10.1016/j.coelec.2017.10.021. URL: https://www.sciencedirect.com/science/article/pii/S2451910317301369.

(*190*) Michelle M Archibald. "NOVEL NANOARCHITECTURES FOR ELECTROCHEMICAL BIOSENSING". PhD thesis. Boston College, 2016. URL: https://dlib.bc.edu/islandora/object/bc-ir:106807.

(*191*) L. Björck and G. Kronvall. "Purification and some properties of streptococcal protein G, a novel IgG-binding reagent." en. In: *The Journal of*

Immunology 133.2 (Aug. 1984), pp. 969–974. ISSN: 0022-1767, 1550-6606. URL: http://www.jimmunol.org/content/133/2/969.

(*192*) U. Sjöbring, L. Björck, and W. Kastern. "Streptococcal protein G. Gene structure and protein binding properties". eng. In: *The Journal of Biological Chemistry* 266.1 (Jan. 1991), pp. 399–405. ISSN: 0021-9258.

(*193*) Evangelina Pensa et al. "The Chemistry of the Sulfur–Gold Interface: In Search of a Unified Model". In: *Accounts of Chemical Research* 45.8 (Aug. 2012), pp. 1183–1192. ISSN: 0001-4842. DOI: 10.1021/ar200260p. URL: https://doi.org/10.1021/ar200260p.

(*194*) Leyla Soleymani et al. "Nanostructuring of Patterned Microelectrodes To Enhance the Sensitivity of Electrochemical Nucleic Acids Detection". In: *Angewandte Chemie International Edition* 48.45 (), pp. 8457–8460. ISSN: 1521-3773. DOI: 10.1002/anie.200902439. URL: https://www.onlinelibrary.wiley.com/doi/abs/10.1002/anie.200902439.

(*195*) Leyla Soleymani et al. "Programming the detection limits of biosensors through controlled nanostructuring". en. In: *Nature Nanotechnology* 4.12 (2009), pp. 844–848. ISSN: 1748-3395. DOI: 10.1038/nnano.2009.276. URL: https://www.nature.com/articles/nnano.2009.276.

(*196*) Jianjun Wang et al. "Glucose oxidase entrapped in polypyrrole on high-surface-area Pt electrodes: a model platform for sensitive electroenzymatic biosensors". en. In: *Journal of Electroanalytical Chemistry* 575.1

(Jan. 2005), pp. 139–146. ISSN: 1572-6657. DOI: 10.1016/j.jelechem.2004.08.023. URL: https://www.sciencedirect.com/science/article/pii/S0022072804004796.

(*197*) Sabahudin Hrapovic et al. "Electrochemical Biosensing Platforms Using Platinum Nanoparticles and Carbon Nanotubes". In: *Analytical Chemistry* 76.4 (Feb. 2004), pp. 1083–1088. ISSN: 0003-2700. DOI: 10.1021/ac035143t. URL: https://doi.org/10.1021/ac035143t.

(*198*) Marc Delvaux and Demoustier-Champagne. "Immobilisation of glucose oxidase within metallic nanotubes arrays for application to enzyme biosensors". en. In: *Biosensors and Bioelectronics* 18.7 (July 2003), pp. 943–951. ISSN: 0956-5663. DOI: 10.1016/S0956-5663(02)00209-9. URL: https://www.sciencedirect.com/science/article/pii/S0956566302002099.

(*199*) Wei Zhang et al. "High sensitivity photonic crystal biosensor incorporating nanorod structures for enhanced surface area". en. In: *Sensors and Actuators B: Chemical* 131.1 (Apr. 2008), pp. 279–284. ISSN: 0925-4005. DOI: 10.1016/j.snb.2007.11.017. URL: https://www.sciencedirect.com/science/article/pii/S0925400507009367.

(*200*) C. Schmädicke et al. "Copper nanowire synthesis by directed electrochemical nanowire assembly". en. In: *RSC Advances* 4.86 (2014), pp. 46363–46368. DOI: 10.1039/C4RA04853A. URL: https://pubs.rsc.org/en/content/articlelanding/2014/ra/c4ra04853a.

(*201*) Leyla Soleymani et al. "Hierarchical Nanotextured Microelectrodes Overcome the Molecular Transport Barrier To Achieve Rapid, Direct Bacterial Detection". In: *ACS Nano* 5.4 (2011), pp. 3360–3366. ISSN: 1936-0851. DOI: 10.1021/nn200586s. URL: https://doi.org/10.1021/nn200586s.

(*202*) Zhichao Fang et al. "Direct Profiling of Cancer Biomarkers in Tumor Tissue Using a Multiplexed Nanostructured Microelectrode Integrated Circuit". In: *ACS Nano* 3.10 (Oct. 2009), pp. 3207–3213. ISSN: 1936-0851. DOI: 10.1021/nn900733d. URL: https://doi.org/10.1021/nn900733d.

(*203*) Darius G. Rackus et al. "A digital microfluidic device with integrated nanostructured microelectrodes for electrochemical immunoassays". en. In: *Lab on a Chip* 15.18 (2015), pp. 3776–3784. DOI: 10.1039/C5LC00660K. URL: https://pubs.rsc.org/en/content/articlelanding/2015/lc/c5lc00660k.

(*204*) Katie A. Edwards and John C. March. "GM1-functionalized liposomes in a microtiter plate assay for cholera toxin in Vibrio cholerae culture samples". In: *Analytical Biochemistry* 368.1 (Sept. 2007), pp. 39–48. ISSN: 0003-2697. DOI: 10.1016/j.ab.2007.04.019. URL: http://www.sciencedirect.com/science/article/pii/S0003269707002527.

(*205*) Soohyoun Ahn-Yoon et al. "Ganglioside-Liposome Immunoassay for the Ultrasensitive Detection of Cholera Toxin". In: *Analytical Chemistry*

75.10 (May 2003), pp. 2256–2261. ISSN: 0003-2700. DOI: 10.1021/ac026428t. URL: https://doi.org/10.1021/ac026428t.

(*206*) A M Svennerholm and G Wiklund. "Rapid GM1-enzyme-linked immunosorbent assay with visual reading for identification of Escherichia coli heat-labile enterotoxin." In: *Journal of Clinical Microbiology* 17.4 (Apr. 1983), pp. 596–600. ISSN: 0095-1137. URL: https://www.ncbi.nlm.nih.gov/pmc/articles/PMC272699/.

(*207*) Claire L. Schofield, Robert A. Field, and David A. Russell. "Glyconanoparticles for the Colorimetric Detection of Cholera Toxin". In: *Analytical Chemistry* 79.4 (Feb. 2007), pp. 1356–1361. ISSN: 0003-2700. DOI: 10.1021/ac061462j. URL: https://doi.org/10.1021/ac061462j.

(*208*) Basudam Adhikari and Sarmishtha Majumdar. "Polymers in Sensor Applications". In: *Progress in Polymer Science* 29 (July 2004), pp. 699–766. DOI: 10.1016/j.progpolymsci.2004.03.002.

(*209*) A. Ramanavicius, A. Ramanaviciene, and A. Malinauskas. "Electrochemical sensors based on conducting polymer—polypyrrole". In: *Electrochimica Acta*. ChargeTransfer at Electrochemical Interfaces "Two Hundred Years of Electrlysis" 51.27 (Aug. 2006), pp. 6025–6037. ISSN: 0013-4686. DOI: 10.1016/j.electacta.2005.11.052. URL: http://www.sciencedirect.com/science/article/pii/S0013468606003252.

(*210*) Maria Serena Chiriaco et al. "EIS microfluidic chips for flow immunoassay and ultrasensitive cholera toxin detection". eng. In: *Lab on a Chip*

11.4 (Feb. 2011), pp. 658–663. ISSN: 1473-0189. DOI: 10.1039/c0lc00409j.

(*211*) Mahmoud Labib et al. "A capacitive immunosensor for detection of cholera toxin". eng. In: *Analytica Chimica Acta* 634.2 (Feb. 2009), pp. 255–261. ISSN: 1873-4324. DOI: 10.1016/j.aca.2008.12.035.

(*212*) Paul T. Charles et al. "A galactose polyacrylate-based hydrogel scaffold for the detection of cholera toxin and staphylococcal enterotoxin B in a sandwich immunoassay format". eng. In: *Analytica Chimica Acta* 578.1 (Sept. 2006), pp. 2–10. ISSN: 1873-4324. DOI: 10.1016/j.aca.2006.04.083.

(*213*) Y. Oku et al. "Development of a highly sensitive bead-ELISA to detect bacterial protein toxins". eng. In: *Microbiology and Immunology* 32.8 (1988), pp. 807–816. ISSN: 0385-5600.

(*214*) Wei Lian et al. "Sensitive detection of multiplex toxins using antibody microarray". eng. In: *Analytical Biochemistry* 401.2 (June 2010), pp. 271–279. ISSN: 1096-0309. DOI: 10.1016/j.ab.2010.02.040.

(*215*) Lin-Xia Wang, Xin-Gui Li, and Yu-Liang Yang. "Preparation, properties and applications of polypyrroles". In: *Reactive and Functional Polymers* 47.2 (Mar. 2001), pp. 125–139. ISSN: 1381-5148. DOI: 10.1016/S1381-5148(00)00079-1. URL: http://www.sciencedirect.com/science/article/pii/S1381514800000791.

(*216*) Wahid Khan, Mamta Kapoor, and Neeraj Kumar. "Covalent attachment of proteins to functionalized polypyrrole-coated metallic surfaces for improved biocompatibility". In: *Acta Biomaterialia* 3.4 (July 2007), pp. 541–

549. ISSN: 1742-7061. DOI: 10.1016/j.actbio.2007.01.006. URL: http://www.sciencedirect.com/science/article/pii/S1742706107000220.

(*217*) Yuh-Ming Uang and Tse-Chuan Chou. "Fabrication of glucose oxidase/polypyrrole biosensor by galvanostatic method in various pH aqueous solutions". eng. In: *Biosensors & Bioelectronics* 19.3 (Nov. 2003), pp. 141–147. ISSN: 0956-5663.

(*218*) M. I. Rodriguez and E. C. Alocilja. "Embedded DNA-polypyrrole biosensor for rapid detection of Escherichia Coli". In: *IEEE Sensors Journal* 5.4 (Aug. 2005), pp. 733–736. ISSN: 1530-437X. DOI: 10.1109/JSEN.2005.845518.

(*219*) Uda Hashim, Muhamad Emi Azri Shohini, and Harbant Singh. "Nanogap Dielectric Biosensor for Label Free DNA Hybridization Detection". en. In: (2007), p. 9.

(*220*) Xing Chen et al. "Electrical nanogap devices for biosensing". In: *Materials Today* 13.11 (Nov. 2010), pp. 28–41. ISSN: 1369-7021. DOI: 10.1016/S1369-7021(10)70201-7. URL: http://www.sciencedirect.com/science/article/pii/S1369702110702017.

(*221*) Hamid Reza Zafarani et al. "Electrochemical redox cycling in a new nanogap sensor: Design and simulation". In: *Journal of Electroanalytical Chemistry* 760 (Jan. 2016), pp. 42–47. ISSN: 1572-6657. DOI: 10.1016/j.jelechem.2015.11.031. URL: http://www.sciencedirect.com/science/article/pii/S1572665715302095.

(*222*) Michael S Wilson and R. David Rauh. "Hydroquinone diphosphate: an alkaline phosphatase substrate that does not produce electrode fouling in electrochemical immunoassays". In: *Biosensors and Bioelectronics*. Special Issue in Honour of Professor Pierre Coulet 20.2 (Sept. 2004), pp. 276–283. ISSN: 0956-5663. DOI: 10.1016/j.bios.2004.01.013. URL: http://www.sciencedirect.com/science/article/pii/S0956566304000314.

(*223*) Erol Akyilmaz and Mehmet Turemis. "An inhibition type alkaline phosphatase biosensor for amperometric determination of caffeine". In: *Electrochimica Acta* 55.18 (July 2010), pp. 5195–5199. ISSN: 0013-4686. DOI: 10.1016/j.electacta.2010.04.038. URL: http://www.sciencedirect.com/science/article/pii/S0013468610005840.

(*224*) Eun Ji Nam et al. "Highly sensitive electrochemical detection of proteins using aptamer-coated gold nanoparticles and surface enzyme reactions". en. In: *Analyst* 137.9 (2012), pp. 2011–2016. DOI: 10.1039/C2AN15994E. URL: https://pubs.rsc.org/en/content/articlelanding/2012/an/c2an15994e.

(*225*) Hossam M. Nassef et al. "Electrochemical Immunosensor for Detection of Celiac Disease Toxic Gliadin in Foodstuff". In: *Analytical Chemistry* 80.23 (Dec. 2008), pp. 9265–9271. ISSN: 0003-2700. DOI: 10.1021/ac801620j. URL: https://doi.org/10.1021/ac801620j.

(*226*) Ning Xia et al. "Comparing the performances of electrochemical sensors using p-aminophenol redox cycling by different reductants on gold

electrodes modified with self-assembled monolayers". In: *Electrochimica Acta* 109 (Oct. 2013), pp. 348–354. ISSN: 0013-4686. DOI: 10.1016/j.electacta.2013.07.118. URL: http://www.sciencedirect.com/science/article/pii/S001346861301387X.

(*227*) D. A. Hall et al. "16.1 A nanogap transducer array on 32nm CMOS for electrochemical DNA sequencing". In: *2016 IEEE International Solid-State Circuits Conference (ISSCC)*. Jan. 2016, pp. 288–289. DOI: 10.1109/ISSCC.2016.7418020.

(*228*) Tom N. Krupenkin et al. "From Rolling Ball to Complete Wetting: The Dynamic Tuning of Liquids on Nanostructured Surfaces". In: *Langmuir* 20.10 (May 2004), pp. 3824–3827. ISSN: 0743-7463. DOI: 10.1021/la036093q. URL: https://doi.org/10.1021/la036093q.

(*229*) Hao-Yuan Guo, Bo Li, and Xi-Qiao Feng. "Line tension effects on the wetting of nanostructures: an energy method". en. In: *Nanotechnology* 28.38 (2017), p. 384001. ISSN: 0957-4484. DOI: 10.1088/1361-6528/aa7f37. URL: http://stacks.iop.org/0957-4484/28/i=38/a=384001.

(*230*) Grace Wu and Muhammad H. Zaman. "WHO | Low-cost tools for diagnosing and monitoring HIV infection in low-resource settings". In: *Bulletin of the World Health Organization* (2012). URL: http://www.who.int/bulletin/volumes/90/12/12-102780/en/.

(*231*) J. N. Hays. *Epidemics and Pandemics: Their Impacts on Human History*. en. ABC-CLIO, 2005. ISBN: 978-1-85109-658-9.

(*232*) Rajul Parikh et al. "Understanding and using sensitivity, specificity and predictive values". In: *Indian Journal of Ophthalmology* 56.1 (2008), pp. 45–50. ISSN: 0301-4738. URL: https://www.ncbi.nlm.nih.gov/pmc/articles/PMC2636062/.

(*233*) *Portable potentiostat*. en-US. URL: https://www.palmsens.com/potentiostat/portable-potentiostat/.

(*234*) *Hardware development*. en-US. URL: https://www.palmsens.com/oem/potentiostat-modules/.

(*235*) Sonthaya Numthuam et al. "Synergistic effects of micro/nano modifications on electrodes for microfluidic electrochemical ELISA". en. In: *Sensors and Actuators B: Chemical* 156.2 (Aug. 2011), pp. 637–644. ISSN: 0925-4005. DOI: 10.1016/j.snb.2011.02.010. URL: https://www.sciencedirect.com/science/article/pii/S0925400511001080.

(*236*) Lilane Coche-Guerente et al. "Electrochemical immobilization of glucose oxidase in poly(amphiphilic pyrrole) films and its application to the preparation of an amperometric glucose sensor". en. In: *Analytica Chimica Acta* 289.2 (Apr. 1994), pp. 143–153. ISSN: 0003-2670. DOI: 10.1016/0003-2670(94)80097-9. URL: https://www.sciencedirect.com/science/article/pii/0003267094800979.

(*237*) Steven Sun et al. "ELISA-LOC: lab-on-a-chip for enzyme -linked immunodetection". en. In: *Lab on a Chip* 10.16 (2010), pp. 2093–2100. DOI: 10.1039/C003994B. URL: https://pubs.rsc.org/en/content/articlelanding/2010/lc/c003994b.

(*238*) Xiao Guan et al. “Rapid detection of pathogens using antibody-coated microbeads with bioluminescence in microfluidic chips”. en. In: *Biomedical Microdevices* 12.4 (Aug. 2010), pp. 683–691. ISSN: 1572-8781. DOI: 10.1007/s10544-010-9421-6. URL: https://doi.org/10.1007/s10544-010-9421-6.

(*239*) Jason R. Wojciechowski et al. “Organic Photodiodes for Biosensor Miniaturization”. In: *Analytical Chemistry* 81.9 (May 2009), pp. 3455–3461. ISSN: 0003-2700. DOI: 10.1021/ac8027323. URL: https://doi.org/10.1021/ac8027323.